Understanding Monomer and Polymer Confinement in Anodised Aluminium Alloys by Dielectric Spectroscopy

GOKUL GANESH MURALI

Master of Science Thesis

This page is intentionally left blank.

UNDERSTANDING MONOMER AND POLYMER CONFINEMENT IN ANODISED ALUMINIUM ALLOYS BY DIELECTRIC SPECTROSCOPY

Thesis report

by,

Gokul Ganesh Murali

in partial fulfilment of the requirements for the degree of

Master of Science

in Aerospace Engineering

at the Delft University of Technology,

to be defended on Tuesday, August 21, 2018

Student Number:	4565800	
Thesis committee:	Prof.dr.ir. S. van der Zwaag	TU Delft, NovAM, Chairperson of thesis committee
	Dr. S.J. Garcia	TU Delft, NovAM, Thesis supervisor
	Dr. M. Nijemeisland	TU Delft, NovAM
	Dr. J.A. Poulis	TU Delft, SIC, External member
	Dr. Y.V. Meteleva	GKN, Fokker Aerostructures B.V., External member

TU Delft

This page is intentionally left blank.

Acknowledgement

I would like to thank my supervisor, Dr Santiago J Garcia for his guidance and support throughout the duration of this study. His directions and motivations greatly aided the progress of this project. The knowledge I gained by following his courses helped me take this thesis forward. I thank him for helping me grow as an effective researcher under his guidance.

I also thank Dr Marlies Nijemeisland, for her assistance on various technical and theoretical problems encountered in this project. Her expertise with BDS equipment was very helpful in resolving the technical difficulties faced. Her help was monumental in timely completion of this project.

Furthermore, I thank Dr Yulia Meteleva (Fokker Aerostructures) for her expert opinion throughout the duration of this project. Her expertise on anodised aerospace aluminium alloys was very helpful to lay a foundation on which this project was built. I also thank Fokker Aerostructures BV for supplying various products required for this project.

I would also like to thank Frans Oostrum of the DASML lab whose importance to this project cannot be overstated. His timely help with instruments in the lab was useful for a steady progress of this project. Materials supplied by the SIC group were also very useful in this project.

In addition, I would like to thank all the members of the NovAM group for their help, motivation and for providing me with a nurturing environment in this regard. I thank NovAM for being a home away from home for me and for supporting me throughout my Masters.

Finally, I would like to thank my family and friends for being a pillar of support throughout my life. Their support and motivation were highly influential in shaping my career. To them, I dedicate this work.

"Research is formalized curiosity. It is poking and prying with a purpose."

- Zora Neale Hurston

"Always pass on what you have learned."

-Master Yoda

This page is intentionally left blank.

Abstract

This thesis investigates the observation and characterisation of molecular dynamics of monomers and polymers confined within the nanoporous oxide layers of anodised aerospace aluminium alloys by the use of Broadband Dielectric Spectroscopy (BDS).

Using BDS, and subsequent data processing by fitting the dielectric data with Havriliak-Negami (HN) curves, Vogel-Fulcher-Tammann (VFT) curves, and Arrhenius curves, the molecular dynamics of monomers and polymers confined within different types of nanopores is investigated. Molecular dynamics is discussed using parameters such as dielectric relaxation time (τ_{HN} and τ_0), transition temperature (Tv and Tx), and activation energy (Ea).

It is found from this project that when monomers are confined within the nanopores of the metal oxide layers, a fraction of them are adsorbed on to the pore wall. This adsorption leads to the formation of a new material morphology that has a relatively high restriction to molecular dynamics. The topology of the confining nanopores also plays an important role in this adsorption. When polymers are confined, the new material morphology shows relatively less restricted molecular dynamics. In this case, sample production methods and nanopore topologies have little influence on molecular dynamics.

From this thesis, it can be seen that BDS shows promising potential to be used to study the molecular dynamics of confined monomers and polymers. Overall, this project lays a groundwork for the development of BDS as a Non-Destructive Testing (NDT) tool to characterise adhesive bonds.

This page is intentionally left blank.

Table of contents

List of figures

List of tables

This page is intentionally left blank.

Chapter 1
Introduction

The molecular interactions of polymeric adhesives (or coatings) with metal oxide layers of anodised metal plates play a major role in governing their macroscopic adhesive properties. This thesis explores the analysis of such molecular interactions using dielectric analysis.

1.1. Coatings and adhesives for aerospace applications

One of the major challenges in the aircraft industry is to optimise the structure, leading to a low cost and lightweight product. For decades, adhesive bonding has been used as an important joining method in aircraft production that helps in achieving this [1], [2]. The introduction of adhesives as a joining method for structural components results in several important desirable outcomes such as lower structural weight, lower cost, fatigue resistance [3], higher durability, improved aerodynamics [4] etc. Some of the important advantages and disadvantages of adhesive bonds are given in Table 1-1. Further, the aerospace industry also relies extensively on functional coatings for purposes such as corrosion protection [5], thermal barrier [6], drag reduction [7], etc.

Table 1-1 Advantages and disadvantages of adhesive bonds.
This table is extracted from the works of Pethrick et al. [4]

Advantages	Disadvantages
Good fatigue strength	Surface cleaning must be proper
Damps vibration and absorbs shock	Needs curing time, temperature, pressure
Hinders corrosion	Needs support structures
Join dissimilar materials	Needs special training
Act as sealant	Inspection is difficult

Coatings and adhesives adhere to the substrates due to the chemical bonding and/or physical interlocking. For coatings and adhesives to applied to a metal substrate, surface treatment is performed. Surface treatment of substrates plays a major role in the adhesion strength of such layers [5]. They remove contaminants and improves surface wettability and roughness [1][6][7]. Surface treatments are done by mechanical, chemical, electrochemical, dry surface treatment, and other methods [3]. Anodisation is an effective surface treatment method for metals since it creates nanometre-sized pores on the metal surface with a layer of metal oxide across the processed surface, as shown in Figure 1-1. This leads to improved wettability of the surface, and better load bearing capability of the adhesive joint compared to non-anodised substrates. The chemical bonds between the polymers and the walls of these nanopores contribute towards the adhesive strength. Furthermore, adhesive infiltration into nanopores of anodised layers allows locking of adhesive nano-pillars into nanopores to

provide improved the load bearing capabilities, similar to a zipper. A full infiltration of adhesives into the nanopores provides better adhesion due to a maximum possible contact area [8].

In general, the strength (contribution of chemical bonding) of an adhesive bond depends on both cohesive forces (between the molecules of the adhesive and/or adherend) and adhesive forces (between the adhesive and the adherend). While cohesive forces are an inherent property of the adhesive material, the adhesive forces can be altered by surface modifications. The adhesive forces between the adhesive and the adherend are due to the Van der Waal's forces, H-bonds, covalent bonds, ionic bonds etc. [7][9].

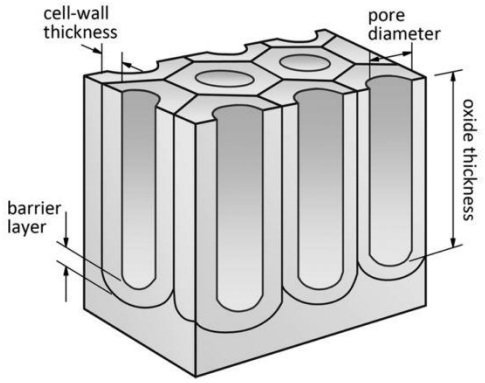

Figure 1-1 Isometric view of an anodised oxide layer of a metal.
This image is extracted from the works of Park et al. [5]

Failure in adhesive can be either due to either adhesive failure or cohesive failure [9][10]. In an adhesive joint between two anodised layers, several types of failures may occur, as shown in Figure 1-2. While cohesive failure is a material property, the adhesive failure depends on the interaction between the coating (or adhesive) with the substrates. For general adhesive applications, it is desirable that any failure that occurs is cohesive, as this is predictable from the material properties. Adhesive failures are highly undesirable as they can be due to a multitude of factors that lead to a poor adhesion between the adhesive and the substrate.

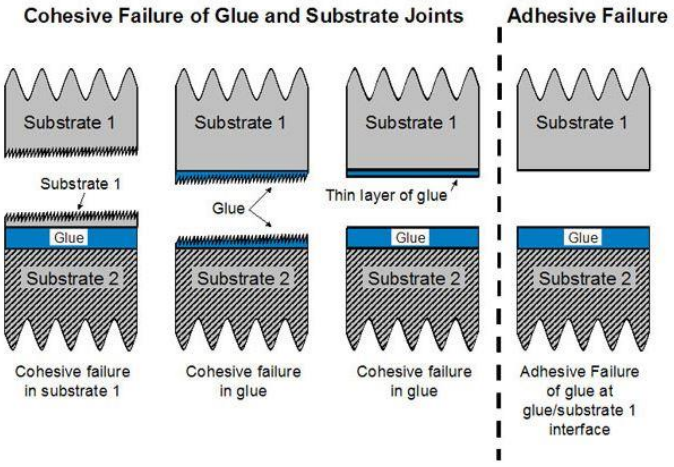

Figure 1-2 Failure modes in an adhesive bond.
This image is extracted from the works of Molitor et al. [11]

Prediction of failures requires robust characterisation methods. Traditionally, the characterisation of the mechanical properties of an adhesive bond or other functional coatings is done by destructive testing methods such peel tests and shear tests [3], [4], [9], [13]–[16]. However, in the field of aerospace engineering, it is preferred to test every single product in order to minimise the probability of failure. In order to analyse every product and bond, it is necessary to develop a non-destructive testing (NDT) method. While current NDT methods (such as ultrasonic scans) can provide information on macroscopic defects, there are no reliable methods to test the bonding properties such as shear strength, bond strength, bond quality, adhesive morphology at the interface, damage assessment etc. Current NDT methods cannot fully verify the integrity of a bond; they only show that the conditions necessary for a good bond have been met [9]. As reliable characterization methods still needed to be identified for industrial scale, adhesive bonds in aircraft are reinforced by rivets called *'chicken rivets'* [16]. These rivets tend to negate the advantages of an adhesive bond. A reliable characterisation of the adhesive bond could potentially lead to the development of methods to eliminate such secondary bonding agents entirely.

Figure 1-3 shows the schematics of the bond interface between an adherend and an adhesive [5]. Here, it can be seen that, at the interface between the adhesive and the adherend, the polymeric structure of the adhesive is different from that of the bulk. This phenomenon of difference in molecular arrangement of polymers can be exploited to characterise their molecular interaction with substrates by dielectric studies using Broadband Dielectric Spectroscopy (BDS). It will be shown later (Chapter 2) that dielectric analysis of a polymer is an important and powerful NDT tool to study the molecular dynamics of a polymeric adhesive. By analysing the molecular dynamics of these polymers, their interactions with substrates can be understood. This could potentially lead to the development of BDS as an NDT method to characterise adhesive bonds.

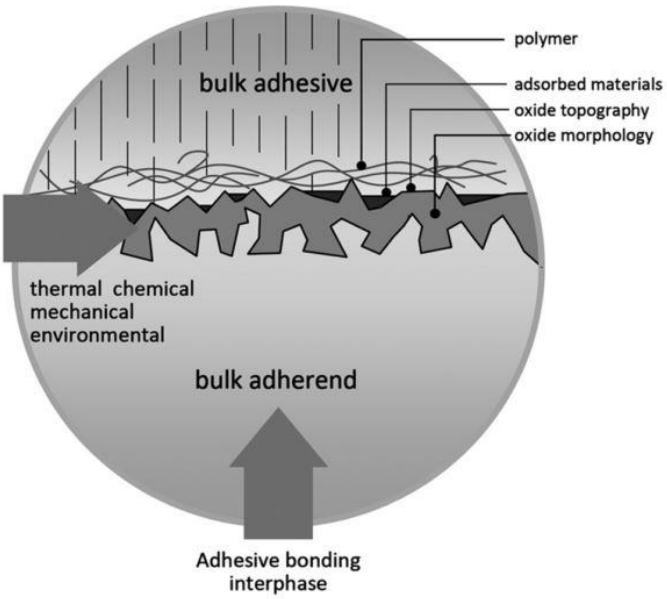

Figure 1-3 Schematic representation of the bond interface.
This image is extracted from the works of Sinmazçelik et al. [3]

1.2. Project goal and hypotheses

The goal of this thesis is to use BDS to understand the molecular dynamics of monomers and polymers that are confined within the reactive nanoporous anodised aerospace aluminium alloys, so that a method can be established for the use of BDS to assess the same. The motivation behind this goal is that the knowledge obtained from this project can be used in the future for the development of BDS to assess the adhesion bonds between polymeric adhesives and metal substrates.

When polymeric molecules are confined within the nanoporous regions, the polymer chains are expected to be rearranged inside the nanopores. This phenomenon is expected to change the local dynamics of the mono/polymers near the walls of nanopores. So, it is hypothesised that the '*Confinement of mono/polymers will introduce altered molecular dynamics in the sample, that could be identified through Broadband Dielectric Spectroscopy (BDS)*'.

Furthermore, the quantity of altered molecules/chains is expected to change with changing topology of the nanopores or area of contact between the mono/polymers and the walls of the nanopores. Hence it is hypothesised that the '*Change in pore topology or contact area between the mono/polymers and the walls of the nanopores will lead to change in the altered dynamics*'.

Finally, it is expected that all the samples with comparable polymers (adhesives) and substrates will show comparable changes in molecular dynamics. So, it is also hypothesised that the *'Data obtained from dielectric studies could be correlated to the strength of the adhesion between the polymeric adhesive and the metal substrates'*.

Chapter 2
State-of-the-art: A literature study

In coatings and adhesives, the polymers are under the confinement of the nanopores formed due to anodisation. These surfaces react with polymers to form primary and secondary bonds. Thus it is necessary to understand how BDS can be used to study polymers in contact with reactive and confining substrates. This chapter provides information on the state-of-the-art in the understanding of the behaviour of polymers under confinement, and under the presence of a reactive surface. The above-mentioned cases are discussed with respect to usage of BDS as a characterisation tool. The aim of this chapter is to provide sufficient background for designing the experiments necessary to validate the hypotheses provided in Section 1.2.

2.1. Molecular dynamics of confined polymers

Molecular dynamics of polymers change dramatically when its chains are under confinement, as the segmental dynamics of polymers are affected [17]. Several studies have been conducted to analyse this phenomenon. Samples based on PVDF [17], PVDF-TrFE [10], [11], PMMA [20] and PS-b-P4VP [9], [13] on porous or non-porous anodised aluminium oxide (AAO) templates [17], [21]–[24] have been produced and studied. In order to analyse the properties of confined polymers, and not that of the bulk, electrodes are used to separate them [19], [22], [23], [25], as shown in Figure 2-1.

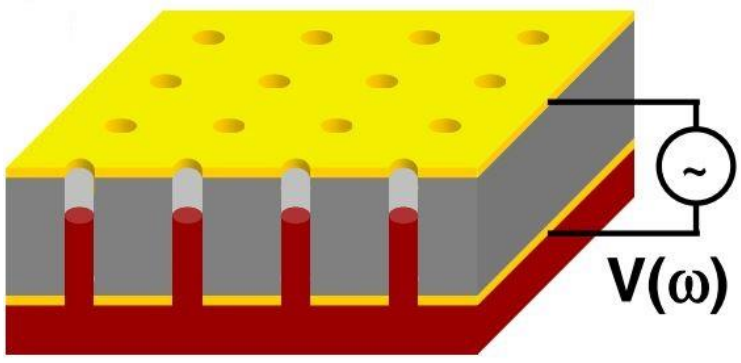

Figure 2-1 Gold electrodes used to study the capillary flow of polymers into nanopores. *This image is extracted from the works of Serghei et al.* [22]

When polymer flows into a nanopore, a new polymer morphology in the generated, as seen by Serghei at al. [25]. Inside the nanopores, the polymer chains interact with the surface of the wall of the nanopores. The interactions, in the case of a non-reacting polymer, are predominantly due to H-bonding or van der Waal's forces. The interfacial effects result in adsorption of polymeric chains to the walls of the pore [26]. These interfacial effects are governed by polarity, adsorption energies, surface coverage etc. [27]. For different polymer-

nanopore combinations, the interfacial effects also change. These interfacial effects cause the polymeric chains to be adsorbed to the surface of the nanopores. The thickness of the such an adsorbed interfacial layer depends on the strength of the molecular interactions [28]. A schematic of such a phenomenon is shown in Figure 2-2.

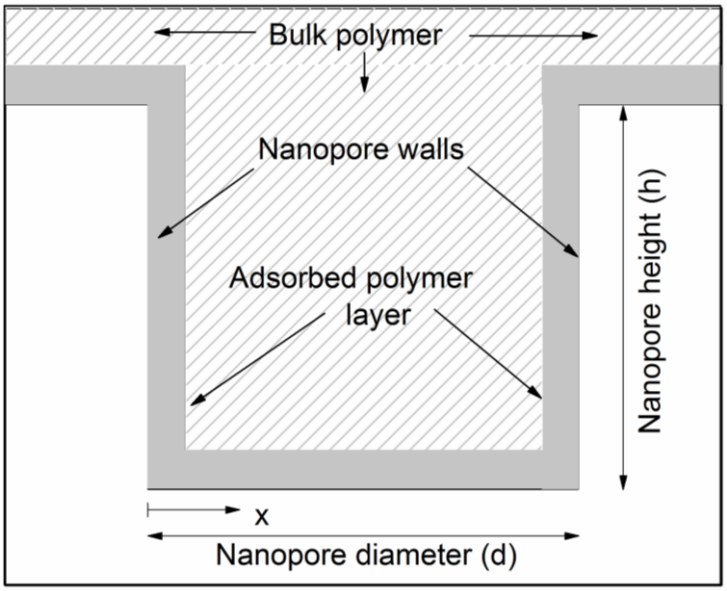

Figure 2-2 Expected schematic of formation of adsorbed interfacial polymer layer close to walls of nanopores

When the polymeric chains are adsorbed to the surface of the nanopores, the local density of the polymer increases with respect to that of the bulk polymer. The local motions of adsorbed chains are restricted more than that of a bulk polymer. This restriction to the motion of molecular chains causes the increase in viscosity, and so prevents the polymer chains to move around and orient themselves.

The higher density of arrangement and the effect of interfacial interactions results in the interfacial layer having a higher glass transition temperature (Tg) than that of the bulk. Thus, it can be considered that the strength of the interfacial interaction governs the changes in Tg of polymer close to the walls of nanopore [29]. Tg depends on the energy required for the motion of chains of the polymer. Due to interactions of the chains closer to the walls, higher energy would be required by the polymer chains to overcome these restrictions and move. Thus, close to walls, the polymer shown higher Tg than that of the bulk. The difference between Tgs (ΔTg) of different regions also remains a function of pore topology. Depending on processing conditions, a polymeric sample with multiple Tgs can be obtained as shown in Figure 2-3 [26]. In certain cases, such a confinement can also lead to lesser Tg due to *'hindered glass transition'*, where correlation length of the glass transition is hindered by pore topology [30]–[32]. These two phenomena are the 'adsorption' and 'confinement' effects respectively i.e. The molecular dynamics of polymers under confinement slows down (increase in Tg) due to adsorption effects and accelerates (decrease in Tg) due to confinement effects [33][34]. A balance of these two phenomena governs the overall molecular dynamics of a polymeric system. Such a balance is governed by factors like pore topology, substrate chemistry, polymer chemistry, and polymer size. For example, as confinement increases (i.e. as $d_{pore}/2R_g$ decreases, where R_g - Radius of gyration of the confined polymer chain), polymer diffusivity into the pores decrease [35].

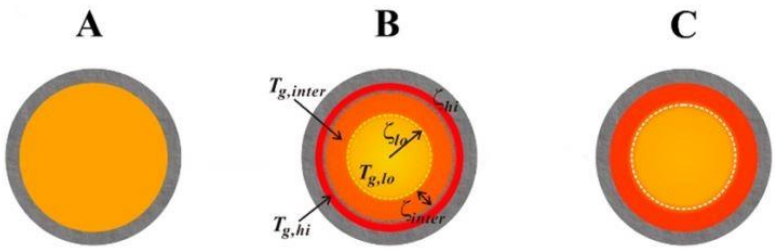

Figure 2-3 Polymers in nanopores, having one (A), three (B), and two (C) Tgs.
This image is extracted from the works of Serghei et al. [26]

This influence of interfacial effects also affects the crystallinity of the polymers. Crystallinity depends on molecular chains orienting in a repetitive fashion to form lamellae and spherulites [36]. As mobility is hindered, the crystallinity of the polymer is inhibited in the case of semi-crystalline polymers, as shown in Figure 2-4 [17], [23]. Confinement of polymers in nanopores also introduces new crystal polymorphs [37][38]. As the distance from the wall increases, the force of adsorption acting on polymer chains decrease. At a particular distance from the wall, the adsorption forces become negligible and the polymer chain arrangement becomes similar to that of the bulk polymer.

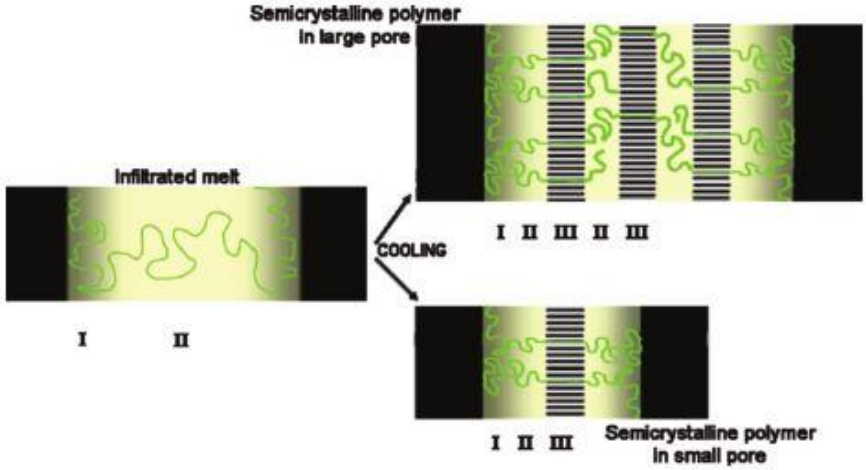

Figure 2-4 Changes in crystallinity with respect to the change in pore size.
This image is extracted from the works of Martín et al. [17]

Polymerisation under the confinement of a nanopore shows a different dynamics than polymerisation in a bulk scenario. Due to interfacial interactions restricting the molecular motion near the walls, the polymerisation is slower near the wall [39]. Overall, the average molecular weight of a polymer inside a nanopore and its PDI are lower than that of the bulk polymer [37][40][41][42]. In the nanopores, only a small number of monomers could react with each other due to geometrical restrictions. Thus, the average molecular weight of the polymer remains small. Similarly, as all monomers are subjected to similar uniform conditions in the nanopores, they statistically tend to form chains of comparable lengths. Thus, the PDI also remains small.

In general, it can be understood that confinement of polymers (or monomers) causes the formation of new morphologies in the samples. This new morphology may be a factor of adsorption, crystallinity, polymerisation etc. These changes in molecular dynamics can be

investigated using BDS. Changes in molecular dynamics reflect as a change in the dielectric response of the sample system to an external electric stimulus. Different relaxation responses are seen at different combinations of frequencies and temperatures [21]. The local molecular dynamics governs these relaxations. From the response spectrum obtained from the BDS experiment, different molecular dynamics can be identified and studied.

Overall, it is seen that the confinement of polymers introduces new relaxations in the system that are not seen in bulk polymers [43]. Due to restriction to molecular motion, the dielectric relaxation lower frequencies of dielectric stimulations [44]. Due to high interfacial effects due to confinement, the molecular motions of molecules are restricted. This causes an increase in relaxation time (slowing down of dynamics) [27],[32],[40],[45]. The interfacial forces do not allow the molecules to respond to dielectric excitation at high frequencies. This phenomenon is seen in BDS as broadening of peaks of normalised dielectric loss curves ($\varepsilon''/\ \varepsilon''_{max}$) [29],[39],[46]. The slowing down of dynamics of polymer chains in the adsorbed region causes the dielectric storage modulus of the sample to start decreasing at lower frequencies. This ultimately results in broadening of the dielectric loss peak towards lower frequency regime. From the relaxation rate, it can be seen that the polymer obeys either Arrhenius type temperature dependence or Vogel-Fulcher-Tammann law based temperature dependence as a function of molecule size and weight, size of nanopore etc [33].

While literature survey sheds light on molecular dynamics of confined polymers and the use of BDS to study them, there is limited information available on the assessment of molecular dynamics of monomers. Usage of BDS to study the interaction between reactive anodised metal oxide layers with polymers (or monomers) is also not explored in detail. However, based on the state-of-the-art, it is expected that confinement of monomers (or polymers) in the nanopores of the anodised metal oxide layers will lead to similar confinement effects as seen in other similar cases in the literature. By the means of assessing the dielectric response of different samples using empirical relations such as Havriliak Negami (HN) fits, Arrhenius fits, and Vogel-Fulcher-Tammann (VFT) fits, the molecular dynamics of samples can be analysed. These methods provide information on the relaxation time, relaxation frequency, temperature dependence of relaxations, etc. Using this information, the validity of the proposed hypotheses can be checked.

2.2. Effect of reactive surfaces on polymers

When polymers are exposed to reactive substrates (as in case of adhesives or coatings), the polymer chains form covalent, ionic or other primary bonds with the substrate. Due to these bonds, the polymer chains will have higher restrictive forces acting on them. Polymers react with the surface because each molecule provides many binding sites for interaction between a polymer and a substrate. For example, Pyridine in the neutral form binds strongly to metals via the formation of the covalent bond and interact with various non-metallic polar surfaces capable of undergoing hydrogen bonding [47]. Such interactions can, for example, be seen in PANI-ZnO, where there is a strong interaction on the surface of ZnO particles with the PANI molecular chains. It causes a decrease in dielectric constant [48]. Similarly, when an oxide is dispersed within a polymer, due to reactions, the molecular dynamics of polymer close to an oxide particle will be restricted. Thus, the dielectric response to BDS study will change similar to that explained in Section 2.1 [48], [49].

The dielectric response also depends on the type of bonds formed. For example, covalent bonding interfaces show a weak frequency dependence of dielectric properties, as shown in

Figure 2-5 [50]. This could be due to the fact that covalent bonds bind the polymer molecules to the surface and does not allow it to move unless a large external energy is supplied.

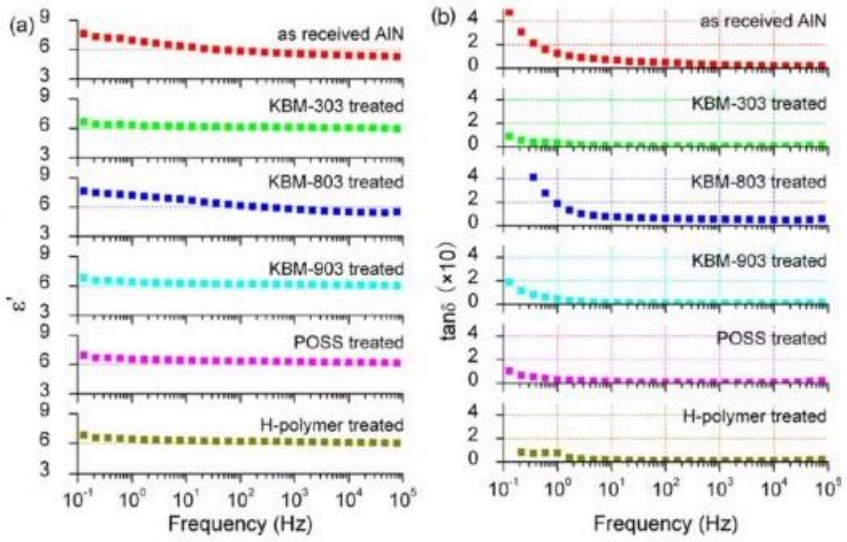

Figure 2-5 Frequency dependence of dielectric response between epoxy and Aluminium nitride particles for different surface treatments.
This image is extracted from the works of Huang et al. [50]

Unlike the explanation provided in Section 2.1, for a reactive substrate, more complex molecular morphologies are expected to be seen. Near the wall of the substrate, in addition to adsorbed layer, there also exists a reactive polymer layer. Due to higher bond energies between the substrate and the polymer, the dielectric response of these layers is expected to be different from that of the bulk. This phenomenon can potentially be used to assess the bonds using BDS as an NDT tool.

2.3. Chapter synopsis

1. Polymers (or monomers) get adsorbed to the inside walls of the nanopores when they are infiltrated into the nanoporous anodised metal oxide layers.
2. Confined polymers (or monomers) may have faster (improved) or slower (retarded) dynamics based on the domination of adsorption or confinement effects respectively.
3. Crystallisation and polymerisation are also affected by confinement. New molecular dynamics are formed in these cases too.
4. Dielectric studies by BDS can be used to study different molecular dynamics.
5. Quantification of dielectric data using HN, Arrhenius, and VFT fits can give information on the molecular dynamics of the polymer (or monomer).

This page is intentionally left blank.

Chapter 3
Methods and methodologies

In this chapter, information regarding the use of BDS as a characterisation tool, and the data processing techniques necessary to extract sufficient information (from dielectric spectroscopy data) on molecular dynamics are provided. The secondary characterisation techniques necessary for validation of BDS data are also listed. Furthermore, the activity flowchart of the project is also provided.

3.1. BDS as a technique

In this thesis, activities are predominantly done on exploring BDS as a characterisation tool. BDS is used to study the dielectric response of the molecules of a specimen to an oscillating electric field across a wide range of frequencies and temperatures. In polymers, the dipole segments in the polymer chains get excited by this field. Depending upon the local molecular dynamics, dielectric excitation of a molecule happens only at certain combinations of temperatures and frequencies. In order to fully analyse the entirety of molecular dynamics of the sample, the BDS study is conducted over a wide range of frequency. It must be understood that for a molecular chain whose motions are restricted, the dielectric response will be witnessed only at low frequencies and for a molecular chain whose motions are unrestricted, the dielectric response will be witnessed even at high frequencies. This can be considered analogous to spring-mass-damper systems having different natural frequencies.

When an electric field is applied, polarisation occurs. The polarisation may be of different types such as: electronic polarisation, atomic or ionic polarisation, dipolar or orientational polarisation etc. [51], [52]. When the field is removed, the atoms and molecules return to their original state. This process is called relaxation [52]. Typically, dielectric relaxation is considered to be only the relaxation with respect to atomic or ionic polarisation and dipolar or orientational polarisation, and it occurs from 10^2-10^{10} Hz, which falls within the domain of BDS. In polymers, the main relaxation processes are dipolar segmental and group relaxation. Among these, dielectric group relaxation can be related to local molecular motion. By studying the rate of change of the dielectric storage modulus, and the corresponding loss modulus, it is possible to study the bonds in a molecule. As BDS depends on molecular motion due to an external electric field, change in polymer structure will cause a change in its dielectric property [53].

3.1.1. Dielectric relaxation

Dielectric relaxation is a type of linear relaxation theory [54]. Dielectric relaxation has been attempted to be quantified by several theories, where the most widely used ones are by Debye, and Havriliak and Negami (HN). These theories quantify the data by fitting the peaks formed in a loss curve with empirical equations.

3.1.1.a. Debye relaxation

In Debye relaxation, it is considered that there exists only one relaxation time. Relaxation time (τ_D) can also be obtained from the complex dielectric function as,

$$\varepsilon^*_D(\omega) = \varepsilon_\infty + \frac{\Delta\varepsilon}{1+i\omega\tau_D} \qquad \text{Eq. 3-1}$$

When this equation is used to fit for the individual peaks in loss curves shown in Figure 3-1, Δε governs the area under the peak and τ_D governs the time-dependent location of the peak. According to Debye relaxation, the loss peaks are sharp and symmetric. While Debye equation was sufficient to describe the processes occurring in most fluid systems, it was not able to explain the processes occurring in more complex polymeric systems [55].

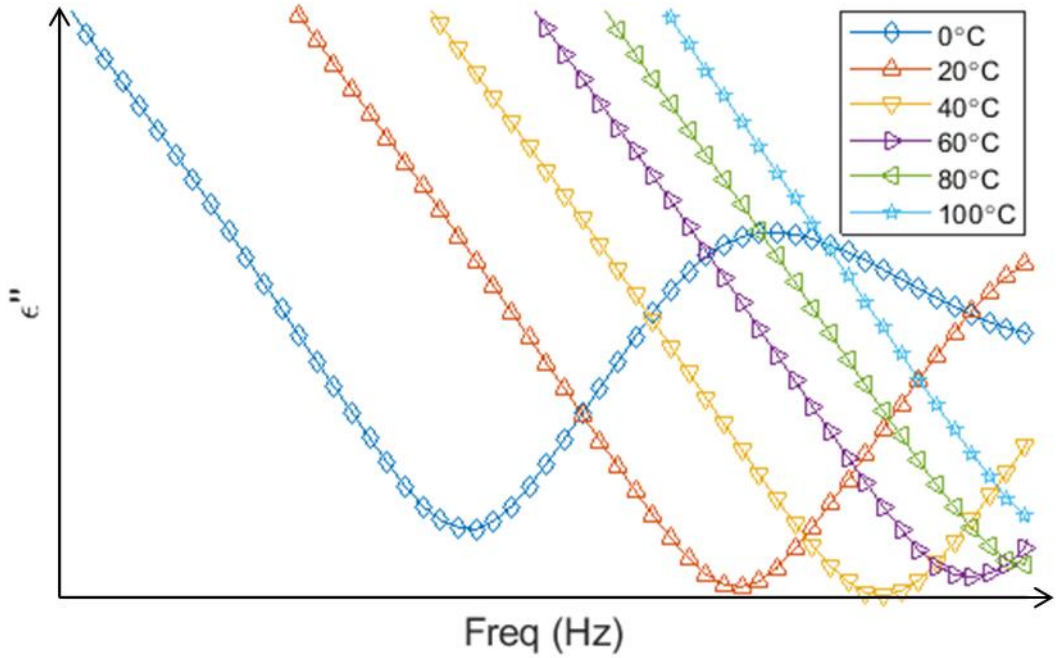

Figure 3-1 Example of dielectric loss curves of a sample at different temperatures

3.1.1.b. Non-Debye relaxation (Havriliak-Negami)

In non-Debye relaxations, the loss peaks are broad and asymmetrical [54]. In reality, most of the samples have this type of relaxation. It is widely accepted that there exists a wide range of relaxation times and activation energies. One of the most effective models for a non-Debye relaxation is given by Harvriliak and Negami [HN] [56],

$$\varepsilon^*_{HN}(\omega) = \varepsilon_\infty + \frac{\Delta\varepsilon}{(1+(i\omega\tau_{HN})^\alpha)^\beta} \qquad \text{Eq. 3-2}$$

where, α and β are the parameters that cause asymmetry. When this equation is used to fit for the individual peaks in loss curves shown in Figure 3-1, Δε governs the area under the peak, τ_{HN} governs the time-dependent location of the peak.

3.1.1.c. Contribution of electrode polarization

In certain conditions, when an external electric field is applied, the cations and anions in the sample tend to travel to the electrodes and form an electrical double layer as shown in Figure 3-2. This phenomenon is called electrode polarisation [57]. The influence of this phenomenon during the observation of BDS response tends to overshadow some of the information on molecular dynamics of the sample.

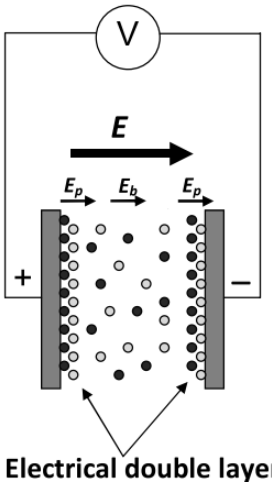

Figure 3-2 Formation of an electrical double layer due to external electric field. *This image is extracted from the works of Ben Ishai et al.* [57]

The electrical double layer can be modelled as a capacitor in series with the sample as its behaviour reflects that of a capacitor as seen in Figure 3-3. Similar to a capacitor, the electrode polarization (EP) acts as a function of frequency (f), as seen in Eq. 3-3.

$$EP\alpha\frac{1}{f} \qquad \text{Eq. 3-3}$$

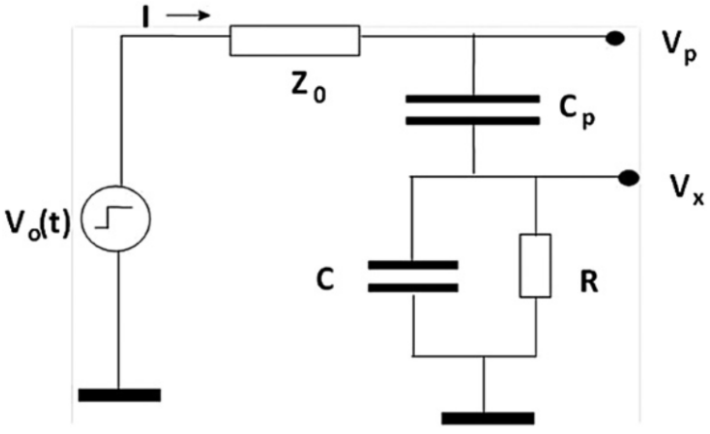

Figure 3-3 Modelling of an electrical double layer as a capacitor (C_p) in series with the sample (modelled by C and R). *This image is extracted from the works of Ben Ishai et al.* [57]

In a ε'' (loss modulus) vs. frequency graph of a sample on a log-log scale, electrode potential leads to the formation of a straight line in the low-frequency region with a fixed negative slope that is determined by the material property of the sample and the experiment

conditions. Such a phenomenon will appear as shown in the low-frequency region of the graph in Figure 3-1*. Here, it can be seen that the electrode polarisation at low-frequency region can overshadow other readings. Detailed analysis can further be done in order to consider these signals as noise and remove them in order to obtain detailed information about molecular dynamics of samples. The contribution of electrode polarisation to the dielectric relaxation is represented by,

$$\varepsilon^*_{EP}(\omega) = -i\left(\frac{\sigma_0}{\varepsilon_0\omega}\right)^n \qquad \text{Eq. 3-4}$$

Thus, the overall dielectric behaviour of the sample is given by,

$$\varepsilon^*(\omega) = -i\left(\frac{\sigma_0}{\varepsilon_0\omega}\right)^n + \sum_{k=1}^{n}\left(\varepsilon_{\infty k} + \frac{\Delta\varepsilon_k}{(1+(i\omega\tau_{HN\,k})^{\alpha_k})^{\beta_k}}\right) \qquad \text{Eq. 3-5}$$

where, k denotes the different superimposing HN curves.

3.1.2. Interpretation of BDS data

In broadband dielectric spectroscopy, the complex dielectric function ε*(ω) is measured for a frequency range of 10^{-6} Hz to 10^{12} Hz [54]. The data obtained from this experiment is complex permittivity ε*= ε'+ iε'', where ε' is storage modulus and ε'' is loss modulus.

While there are several ways to interpret BDS response graphs, this section concentrates on the interpretation of only the information relevant to this study. Of the several parameters observed in a BDS study, *ε'* and *ε''* can be used to obtain information regarding the molecular dynamics of a sample. A sample frequency domain BDS response is shown in Figure 3-4. Here, it can be seen at certain frequencies, there are drops in storage modulus (ε'). It indicates the existence of a certain type of bonds in the system. i.e. for certain bonds, the frequency of dielectric excitation might become too high and so, they stop getting excited. This drop in ε' can be considered analogous to the transmittance behaviour of a mass-spring-damper system around its natural frequency. So, each drop in ε' can be related to different mass-spring-damper systems (corresponding to different molecular dynamic systems) with their respective transmittance dropping to 0 at various critical frequencies.

* Interpretation of BDS graph can be found in Section 3.1.2

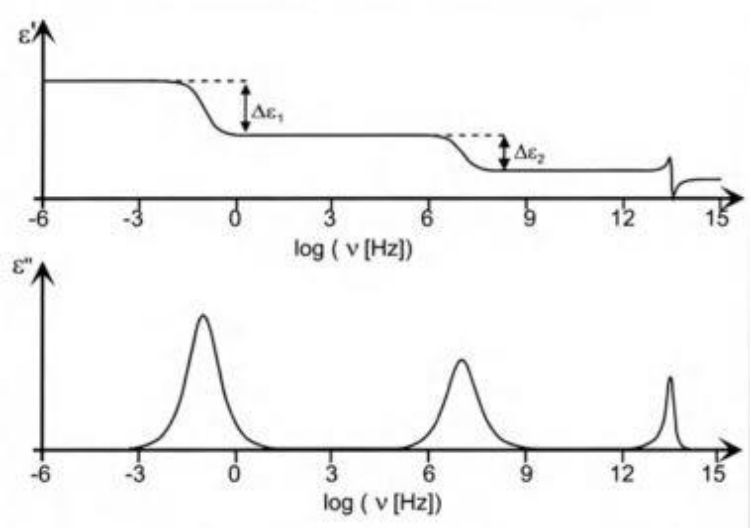

Figure 3-4 Sample frequency domain BDS response.
This image is extracted from the works of Kremer et al. [54]

When the sample under test undergoes any changes with respect to a control sample that does not undergo change, there is a possibility of observing the change in its molecular dynamics. For example, in a polymeric sample, polymerisation and increase in cross-links can increase the local inertia of the polymeric chains that leads to a decrease in the molecular dynamics of the sample (slowing down). This might cause a shift of loss peak towards the low-frequency region, as seen in Figure 3-5 (a). Similarly, increase in polymeric dynamics can occur due to increase in energy of the system, or breakage of bonds etc. In such cases, the peak of the loss modulus shifts to higher frequency region as the inertia of the sample tends to decrease, as seen in Figure 3-5 (b).

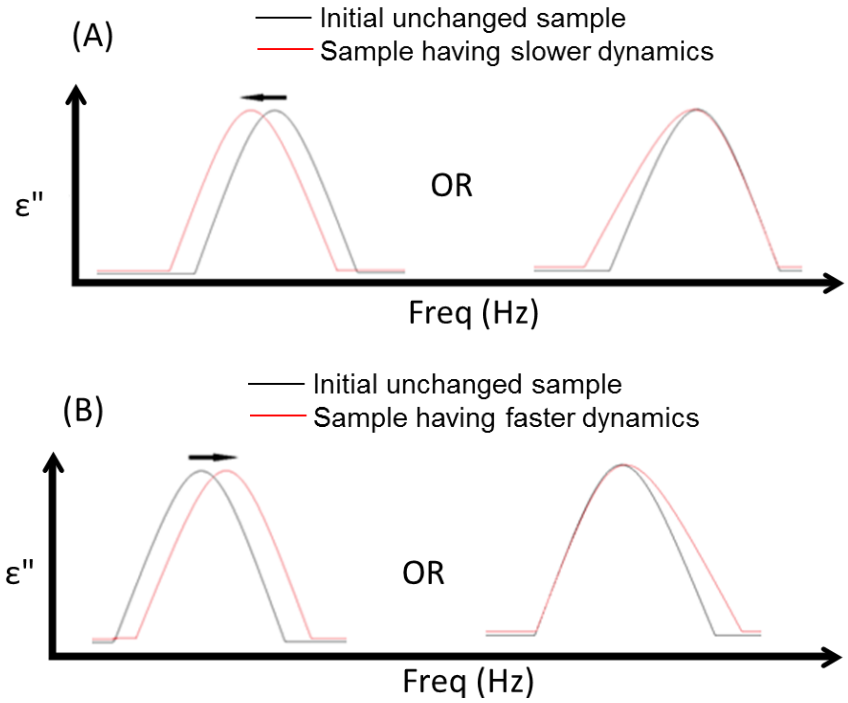

Figure 3-5 Expected BDS response of an initial undisturbed sample and a similar sample with (A) slower or (B) faster molecular dynamics

3.1.3. Data analysis

In order to obtain necessary information on molecular dynamics from the dielectric data, the observed data can be fitted with HN curves and VFT curves. Their significance is explained below. The upcoming chapters (Chapter 4 and Chapter 5) use these methods to extract necessary information from dielectric data that can be used to discuss regarding molecular dynamics.

3.1.3.a. Curve fitting using HN curves

In order to analyse the molecular dynamic behaviour of the sample, the loss peaks of dielectric samples can be fitted with HN curves that are described mathematically using Eq. 3-5. The loss peaks can be fitted with either a single HN curve or it can be de-convoluted and fitted with multiple HN curves. From this method, information such as relaxation time of a relaxation process can be obtained.

i. Single-HN curve fit

In this type of fitting, the entire loss peak of a sample is fitted with one HN curve. The use of this fitting is two-fold. Firstly, the entire sample is assumed to have only one type of relaxation that is represented by the single HN peak. So, the overall change in the dynamics of the sample is seen. Secondly, it allows us to observe that behaviour of the bulk sample. This observation is useful for deconvolution of loss peaks into bulk behaviour curve (HN1) and new behaviour curve (HN2) when the loss peaks are witted with more than one HN curves. A sample single HN fit is shown in Figure 3-6.

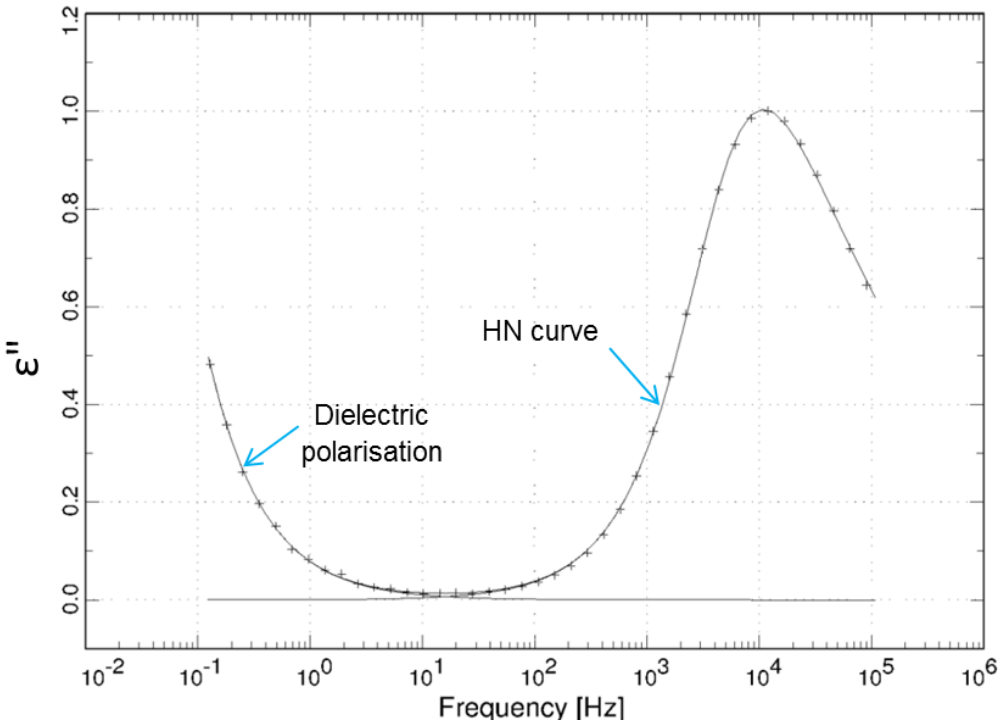

Figure 3-6 Sample Single-HN curve fitting for the loss peak of DGEBA monomer

ii. Double-HN curve fit

In order to understand and characterise changes in molecular dynamics separately, the loss peaks can be fitted with two (or more) HN peaks: one peak (HN1) simulating the bulk effects of the sample and another peak (HN2) simulating the rest of the sample. In one HN (HN1)

curve, the α and τ parameters can be fixed using Single-HN fit data of bulk monomer. The idea behind this process of selection of α and τ for HN1 is that it will represent the dielectric behaviour of the fraction of the DGEBA monomer that behaves as bulk by replicating the shape of the peak at low frequencies using variables obtained from Single-HN fitting of bulk DGEBA data. For the second HN (HN2) curve, α and β can be forced as value 1 so that a distinct second HN curve can be fitted. This fitting assumes that the HN2 peak behaves like a Debye peak and not an HN peak. The only reason to do this is to ensure that a fully formed HN2 peak is obtained within the frequency range under consideration. A sample Double-HN fit is shown in Figure 3-7. If required, the loss peaks can also be fitted with more than two HN peaks (depending on the situation).

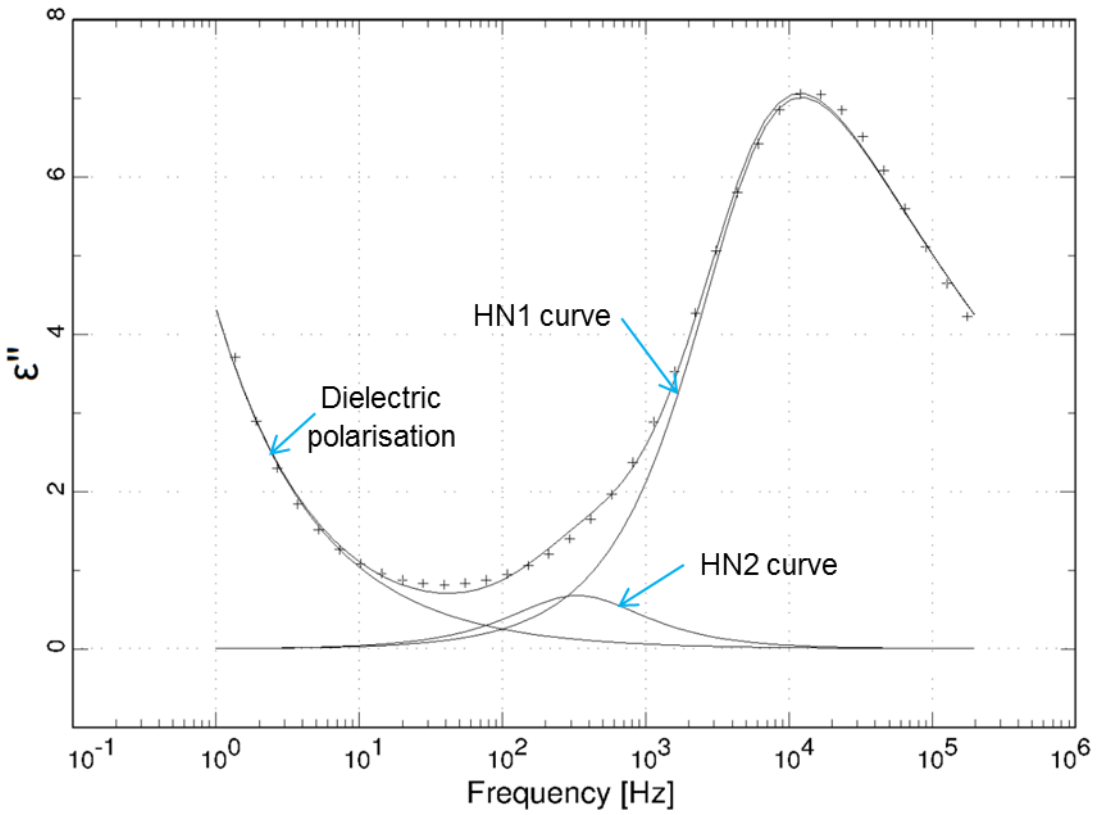

Figure 3-7 Sample Double-HN curve fitting for the loss peak of DGEBA monomer interacting with a metal substrate

3.1.3.b. Curve fitting using VFT curves

Based on the temperature dependence of the relaxation time of different samples, Vogel-Fulcher-Tammann (VFT) law can be used to identify the behaviour of the sample. For this method, the necessary relaxation times are extracted by fitting the loss peaks with Double-HN curves. At times, Arrhenius fits may also be used. VFT equation that governs the behaviour of the sample is given as,

$$\tau(T) = \tau_0 \exp\left(\frac{E_a}{k_B(T - T_V)}\right) \quad \text{Eq. 3-6}$$

where, E_a is the activation energy of a particular relaxation process, k_B is the Boltzmann constant and T_V is the Vogel temperature which is defined as the temperature below which a

particular dynamics completely ceases to exist. Tv is often considered as the ideal gas transition temperature, and is generally considered to be 40-70 K lesser than the practical glass transition temperature [54][58]. In some cases, glass transition temperature is considered as the temperature when the Arrhenius for $\tau_{max}(T)$ crosses 100 s [53][59]. Since both the cases are scientifically acceptable, both of them are considered in this thesis.

3.2. Supporting characterisation techniques

While this thesis focuses on the use of BDS as an NDT tool, other secondary tests must also be done in order to validate its data. Such tests used in this thesis (listed below) are commonly used characterisation techniques; and so, detailed descriptions and development of these methods are not provided.

3.2.1. Fourier transform infrared spectroscopy (FTIR)

FTIR allows users to closely follow the chemical reaction taking place in a sample. This technique is highly useful to ensure that the sample chemistry remains under controlled changes. Within the scope of this project, FTIR is used to eliminate (or identify) any variables arising due to changes in sample chemistry. The equipment used for this purpose is PerkinElmer Spectrum 100 FT-IR Spectrometer.

3.2.2. Differential scanning calorimetry (DSC)

DSC is a thermodynamic technique that measures the heat change in a sample as a response to change in temperature, with respect to a reference. This method allows the user to closely follow the phase transitions in a sample. Within the scope of this project, this technique is useful in identifying transition temperatures in a sample. The equipment used for this purpose is PerkinElmer DSC 8000 Differential Scanning Calorimeter.

3.2.3. Scanning electron microscopy (SEM)

This type of microscopy allows the user to observe the samples visually, on a nanometre scale. Within the scope of this project, SEM is useful for characterisation of the substrate topography and polymer infiltration into the nanopores of the substrates. The equipment used for this purpose is JEOL JSM-7500F Field Emission Scanning Electron Microscope. In these experiments, the samples are first sputtered with Gold nanoparticles so that charge accumulation is prevented while SEM is done.

3.2.4. Bell peel test

Bell peel test (or roller peel test) is a common destructive technique used in identifying the adhesive strength between two substrates. In this project, the adhesive strength of polymeric samples is tested using this method. These tests (and preparation of required samples) were done at Fokker Aerostructures B.V. (Papendrecht, The Netherlands).

3.3. Thesis methodology

In order to validate the proposed hypotheses (Section 1.2), it was necessary to take a structured approach. Using the information on molecular dynamics of the systems obtained through curve fitting (HN, VFT, Arrhenius) of data obtained from the dielectric analysis (BDS), and supporting characterisation techniques (SEM, FTIR, DSC), the validity of the hypotheses can be tested. The flowchart provided in Figure 3-8 provides the methodology that was used for this purpose.

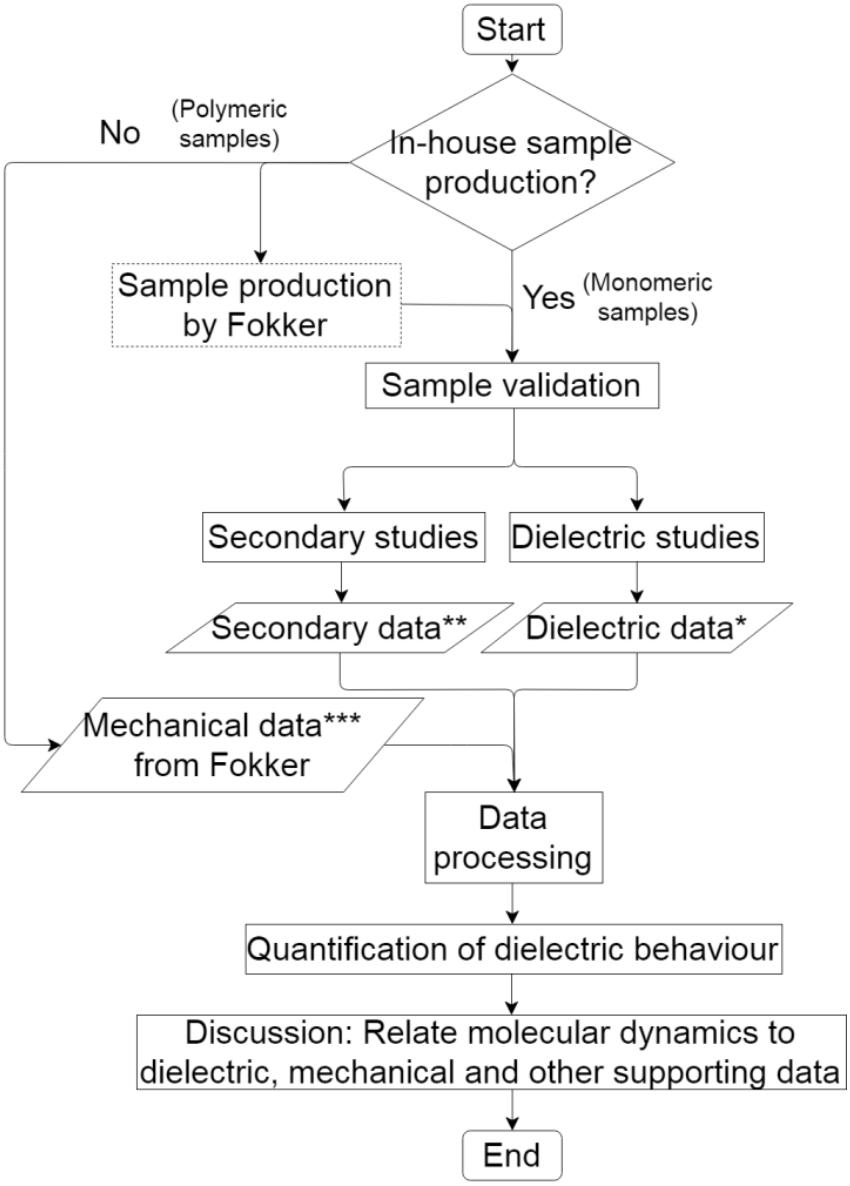

Figure 3-8 Flowchart of the methodology used in this project

*Dielectric data: Data from BDS.
**Secondary data: Data from SEM, DSC, and FTIR.
***Mechanical data: Data from Bell peel test.

Here, it must be noted that the polymeric samples, and mechanical data of polymeric samples were obtained from Fokker Aerostructures B.V. Further information on the contribution of Fokker is shown later, in Chapter 5.

This page is intentionally left blank.

Chapter 4
DGEBA monomers confined within nanoporous oxides of anodised aerospace aluminium alloys

The first step in a structured approach to the investigation of molecular dynamics of polymer under confinement would be to understand how the monomers behave under similar conditions. In this chapter, information is provided on the selection of materials for testing, sample production, production validation methods, dielectric tests and finally, the analysis and discussion of dielectric data to understand the molecular dynamics of monomers under confinement.

4.1. Materials

In order to perform experiments to validate the hypotheses that monomers under confinement have altered molecular dynamics (Section 1.2), a monomer and a nanoporous substrate were selected. Diglycidyl ether of bisphenol A (DGEBA), procured from Sigma Aldrich, was selected as a monomer since it is one of the most commonly used epoxy-terminated monomer used in adhesives [10], [60]. The molecular structure of DGEBA monomer is given in Figure 4-1.

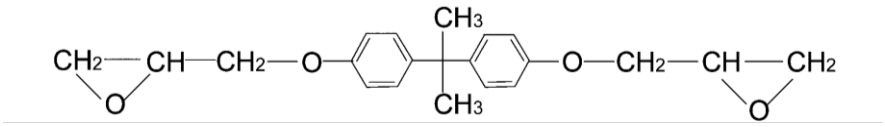

Figure 4-1 DGEBA molecule

Anodised aerospace aluminium alloy plates were selected as the substrate due to the presence of nanopores. In order to study the effect of nanopore topography on molecular dynamics of monomers, different types of anodised plates were selected, as specified in Table 4-1. Here, Bare Al-2024-T3 alloy plates are anodised using Phosphoric Sulphuric Acid (PSA), and have a nanoporous oxide layer with a spongy texture and three-dimensional pore network; they are referred to as N-series (for Network) plates. Similarly, Clad Al-7075-T6 alloy plates anodised using PSA, and having highly ordered monodirectional nanopores; they are referred to as M-series (for Monodirectional) plates. The different nanopores topologies that inspired such a nomenclature can be seen in Figure 4-2. In this report, different plates will be referred to using different sample codes as shown in the example below:

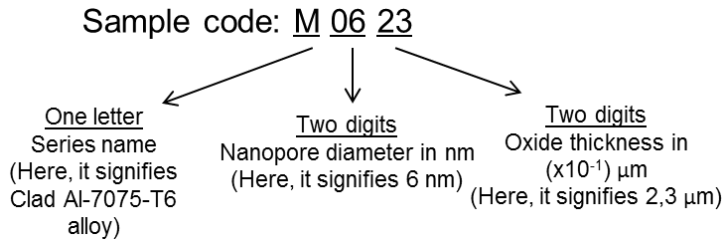

Table 4-1 Specification of nanoporous substrates

S.No.	Alloy	Metal plate series	Nanopore diameter (nm)	Oxide layer thickness (µm)	Substrate code
1	Bare Al-2024-T3	N	10	1,5	N1015
2			10	3,0	N1030
3			15	1,2	N1512
4			40	1,1	N4011
5	Clad Al-7075-T6	M	6	2,3	M0623
6			30	1,2	M3012
7			7	5,6	M0756
8			25	1,5	M2515

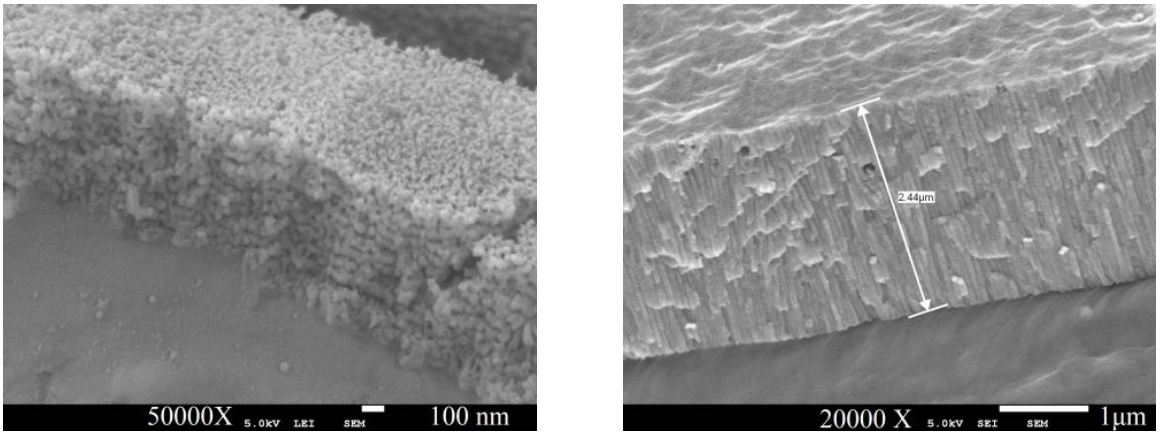

(a) (b)

Figure 4-2 Topology of oxide layers on a) N-series, and b) M-series metal plates

4.2. Comparison methodology

From the descriptions of the porous substrates, it can be seen that there are many variables such as the type of pores, pore diameter, and pore depth that come into play. However, in order to provide a common ground for comparison of different substrates, non-dimensional parameters, CSA (contact surface area) and TF (topology factor), are developed for each substrate. Their descriptions and the motivation behind their selection are given below.

The adsorption of the monomer chains is expected to happen on the surface of the walls of the nanopores. So, it is expected that this is a surface phenomenon. In order to understand the effect of the change in surface area on the dielectric analysis, the surface area of these nanoporous substrates was calculated. For this purpose, these nanopores were mathematically modelled as one dimensional (mono-directional) and three dimensional (network) pores for M-series and N-series plates respectively. A simple model of these approximations can be seen in Figure 4-3. The approximations are made with the assumption that all the pores are perfectly straight and one-directional. It must be noted that these approximations do not reflect the physical conditions perfectly, but are used for the approximate representation of the surface area in different metal plates. In the approximations for M-series plates, all the nanopores of a particular plate are assumed to have similar pore sizes and pore height equal to the oxide layer height. In the approximations

for N-series plates, all the nanopores on the surface of a particular plate are assumed to have similar pore sizes and pore height equal to the oxide layer height, while the nanopores on the cross-section of oxide layers vary from that of the surface, as seen in Table 4-2.

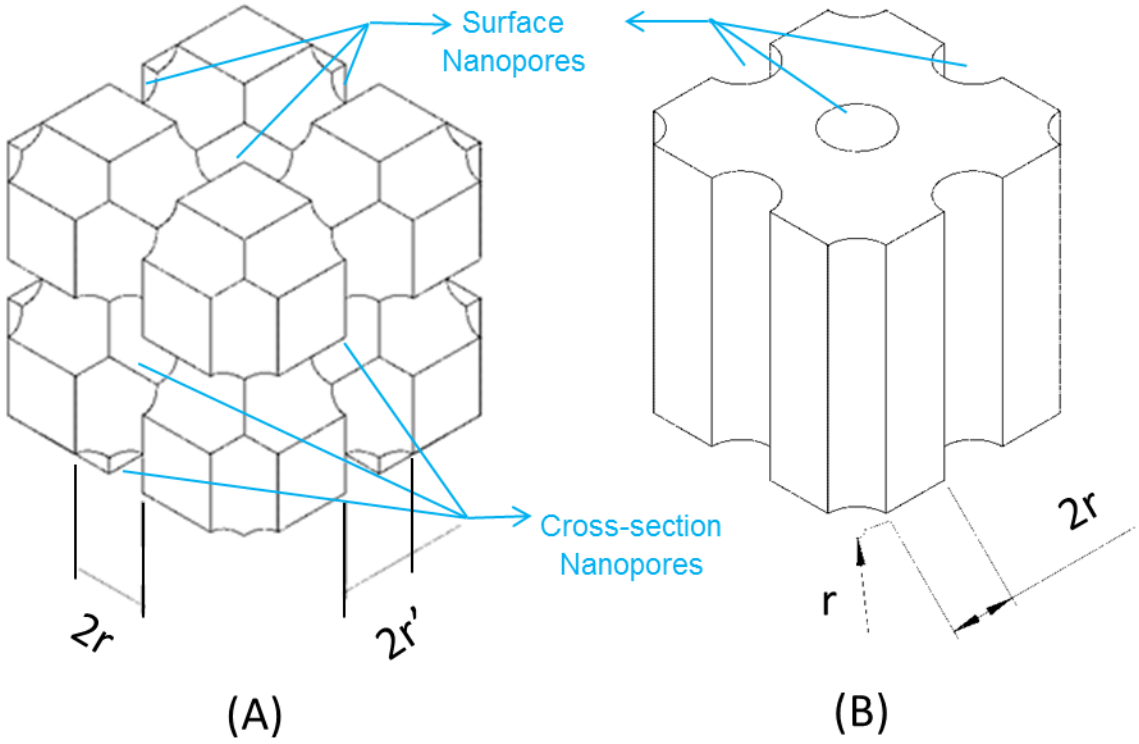

Figure 4-3 Approximate model for (A) N-series nanopores and (B) M-series nanopores in oxide layers of anodised metal

Table 4-2 Specification of some 3D network nanopore substrates

Series	Surface nanopore diameter (nm)	Oxide layer height (µm)	Cross-section nanopore diameter (nm)
N	20	0,5	25
	50	1,5	38
	8	1,1	29
	30	0,7	29
	35	1,0	28

Based on these models, the maximum possible contact surface area (CSA) between the monomers and the walls of the nanopores can be calculated through equations Eq. 7 and Eq. 8 for M-series and N-series substrates respectively. CSA per unit square centimetre shadow area of the metal plate is calculated for different metals and is provided in Table 4-3. If a mono/polymer fully infiltrates the nanopores, then it would be possible to establish a relationship between the CSA and the restriction in molecular dynamics. CSA also allows us to assess how the substrate surface area plays a role in the molecular dynamics of the samples.

$$CSA = x^2\left[1+\frac{\pi}{8r}(h-2r)\right] \quad \text{Eq. 7}$$

Where, x – Length of one side of the shadow area of a square metal plate
r – Radius of the nanopores
h – Height of the nanopore = Height of the oxide layer

$$CSA = x^2\left[1-\frac{\pi}{16}+\frac{\pi h}{8r}+\frac{\pi h}{4r'}\right] \quad \text{Eq. 8}$$

Where, x – Length of one side of the shadow area of a square metal plate
r – Radius of the surface nanopores
r' – Radius of nanopores on the cross-section of the oxide layer
~15 nm (approximated from Table 4-2)
h – Height of the nanopore = Height of the oxide layer

Furthermore, in order to see if the geometry of the pores plays a role, a non-dimensional geometry parameter called 'Topology factor (TF)' was defined. Topology factor was defined as shown in Eq. 9, and their values are provided in Table 4-3. Based on the definition of TF, only series-2 plates can have TF, as series-1 plates have a complex oxide structure with network nanopores. TF also allows us to assess how the pore topology plays a role in the molecular dynamics of the samples.

$$TF = \frac{PD}{PH} \quad \text{Eq. 9}$$

Where, PD – Pore diameter (nm)
PH – Pore height (μm)

Table 4-3 CSA and TF for different metal plates used as substrates for samples

Substrate code	CSA (cm^2/cm^2)	TF (10^{-3})
N1015	193	-
N1030	390	-
N1512	128	-
N4011	81	-
M0623	307	3
M2515	47	17
M0756	622	1
M3012	30	26

Finally, in order to observe the dielectric behaviour of bulk DGEBA, a Teflon cell was used as it is a standard used for measuring the dielectric behaviour of liquids. The CSA for this particular case is approximated to be 1.

4.3. Sample preparation

In order to understand the change in molecular dynamics due to adsorption different samples with DGEBA monomers fully infiltrating the nanopores (on the metal surface) were produced. The steps followed in this production process are,

Step 1 - The surface of the metal plate was cleaned using ethanol
Step 2 - The metal plate was placed under a vacuum to remove air from the nanopores
Step 3 - DGEBA (~3 ml) was added on the surface of the metal plate under vacuum
Step 4 - The metal plate with DGEBA is then removed from vacuum, placed in an oven, heated to 80°C and held at this temperature for 20 hours. This step is aimed at decreasing the viscosity of the DGEBA so that it could flow into the nanopores that are now under vacuum
Step 5 - The sample was removed from the oven and DGEBA on the surface was spread evenly into a thin layer using a scalpel

The schematics of the production process with expected conditions of the sample in the different processing steps are shown in Figure 4-4. Here, it must be noted that optimisation of process to obtain ideal infiltration conditions has not been performed.

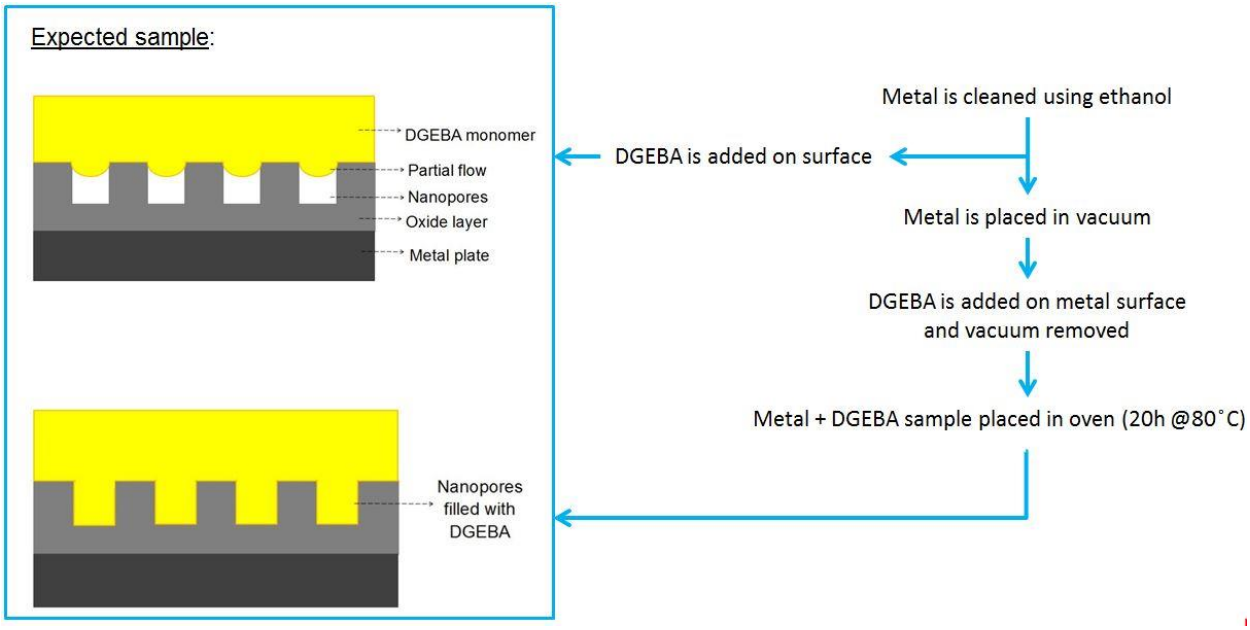

Figure 4-4 Schematic of the sample production process

In order to validate the production method, the cross sections of the samples were observed through SEM. It can be seen from Figure 4-5 that the infiltration of monomers into the nanopores is visually verified. It is evident from the images that the production method results in the production of samples with DGEBA monomers fully infiltrating the nanopores on the substrates.

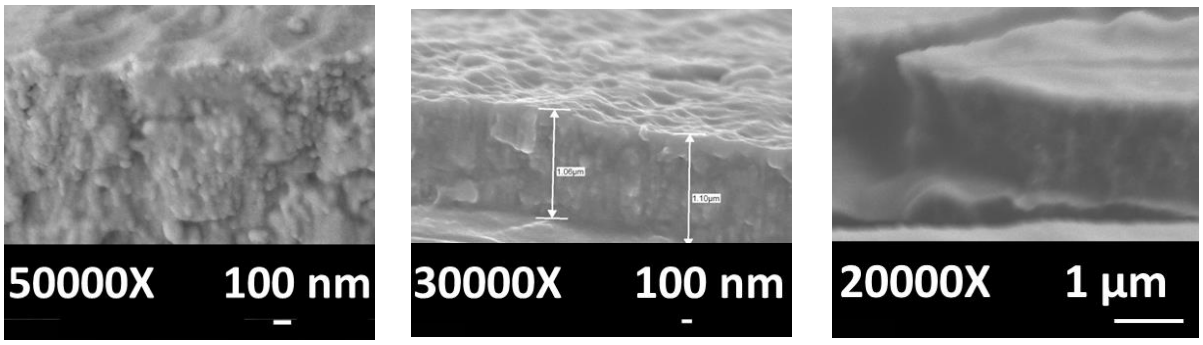

(a) (b) (c)

Figure 4-5 Cross-sectional view of full infiltration of DGEBA into nanopores of oxide layers of a) M0756, b) M3012, and c) N1015

In order to observe any chemical changes in DGEBA monomer due to the processing technique, the samples were also tested using FTIR from 4000 cm^{-1} to 600 cm^{-1}. From the transmittance graph normalised from 0 to 100 (as seen in Figure 4-6) of the pristine DGEBA and processed DGEBA, it can be seen that there are no changes in the transmittance for the peaks corresponding to cyclic C-O-C bonds of oxirane rings (1280-1240 cm^{-1}) or linear C-O-C bonds (1240-1070 cm^{-1}). This is an indicator that epoxy rings have not opened due to this process and so, (homo)polymerisation has not happened during the sample manufacturing process. This signifies that any changes in molecular dynamics that will be observed during dielectric studies will be due to the interaction (and subsequent adsorption) of monomers with the nanopore walls, and not due to any chemical changes in DGEBA.

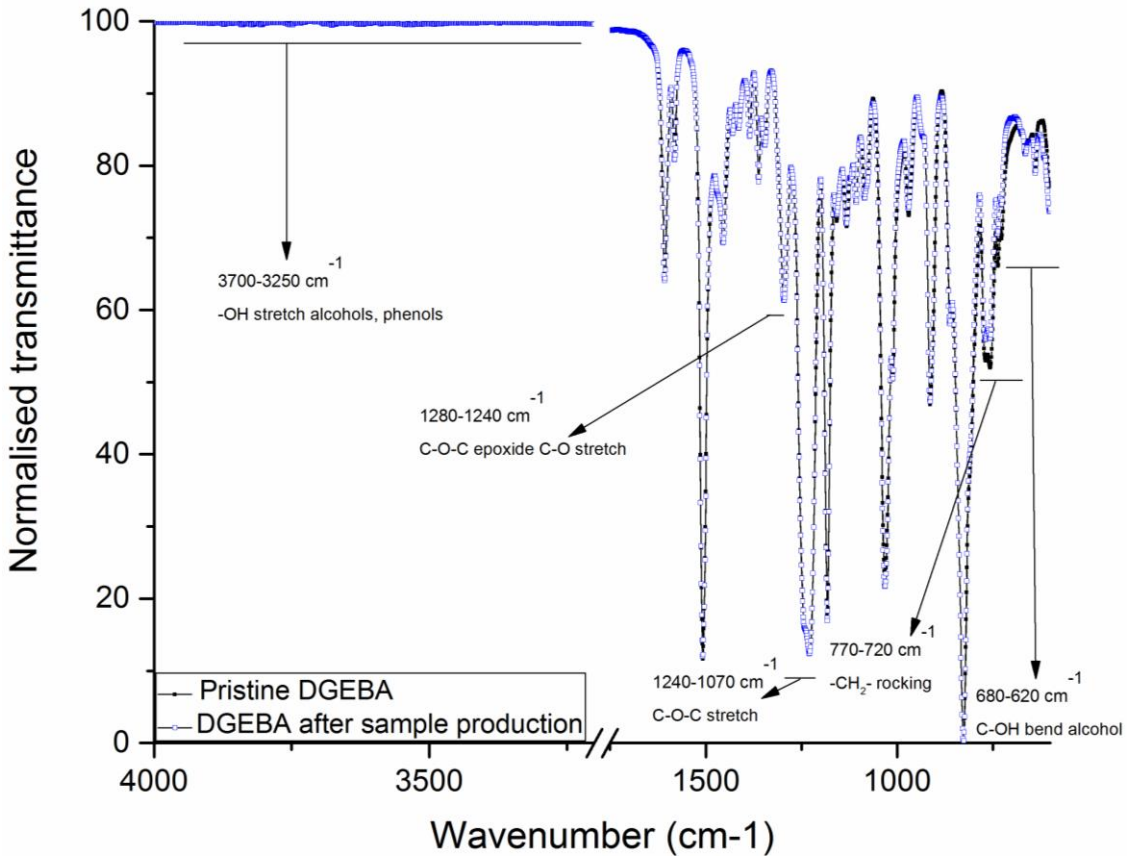

Figure 4-6 FTIR transmission spectrum of pristine and processed DGEBA

4.4. Dielectric analysis

The metal plates with a thin layer of DGEBA that were obtained from the production process explained in Section 4.3, were used as samples for dielectric analysis. The setup used for this dielectric analysis was Novocontrol ALPHA-A dielectric analyser that was coupled with a Novocontrol Quatro cryogenic system for temperature control, and a computer that serves as an experiment control panel. This setup can be seen in Figure 4-7.

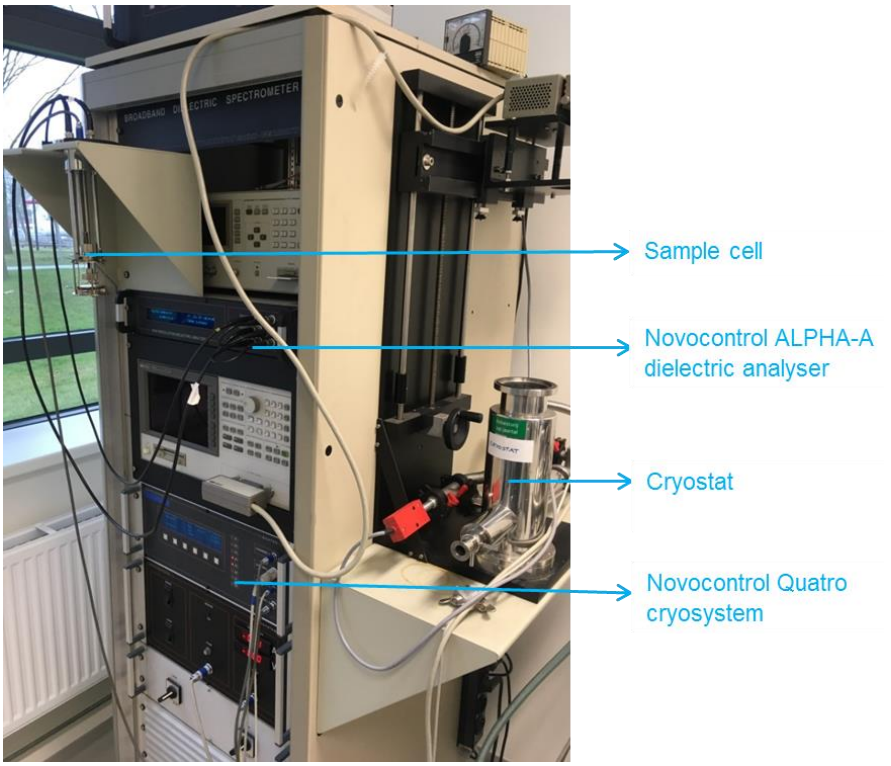

Figure 4-7 BDS equipment

4.4.1. Experiment setup

The samples were mounted between two gold-plated external electrodes inside the sample cell, as shown in Figure 4-8. The sample cell was then placed inside the cryostat where the temperature control over the sample was established. For all the samples, dielectric analysis was performed with:

- Frequency range: 10^{-2} to 10^{6} Hz (63 discrete values with logarithmic growth)
- Temperature range: -20°C to +20°C (9 discrete values with linear growth)
- Voltage settings: 1 V (Vrms-AC) and 0 V (DC).

The use of a wide range of frequencies and temperatures is due to the fact that the dielectric response of the sample will vary as a function of both frequency and temperature, as both of them affect the molecular dynamics of the molecules (or chains, in case of polymers) of the samples.

The data obtained from the dielectric relaxation analysis of a sample includes (and not limited to) ε' (storage modulus) and ε'' (loss modulus). Even though several other information such as capacitance, resistance, etc. are obtained, only the above-mentioned parameters are used extensively in this project.

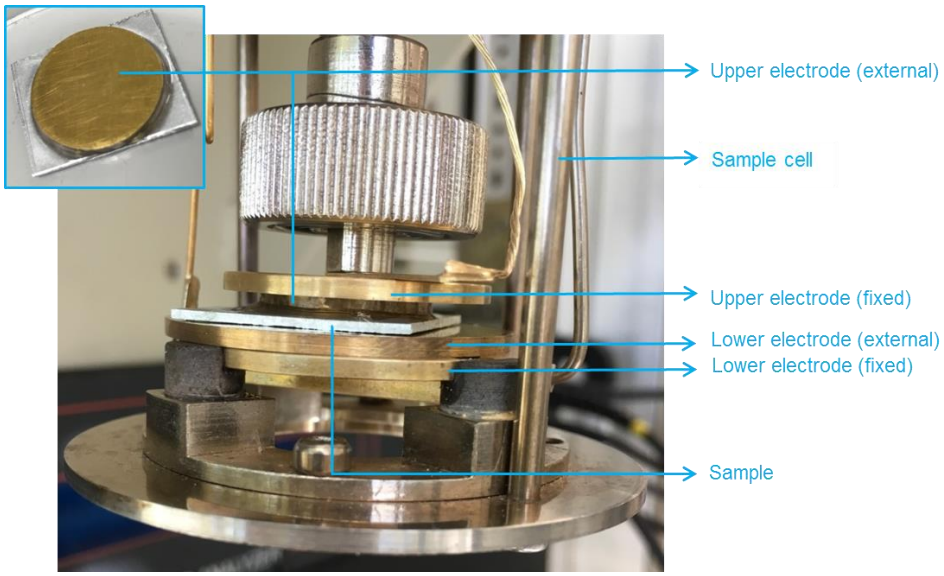

Figure 4-8 Sample mounted in a sample cell for a BDS test (Inset: A sample)

4.5. Results and discussions

In this section, the results of the experiment described in Section 4.4 is provided. Descriptions are also provided on how the data analysis methods explained in Section 3.1.3 are used to extract necessary information on molecular dynamics of the samples. Also, discussions based on these observations are provided in parallel in order to maintain coherence to the provided explanations.

4.5.1. Dielectric behaviour of bulk monomer (DGEBA)

Over the recorded frequency and temperature range, the behaviour of Storage modulus (ε'), Capacitance, and Loss modulus (ε'') of bulk DGEBA is given in Figure 4-9, Figure 4-10, and Figure 4-11 respectively. From these graphs, the dielectric behaviour of bulk DGEBA can be observed.

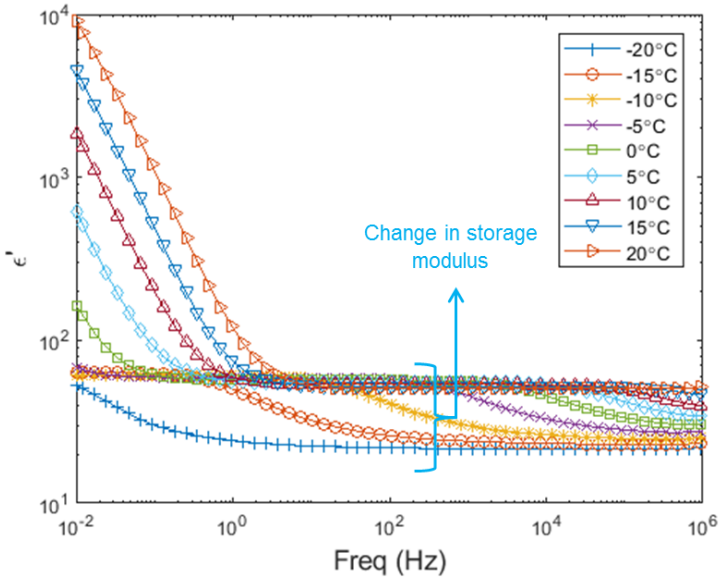

Figure 4-9 Storage modulus (ε') of bulk DGEBA, as observed through dielectric analysis

From Figure 4-9, it can be seen that for each temperature, there is a drop in storage modulus (ε') within the observed frequency range for the temperature range of -15°C to +10 °C. At temperatures lower than -15° C and over +10 °C, the change in dielectric behaviour probably occurs at a frequency that is outside the frequency band that is recorded. Within the observed frequency range, there is a drop in storage modulus (Δε) when the response is followed from lower frequencies to higher frequencies, after which the response of the sample achieves a constant value of ε∞.

As expected, the frequency range of this change in modulus coincides with the frequency range where a drop in capacitance of the sample is observed (Figure 4-10). This drop in charge storage capacity (related to capacitance) can be attributed to the drop in storage modulus of the sample. The observed capacitance also sheds some light on the thickness of the DGEBA layer on the sample. As the sample production and testing methods do not lead to a controllable DGEBA thickness on the metal plates, observation of capacitance of a similar order of magnitude can indicate that the different samples have a similar or comparable thickness of DGEBA layer.

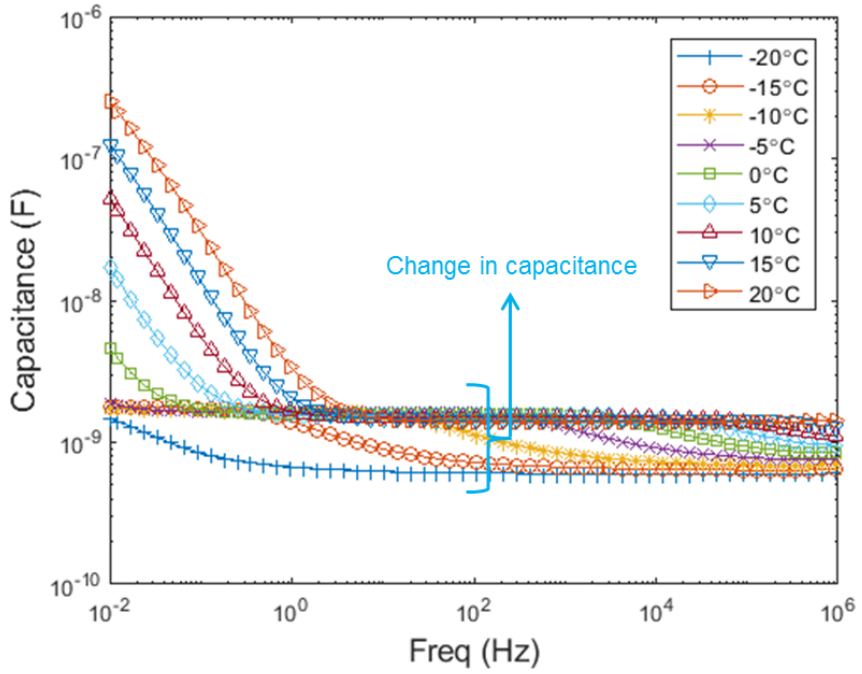

Figure 4-10 Capacitance of bulk DGEBA, as observed through dielectric analysis

By comparing Figure 4-9 and Figure 4-11, it can be seen that the drop in storage modulus (ε') graph reflects as a peak in the loss modulus (ε'') graph, as loss modulus is a mathematical derivative of storage modulus. These relaxation peaks are used extensively in further analyses to characterise the molecular dynamics of the samples. In general, it can be seen that the relaxation peaks tend to become more broad and asymmetrical as the temperature of analysis decreases, in accordance with the literature [59].

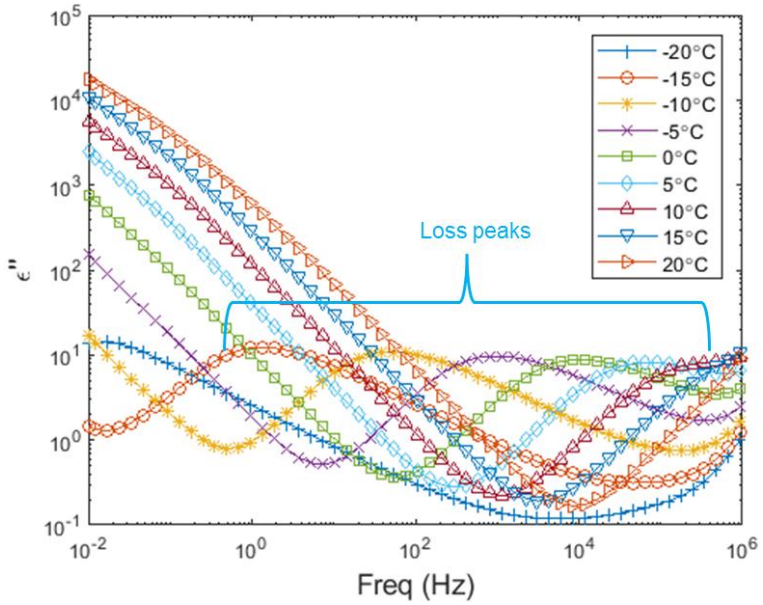

Figure 4-11 Loss modulus (ε'') of bulk DGEBA, as observed through dielectric analysis – 2D

The behaviour of relaxation peak the can be further understood and easily visualised through a 3D image of this phenomenon as provided in Figure 4-12.

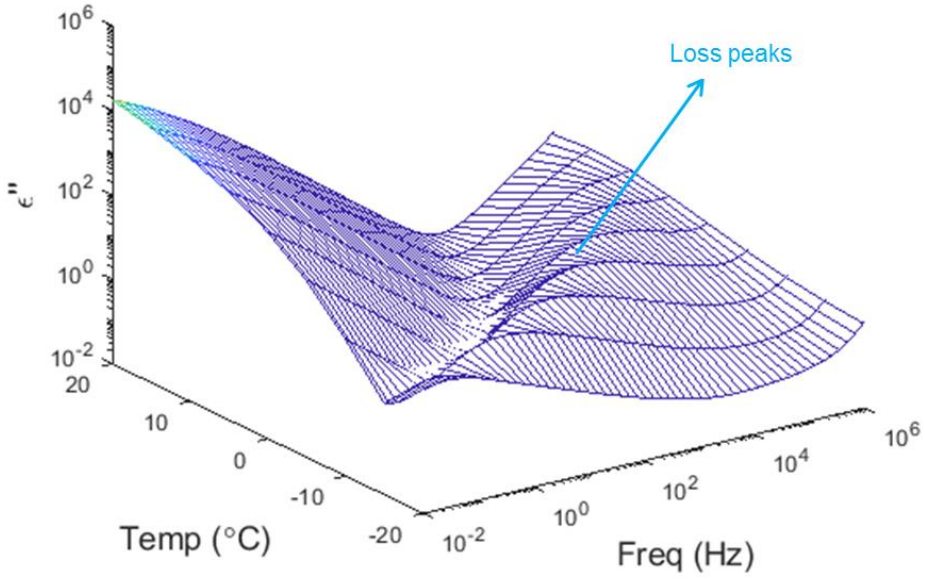

Figure 4-12 Loss modulus (ε'') of bulk DGEBA, as observed through dielectric analysis – 3D

4.5.2. Broadening of normalised loss (ε") peaks

It can be observed from Figure 4-11 that fully formed peaks corresponding to dielectric losses are formed within the observed frequency range for the temperature range of -15˚C to 5˚C. For the sake of observation, comparison and interpretation of molecular dynamics, the ε'' peaks (loss peaks) of the samples at temperature 0˚C have been considered for further use (in Section 4.5.3 for curve fitting) involving the correlation between curve shape and molecular dynamics of the samples. The compiled set of loss peaks, that have been normalised for both frequency and ε'' for different samples can be seen in Figure 4-13. Normalisation of peaks allows us to eliminate the effect of minor drift in frequency of the maximum of the peak and also the changes in its intensity.

It can be seen that with an increase in CSA, there is an increase in the breadth of the curve along the low-frequency side. Although this phenomenon is apparent from Figure 4-13, these curves are fitted with HN and VFT equations to quantify their molecular dynamics.

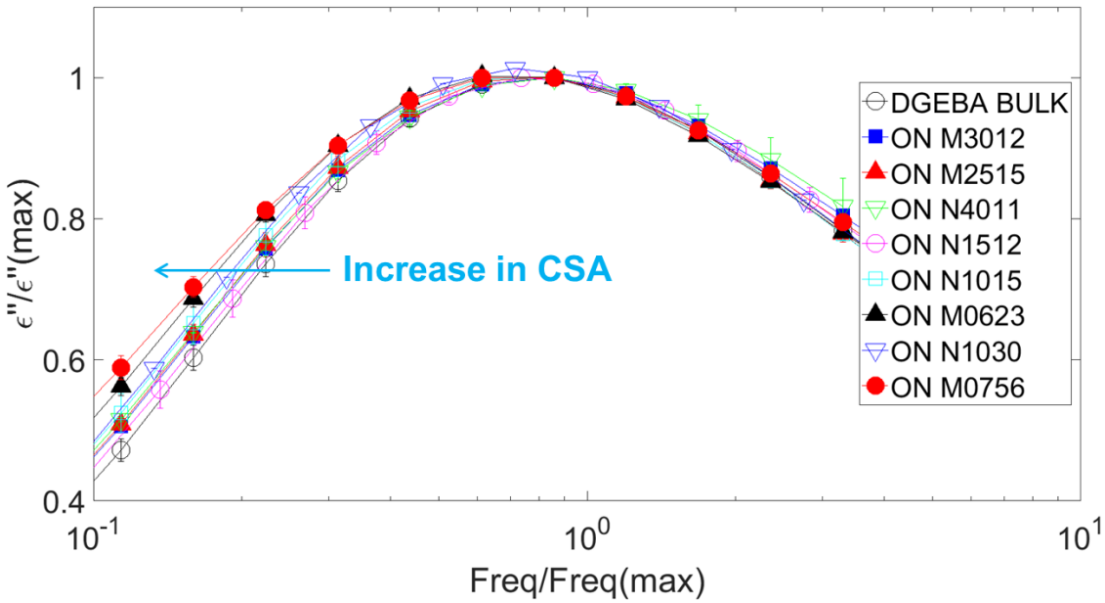

Figure 4-13 Compiled loss peaks for DGEBA on different substrates (normalised about both frequency and ε")

4.5.3. Curve fitting parameters

The dielectric data (loss peaks) were fitted with the following: (a) Single-HN peaks, (b) Double-HN peaks, and (c) VFT curves, as explained in Section 3.1.3, where the fitting procedures and equations are provided. These fitting parameters are discussed in the upcoming sections.

For Single-HN curve fit, the different fitting parameters of different samples, such as Δε, τ_{HN}, α and β are provided in Table 4-4. It can be seen that Δε and τ_{HN} of different samples are comparable to each other. However, significant changes can be observed in the α parameter for different samples. i.e. even as the peaks show comparable area and relaxation time, their respective shapes show significant differences.

Table 4-4 HN curve fitting parameters for different monomeric samples (Single-HN curve)

Sample substrate	CSA (cm^2/cm^2)	σ_0	n	Δε	τ_{HN} (s)	α	β	αβ
Bulk	1	6E-12	1,0	3,7	3,7E-05	0,95	0,36	0,34
M3012	30	3E-12	0,8	4,3	4,2E-05	0,93	0,29	0,27
M2515	47	3E-13	0,9	3,8	2,5E-05	0,91	0,38	0,35
N4011	81	8E-13	0,9	4,2	4,2E-05	0,90	0,34	0,31
N1512	128	2E-12	0,9	3,7	2,6E-05	0,89	0,40	0,36
N1015	193	2E-12	1,0	3,7	3,1E-05	0,89	0,41	0,36
M0623	307	2E-12	1,0	3,9	1,9E-05	0,89	0,37	0,33
N1030	390	1E-13	0,8	3,7	3,0E-05	0,88	0,43	0,38
M0756	622	6E-12	0,6	3,9	2,5E-05	0,79	0,46	0,36

When the loss peaks were fitted with Double-HN peaks, has a set of fitting parameters, as seen in Table 4-5 was obtained*. It can be observed that the HN2 curve appears to be smaller than the HN1 peak ($\Delta\varepsilon_{HN2} < \Delta\varepsilon_{HN1}$). Also, it can be observed that $\Delta\varepsilon_{HN2}$ and $\Delta\varepsilon_{HN1}$ values tend to have comparable values across different samples. The relaxation time of HN2 peak (τ_{HN2}) is observed to be slower than that of the HN1 peak (τ_{HN1}).

Table 4-5 HN curve fitting parameters for monomeric samples (Double-HN curves)

Sample substrate	CSA (cm^2/cm^2)	σ_0	n	$\Delta\varepsilon_{HN1}$	τ_{HN1} (s)	α_{HN1}	β_{HN1}	$\Delta\varepsilon_{HN2}$	τ_{HN2} (s)	α_{HN2} , β_{HN2}
Bulk	1	6E-12	1,0	3,7			0,36	-	-	
M3012	30	2E-13	0,9	4,5			0,25	0,12	6E-5	
N4011	81	1E-12	0,9	4,9			0,22	0,01	2E-3	
N1512	128	5E-14	0,9	3,9	~3,9 E-5	0,9	0,33	0,03	3E-3	1,0
N1015	193	2E-13	1,0	3,7			0,35	0,05	3E-4	
M0623	307	1E-11	0,7	5,0			0,21	0,09	4E-3	
N1030	390	1E-13	0,9	3,9			0,32	0,04	2E-3	
M0756	622	6E-12	0,6	4,2			0,28	0,19	5E-4	

Based on the dielectric behaviour of the samples at different temperatures, VFT fit was done. The VFT based fits are provided in Figure 4-14, and the fit parameters are provided in Table 4-6. It can be observed that for HN1 curves, fit parameters are of comparable values for different CSA. For HN2 curves, an increase in the CSA of the samples leads to an increase in τ_0 and T_v, and decrease in E_a.

Table 4-6 VFT fit parameters for different monomeric samples

Sample substrate	$\tau_{o\ HN1}$ (s)	$E_{a\ HN1}$ (eV)	$T_{v\ HN1}$ (K)	$\tau_{o\ HN2}$ (s)	$E_{a\ HN2}$ (eV)	$T_{v\ HN2}$ (K)
Bulk	1,1E-01	4,2E-15	218	-	-	-
M3012	1,1E-01	2,6E-15	218	3,1E-11	4,8E-02	236
N4011	9,7E-02	2,1E-14	221	1,4E-09	5,0E-02	230
N1512	9,0E-02	4,2E-14	223	1,9E-07	3,7E-02	242
N1015	9,2E-02	3,9E-14	222	4,0E-08	2,2E-02	233
M0623	9,2E-02	3,9E-14	222	7,1E-08	2,6E-02	243
N1030	8,1E-02	3,8E-14	226	2,0E-05	2,8E-02	254
M0756	9,5E-02	2,3E-14	221	2,0E-05	0,5E-02	239

* In one particular case (one repetition of M3012 sample), due to a high drift in data along frequency axis, α and β were fixed for HN1 peak to simulate bulk behaviour.

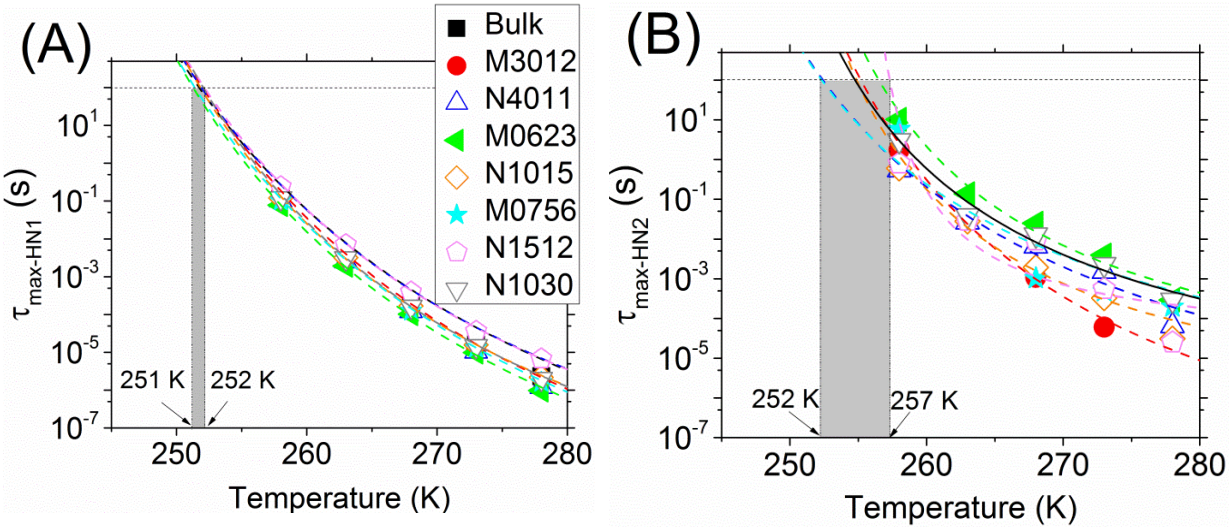

Figure 4-14 VFT fit for the (A) HN1, and (B) HN2 peaks of different monomeric samples

4.5.4. Significance of different fits

It can be seen that the HN and VFT fittings were performed on dielectric data of different samples in order to extract necessary information. Each fitting performed here has its own significance. Fitting the loss peaks with a Single-HN curve enabled the quantification of peak broadening as a shape factor. Fitting the loss peaks with Double-HN peaks allowed the quantification as the formation of a new region of different molecular behaviour. And curve fitting using VFT fits enabled the analysis of temperature dependence of these HN curves. In this report, discussions on electrode polarisation and its parameters (σ_0 and n) are not done as they are outside the scope of this project.

Based on the mean squared deviation (MSD) of the fits provided in Appendix A, it can be seen that the error decreases when the loss peaks are fitted with Double-HN peaks. It appears that Double-HN peaks are a better representation of the behaviour of the samples. It is expected that density distribution of DGEBA monomers is continuous as we move from the nanopore wall towards the centre of the nanopore, thus allowing multiple regions of distinct dynamics each could each be represented by an HN curve. However, since distinguishing several HN curves is not feasible in this case, an arbitrary selection is made to separate the DGEBA into two regions of different dynamics, each represented by an HN curve. This selection is automatically done in such a way as to get the best mathematical fit with the least MSD.

When the loss peaks are fitted with Single-HN curve, it is seen that $\Delta\varepsilon$ and τ_{HN} for all the samples tend to be of comparable values. Since the loss peaks are normalised about their respective maximums, there is not much difference observed in $\Delta\varepsilon$. Similarly, since all the loss peaks are considered for similar sample materials and experimental conditions (0°C), there are no significant changes observed in τ_{HN}. The minor changes observed in $\Delta\varepsilon$ and τ_{HN} are probably due to various factors such as the effect of a fraction of monomer adsorbed, normalisation parameters, and drift in data along the frequency axis. While this fit does not show any difference between samples in terms of relaxation time, it indirectly shows the change in the molecular dynamics of different samples by the change in α. This change, along with an (almost) constant $\alpha\beta$ term, clearly indicates broadening of peak towards lower frequencies.

When the loss peaks are fitted with Double-HN curves, it is seen that Δε for HN1 and HN2 are comparable for different samples. It is an indicator that there is no significant change in the quantity of monomer chains represented under HN1 and HN2. However, it is quite apparent from fitting parameters of Double-HN fitting (Table 4-5) that HN2 peaks have slower dynamics compared to HN1 peaks, as seen in Figure 4-15. This fitting establishes a clear presence of an HN2 peak (having slower dynamics than HN1) that is expected to represent the behaviour of the adsorbed monomers. The slow dynamics of HN2 peaks appears to reinforce the hypothesis that adsorbed monomers have slower dynamics than bulk monomers. Further, data obtained from this fitting was used in VFT fits to identify the temperature dependence of the samples.

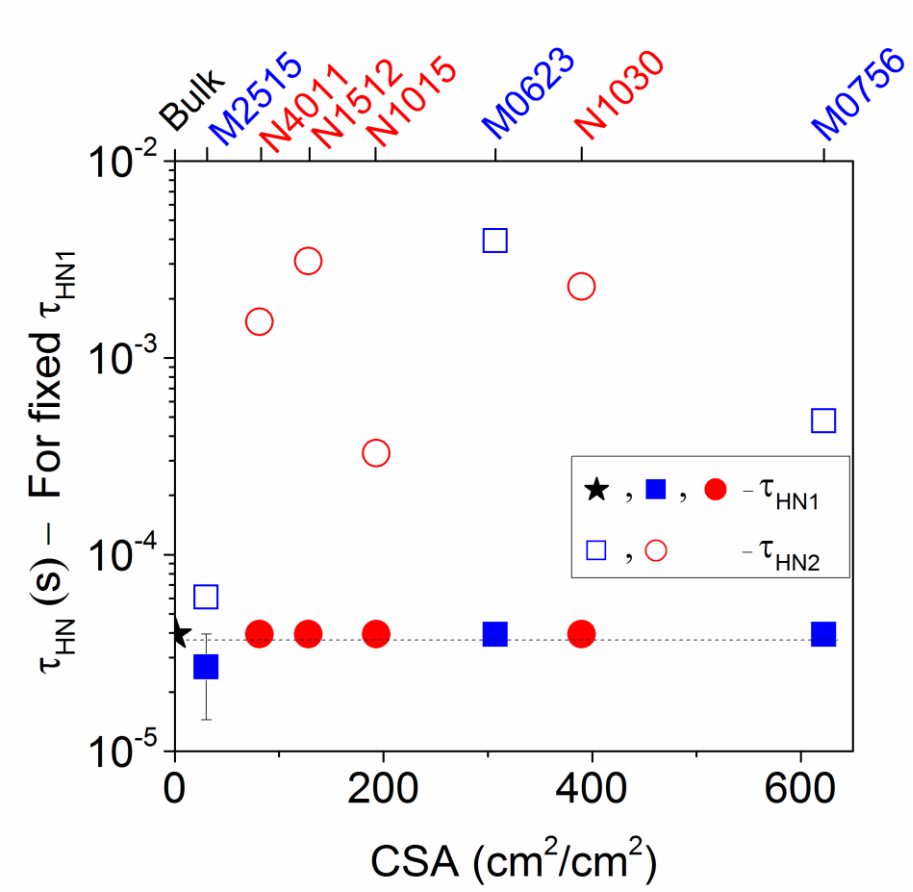

Figure 4-15 τ_{HN} for the Double-HN curves fitted for loss peaks of DGEBA on different substrates

VFT fitting for different samples allows us to identify the temperature dependence of the samples. This fitting was useful in eliminating the drift observed during Double-HN fits. The fitting parameters obtained from this fitting were paramount in deducing the molecular dynamics of different samples. The information obtained from this fitting is further discussed in the upcoming sections.

4.5.5. Slowing down of molecular dynamics

Depending on the frequency and temperature dependence of the loss peaks, the relaxation times are extracted from both HN fit and VFT fit.

4.5.5.i. Havriliak-Negami relaxation time

It is expected that the major fraction of the sample will behave like the bulk monomer and only a small fraction of the sample is expected to behave like the adsorbed monomer. It can

be seen from Figure 4-15 and Table 4-5 that while τ_{HN1} for different sample remains constant (as it was enforced)*, τ_{HN2} changes for all the samples. While the HN1 loss peaks for different samples remain stationary with respect to frequency, the HN2 loss peaks tend to drift towards lower frequencies. An increase in the fraction of monomers under confinement is expected to shift the loss peak of adsorbed monomer to lower frequencies.

If all the samples have a similar morphology of adsorbed region, it is expected that when the fraction of monomer corresponding to HN2 increases, the τ_{HN2} must be constant while $\Delta\varepsilon_{HN2}$ increases. However, it is not the case here as no conditions were provided to force τ_{HN2} to be constant, as it is unknown. Further, since in $\Delta\varepsilon_{HN2}$ tends to be very small compared to $\Delta\varepsilon_{HN1}$, it was easier to perform a fit with (almost) constant $\Delta\varepsilon$ and a variable τ_{HN2} so that the decrease in MSD (and subsequent convergence) can be attained. It could also be due to the enforcement of HN2 to behave like a Debye peak i.e. peak broadening is defined as a change in relaxation time (with constant peak area), and not change in peak area (with constant relaxation time).

While HN2 peaks have slower relaxation times, a clear trend between different samples and substrates are missing. It is possible that uncontrolled minor drift along frequency axis could be a possible reason for this. So, it appears that it might be difficult to observe a trend in slowing down of the dynamics.

4.5.5.ii. Vogel-Fulcher-Tammann relaxation time

VFT fit provides information of the theoretical relaxation time (τ_0) of different samples at an infinite temperature (or, maximum energy). It can be seen from Figure 4-16 that the relaxation time τ_{0-HN1} appears to be constant, while τ_{0-HN2} appears to increase. The trend of increase in τ_{0-HN2} with an increase in CSA appears to be shed more light on the trend observed for τ_{HN2} seen in Section 4.5.5.i.

Here, it is explicitly seen that increase in CSA leads to slowing down of the dynamics of the adsorbed region (represented by HN2). It appears that HN2 represents a fraction of sample that is dominated by adsorbed monomer (constant $\Delta\varepsilon_{HN2}$ and changing τ_{HN2}). So, an increasing trend observed in this case could be considered an indicator that an increase in CSA leads to an increase in adsorption of monomers to nanopore substrates, leading to slowing down of dynamics.

Unlike HN fits, VFT fits provide a clear insight into the change in relaxation time of the samples with changing topography. Based on the data points available in Figure 4-16, it can be seen that increase in CSA is coupled with an increase in τ_{0-HN2}. So, it can be understood that an increase in contact between monomers and substrates improved adsorption leads to slowing down on molecular dynamics of the monomers. Further, in VFT fit, the effect of drift of data along the frequency axis becomes negligible as the drift was found to be constant/comparable across the temperature range. Thus, the information extracted from this method (Figure 4-16) shows lesser noise than that obtained by HN fitting (Figure 4-15).

Overall, the combination of constant $\Delta\varepsilon_{HN2}$ and increased τ_{HN2} (or τ_{0-HN2}) strengthens the following ideas: (1) the monomers corresponding to the HN2 peak have slower dynamics due

* Except in case of M3012 due to reason explained in footnote in page 32.

to adsorption, and (2) fraction of DGEBA under HN2 relaxation changes with a change in the substrate.

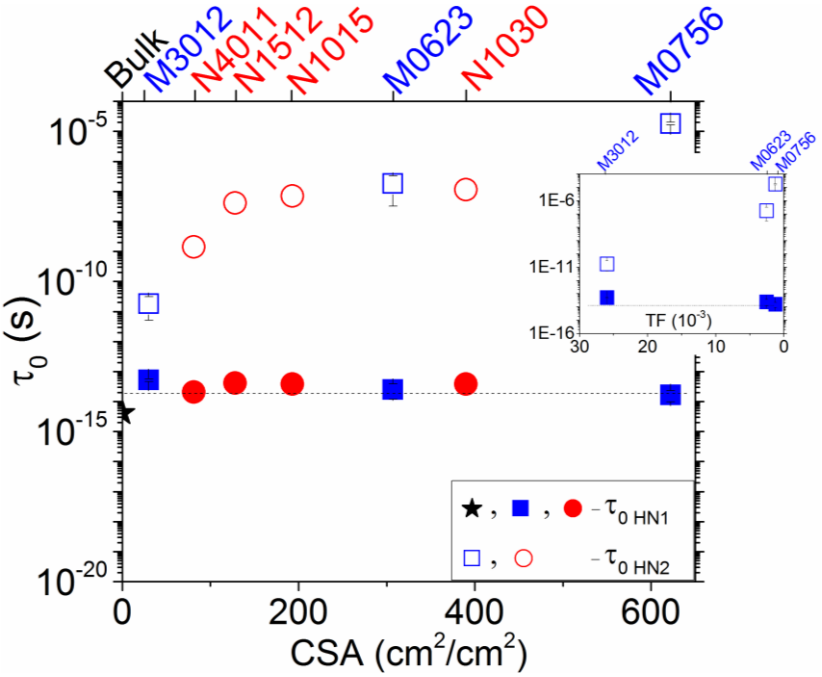

Figure 4-16 τ_0 for the two relaxations (HN1 and HN2) of DGEBA on different substrates *(Inset: Same, but as a function of TF)*

4.5.6. Transition temperature of dielectric relaxation

The given material (DGEBA monomer) is a monomer and hence, will not have a Tg. Thus, the transition temperatures corresponding to the samples in this study correspond to the temperature at which the molecular motions corresponding to relaxations shown in Figure 4-11 and Figure 4-12 cease to exist. For the sake of representation, this temperature will be considered as a transition temperature that is referred to as Tx, for further use in this chapter.

It can be seen from Table 4-6 and Figure 4-17 that Tv for HN1 tends to remain constant at around 221 K for different samples while Tv for HN2 increases. When considering the condition of when $\tau_{max}(T)$ crosses 100 s, it can be seen from Figure 4-18 and Table 4-7 that Tx(HN1) tends to be a constant at around 251-252 K, and Tx(HN2) increases with increase in CSA.

In order to validate this observation, DSC tests were done on pristine DGEBA from -50°C to +100°C at ±10°C/min ramp up/down rate under Nitrogen. From the deflection in the graph, the onset of a transition at around 252 K is seen (Figure 4-19). In all cases, Tv, Tx, and transition temperature from DSC fall within the acceptable limits of each other. This is a validation of the method followed until now. It can be safely concluded that the Tv (and Tx) data observed here are accurately predicted transition temperatures, and not arbitrary theoretical values.

When Tv of HN2 peaks is analysed, it can be observed that there is an increasing trend with respect to CSA, as shown in Figure 4-17. It indicates that with increasing CSA, the temperature at which dynamics stop increases. It is an indicator of an increase in restriction

to molecular motion of the monomers corresponding to HN2. These monomers require higher energies for the observed relaxations.

Compared to HN1, HN2 has a wide range of Tx, as shown in Table 4-7 and Figure 4-18, where the distribution of Tx as a function of CSA is provided. The increasing trend can be contributed to an increasing fraction of adsorbed monomers under the HN2 domain. Such a trend is also observed in Figure 4-17. From Sections 4.5.5, it was already discussed that the dynamics of adsorbed monomers (represented by HN2) is slower compared to that of bulk monomers. The observations in this section further strengthen this idea by the observation of change in transition temperature. These observations in a change in transition temperature appear to be consistent with similar analysis by Schönhals et al. [32], where an increase in Tg was observed for Propylene glycol monomers confined in nanoporous glasses.

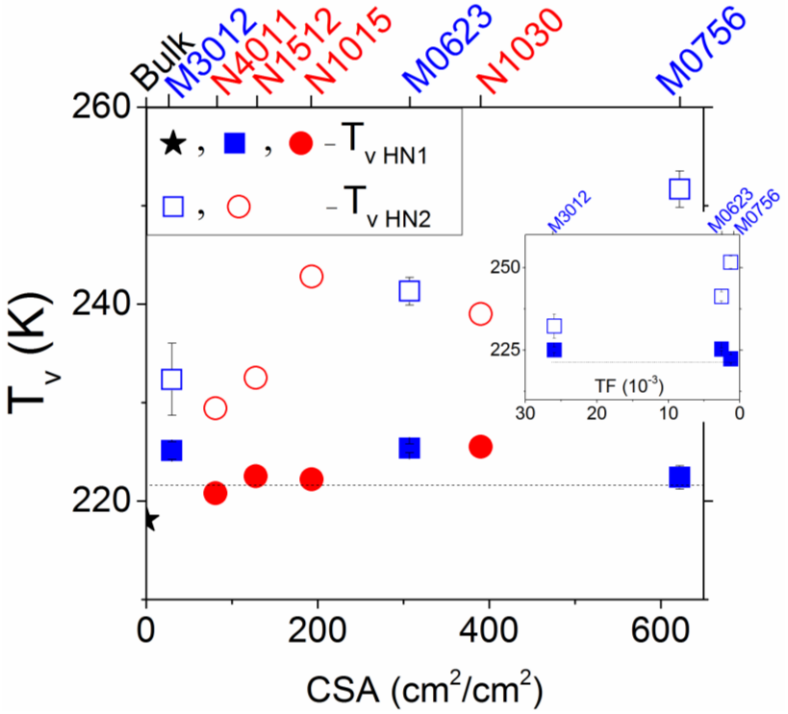

Figure 4-17 Tv for the two relaxations (HN1 and HN2) of DGEBA on different substrates *(Inset: Same, but as a function of TF)*

It can be considered based on these observations that the fraction of sample represented by HN2 stops relaxations at temperatures higher than that represented by HN1. This is a strong indicator of the fact that adsorbed monomers (HN2) would have a slower dynamics probably due to either attraction forces with the nanopore walls, or due to an increase in density of monomers close to the wall.

Table 4-7 Transition temperature (Tx) of DGEBA on different substrates corresponding to τ_{max}=100s for HN1 and HN2 peaks

Sample substrate	Bulk	M3012	N4011	N1512	N1015	M0623	N1030	M0756
CSA (cm^2/cm^2)	1	30	81	128	193	307	390	622
Tx (HN1)	251,5	252,0	251,8	251,4	251,8	251,4	252,0	251,4
Tx (HN2)	-	254,7	255,3	255,3	254,9	256,5	255,0	257,0

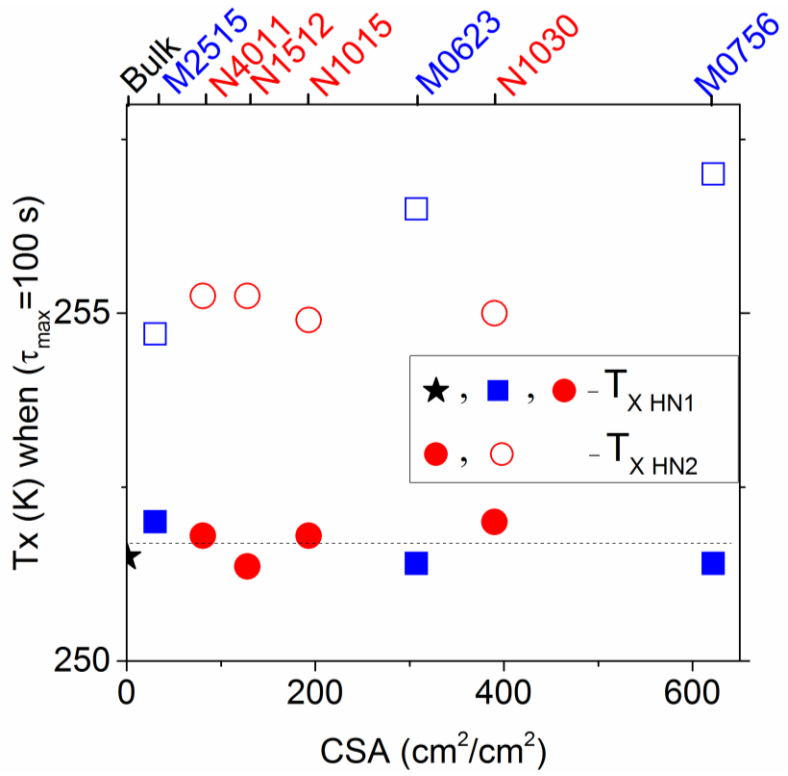

Figure 4-18 Transition temperature of DGEBA on different substrates corresponding to τ_{max}=100s for HN1 and HN2 peaks

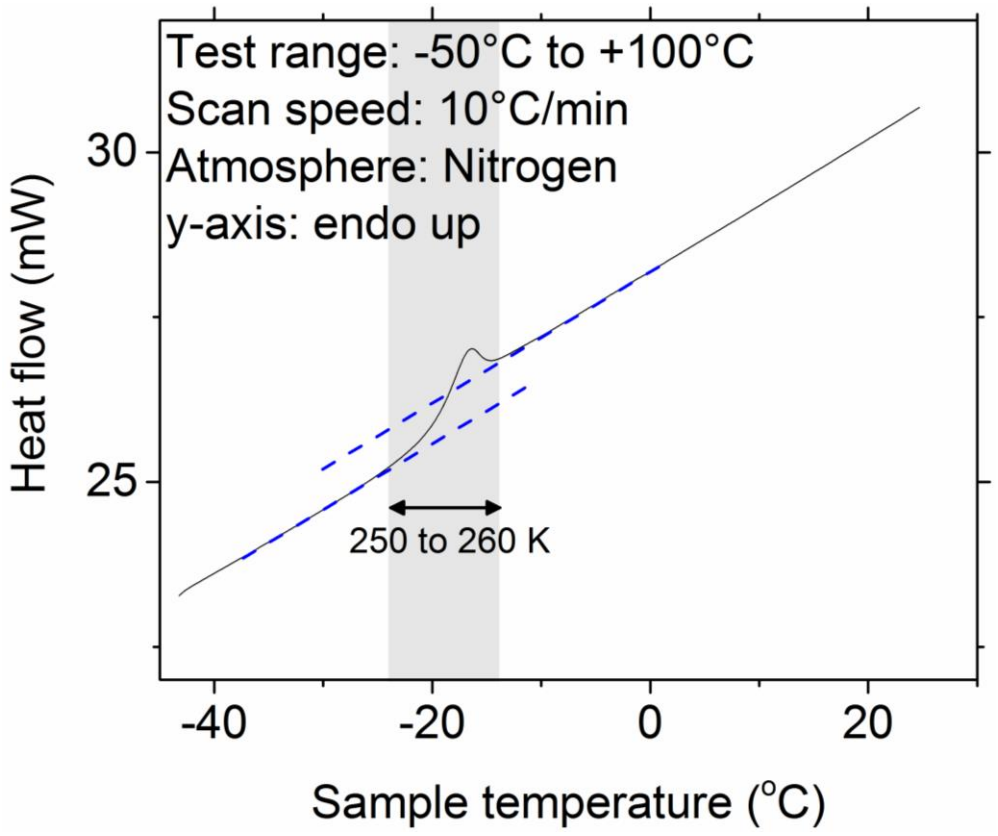

Figure 4-19 DSC data of pristine DGEBA

4.5.7. Activation energy required for dielectric relaxation

With an increase in density of monomers near the surface of the nanopores due to increase in confinement (increase in CSA), it is expected that the activation energy of the system must increase, as observed by Schönhals et al. in poly(propylene glycol) (PPG) confined in nanoporous glass substrate [61]. Further, the attraction between the monomers and the surface of the nanopores that causes adsorption must also lead to an increase in activation energy. However, it is not the case in the observed phenomenon, as evident from Figure 4-20.

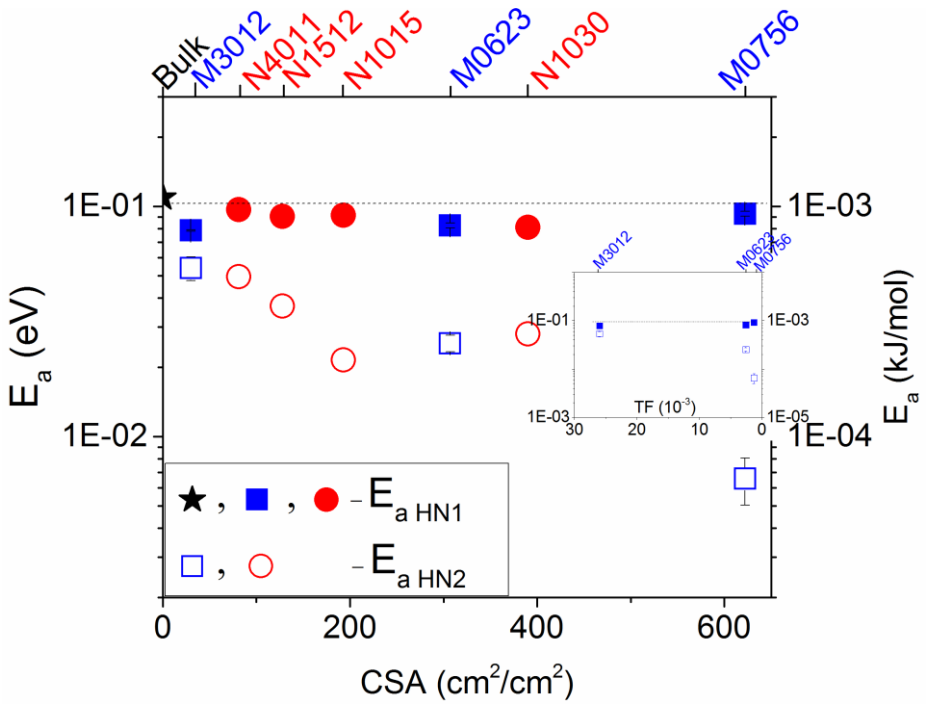

Figure 4-20 E_a for the two relaxations (HN1 and HN2) of DGEBA on different substrates *(Inset: Same, but as a function of TF)*

Here, it is observed that the activation energy (E_a) of HN1 remains a constant. A consistent E_a is a strong indicator that HN1 peaks represent the behaviour of a single type of molecular arrangement (that of bulk monomers). Further, with an increase in CSA, it is seen that E_a of HN2 decreases. This change in E_a of HN2 appears counter-intuitive to the current thought flow. Here, it must be noted that such an assessment of E_a based on changes in monomer confinement inside metal oxide pores is a fairly unexplored regime.

Based on the observations, it appears the origin of this change in E_a can be traced to the molecular arrangement of the monomers close to the nanopore walls, that causes $E_{a\ HN2} < E_{a\ HN1}$. Conclusive discussions on this particular phenomenon need further detailed experiments or simulations to understand the arrangement of individual monomer molecules close to the nanopore walls.

4.5.8. Effectiveness of CSA and TF

The dependence of the molecular dynamics parameters on CSA indicates that the adsorption of monomers is a surface phenomenon. No such dependence is seen for the TF of the samples. As the size of the monomers (~1,9 nm) is several times smaller than the nanopore dimensions, it is probable that the pore dimensions (TF) did not directly affect adsorption. This observation validates the idea of using CSA as a common comparison parameter for different substrates.

4.5.9. Influence of substrate topography

The dynamics of the samples also appears to vary with the types of oxide layers (N-series or M-series). It can be seen that the fitting parameters of M-series samples show a continuous trend as explained previously. This consistency appears to be lacking in case of N-series samples. Based on the τ_0, Ea, Tv and Tx values of different samples, it can be seen that N-series samples show significant difference with respect to trend followed by M-series samples.

Further, it is also seen that all the N-series samples have comparable behaviour when considered separately. While it is quite apparent that N-series and M-series samples show different trends, it is difficult to conclude whether the different trends are due to, (a) difference in substrate topography, or (b) a limited number of data points that gives a false-sense of difference in trends. Thus, based on the available data, discussions on the difference in trends for different substrate types cannot be conclusively performed. While the evidence point towards difference in trends, there is a need for further tests to validate it (preferably using more samples having different CSA than current samples).

4.5.10. Validity of hypotheses

Based on the above discussions, it is quite evident that confinement of monomers within nanopores of the anodised aerospace aluminium alloys lead to change in the molecular dynamics of the monomers. Here, it is seen that a fraction of monomer with slower dynamics is formed in such a case. This phenomenon is attributed to the adsorption of monomers to the walls of the nanopores. It is also seen that this adsorption effect appears to become more pronounced when there is an increase in contact area between substrate and monomer. Furthermore, as this chapter deals with only the monomers, it was not possible to study the adhesive effects.

Overall, this experiment appears to validate the following hypotheses: (1) *Confinement of mono/polymers will lead to restricted molecular dynamics in one part of the sample, that could be identified through Broadband Dielectric Spectroscopy (BDS)*, and (2) *Change in contact area between the mono/polymers and the walls of the nanopores will lead to change in the fraction of molecules under restricted dynamics*.

4.6. Chapter synopsis

From the discussions provided in Section 4.5, it can be seen that multiple factors point towards the formation of a region of new molecular dynamics within the samples when DGEBA monomers are confined within the nanoporous substrates.

When the DGEBA monomers are under confinement, the area under the curves of loss peaks shows broadening towards the low-frequency region (Section 4.5.2), indicating the movement of the observed relaxation dynamics to lower frequencies. This is further quantified by fitting the peaks with Single-HN curve each, where this broadening is reflected as an increase in the non-dimensional parameter α (Section 4.5.3). This change follows a trend with respect to the CSA of the samples.

When the peaks were fitted with Double-HN peaks in order to differentiate and observe the contribution of bulk monomer and adsorbed monomer, it was found that the frequency of the peaks corresponding to adsorbed monomers (HN2) drifted away from that of bulk monomers (HN1), as discussed in Section 4.5.5. This is a clear indication of a different dynamics within the sample that behaves different from the bulk. Based on the frequency of their peaks, it is

also seen that these dynamics are slower than that of bulk monomer. This drift in frequency of peak was found to follow a trend with respect to CSA. This indicates the increased adsorption of monomers with a change in CSA.

VFT fits allowed the study of the temperature dependence of different relaxation processed by studying different HN peaks separately. In this scenario, HN2 corresponded to a relaxation that required higher temperatures to initiate relaxations (Section 4.5.6). This relaxation temperature varied with changes in CSA. With increased adsorption of monomers to the nanopore walls, an increase in transition temperature is observed. So, it is safe to conclude that the adsorbed monomers have a different molecular arrangement that they need higher temperatures (or energies) for the relaxations to occur. This discussion was however opposed by the observation of the activation energy of the processes (Section 4.5.7). More study is needed to understand this behaviour.

Overall, from these different discussions, it can be concluded safely that confinement of monomers within the nanopores introduces highly restricted and slower molecular dynamics to the samples. With an increase in confinement (increase in CSA), this effect was found to be more pronounced. Thus, an increase in confinement causes an increase in adsorption of monomers to nanopore surfaces.

In this case, when adsorption is considered as a function of CSA, and a good trend is observed between adsorption and CSA. It can be concluded that confinement of monomers within the nanopores is a surface.

4.6.1. Summary

The summary of this chapter can be stated as follows:

1. Monomers infiltration into nanopores leads to adsorption of monomers to nanopore walls
2. This adsorption layer has highly restricted monomers that have slower dynamics i.e. domination of adsorption effects
3. Slowing down of dynamics is identified through changes in the shape of loss peak, relaxation time, and transition temperature of the samples
4. The fraction of monomers under adsorption differs based on the confining geometry
5. Adsorption of monomers is a surface phenomenon, not topology phenomenon
6. Further studies (preferably theoretical or simulation) needs to be done to understand the unexpected behaviour of Ea for different samples

This page is intentionally left blank.

Chapter 5
AF163-2K0.060 confined within nanoporous oxides of anodised aerospace aluminium alloys

From the inferences from the dielectric studies of monomers under confinement (Chapter 4), it was decided to explore the possibility of applying similar concepts to a polymeric system. In this chapter, information is provided on the materials selection for testing, production validation methods, dielectric tests and finally, the analysis and discussions of dielectric data to understand the molecular dynamics of polymers under confinement. Further, it must also be noted that due to limited data due to a limited variety of samples, and subsequent limitation in mechanical test data (Appendix B), attempts to relate dielectric data to the mechanical strength of the adhesive bonds of the samples were not made.

5.1. Materials and sample preparation

Monodirectional (M-series) porous substrates (Figure 4-2 (b)), with a commonly used polymeric film adhesive (PFA), 3M™ Scotch-Weld™ AF 163-2K0.060 (as the polymer adhesive), were provided by Fokker Aerostructures (Papendrecht, The Netherlands). The surface topologies of the metal plates are provided in Figure 5-1. As described in Section 4.1, the clad Al-7075-T6 metal substrate was anodised using PSA to achieve monodirectional 1D pores (M-series). In one set of samples, the adhesive film was placed on the metal substrate and cured in an autoclave at 6 bar pressure, and another set was cured in an autoclave at 1 bar pressure. The temperature cycle for curing was maintained as suggested by the PFA manufacturer. The different samples and their corresponding processing conditions are specified in Table 5-1. In the sample code, H and L suffixes respectively refer to high and low pressures used during sample preparation. The motivation behind these two processes is that the polymeric film is expected to not infiltrate the nanopores in absence of excessive pressure, leading to poor adhesion as evident from Appendix B. In order to analyse bulk effects, a strip of PFA was cured on a Teflon substrate (1 bar pressure, suggested curing temperature cycle) and then peeled off for further analysis. Furthermore, Figure 5-2 shows the overview of a sample (M3012L), where it can be seen how the film adhesive is present on top of a metal substrate. It can also be seen that the adhesive film is supported by a carrier mesh that keeps the film intact, without providing any significant structural reinforcement to the film.

Table 5-1 Specifications of samples with PFA coated metal substrates

Metal plate	Polymer	Curing temperature (^{0}C)	Curing pressure (bars)	Sample code	CSA (cm^2/cm^2)	TF (10^{-3})	Pore diameter (nm)
-	3M™ Scotch-Weld™ AF 163-2K0.060	~120	1	Bulk	1	-	0
M0623			6	M0623H	307	3	6
M3012				M3012H	30	26	30
M0756				M0756H	622	1	7
M2515				M2515H	47	17	25
M0623		~120	1	M0623L	307	3	6
M3012				M3012L	30	26	30
M0756				M0756L	622	1	7
M2515				M2515L	47	17	25

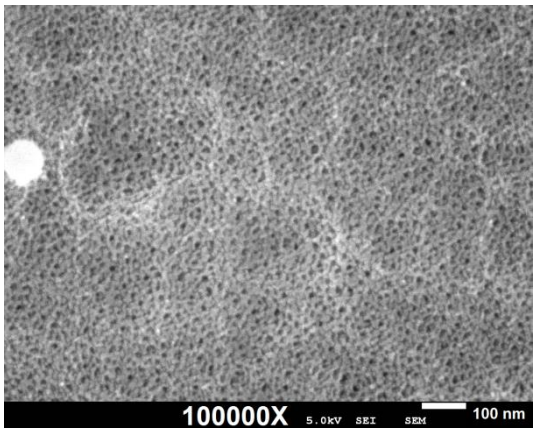

(a)

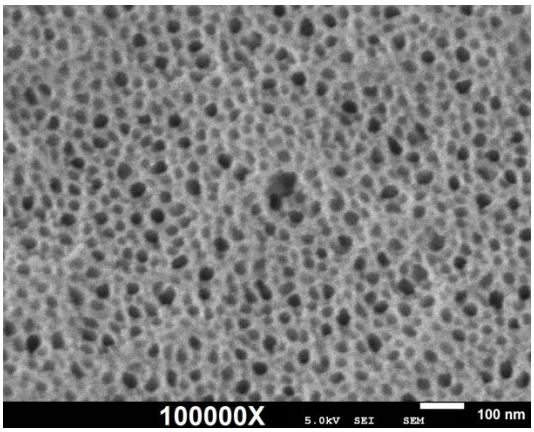

(b)

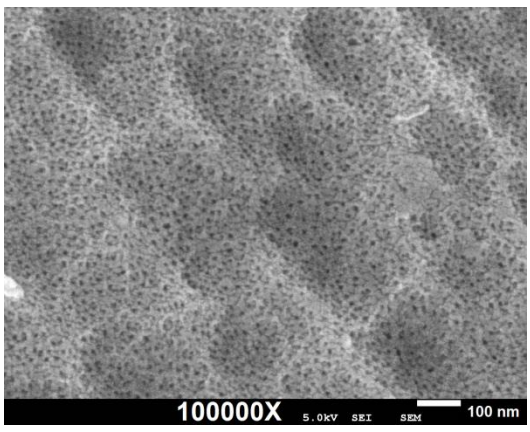

(c)

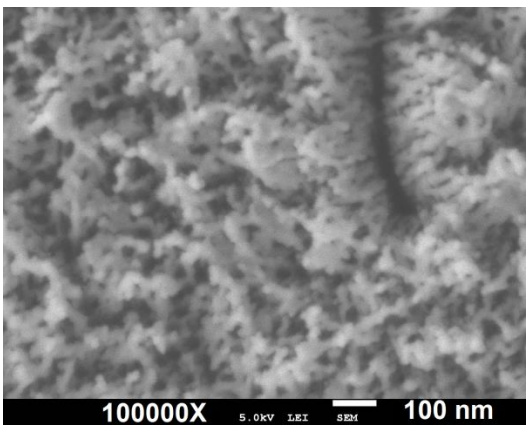

(d)

Figure 5-1 Surface topologies of the metal plates M0623 (a), M3012 (b), M0756 (c), and M2515 (d)

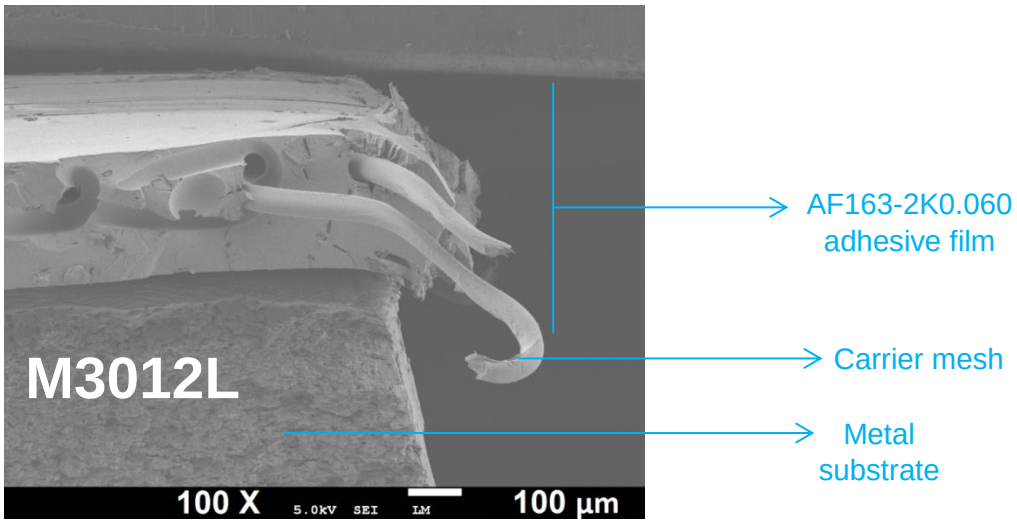

Figure 5-2 Overview of adhesive film cured on a metal substrate (M3012L)

5.2. Dielectric analysis

The metal plates with a layer of PFA that were obtained from the Fokker, were used as samples for dielectric analysis. The setup used for this dielectric analysis was Novocontrol ALPHA-A dielectric analyser that was coupled with a Novocontrol Quatro cryogenic system for temperature control, and a computer that serves as an experiment control panel. This complex setup can be seen in Figure 4-7.

5.2.1. Experiment setup

The samples were mounted in between two gold-plated electrodes inside the sample cell. The sample cell was then placed inside the cryostat where the temperature control over the sample was established. For all the samples, dielectric analysis was performed with:

- Frequency range: 10^{-2} to 10^{6} Hz (63 discrete values with logarithmic growth)
- Temperature range: -100 °C to +100 °C (11 discrete values with linear growth)
- Voltage settings: 1 V (Vrms-AC) and 0 V (DC).

The data obtained from the dielectric relaxation analysis of a sample includes (and not limited to) ε' (storage modulus) and ε'' (loss modulus).

5.3. Results and discussions

In this section, the results of the experiment described in Section 5.2 is provided. Descriptions are also provided on how the data analysis methods explained in Section 3.1.3 are used to extract necessary information on molecular dynamics of the samples. Also, discussions based on these observations are provided in parallel in order to maintain coherence to the provided explanations.

5.3.1. Validity of samples

The samples were analysed using SEM in order to visually confirm the infiltration of PFA into the nanopores of the oxide layer. For this, the cross sections of the samples were observed through SEM. Figure 5-3 shows the cross-section view of the oxide layers with polymers for different samples. From the SEM analysis, it can be observed that for samples where high pressure was applied (M0623H, M3012H, M0756H), PFA appears to stick on to the surface, or show minor infiltration into the pores. However, in the case of M0756H, it appears that the failure was interfacial. In these samples, it appears that only M0623H and M3012H show proper infiltration into pores and look comparable. When high pressure is not applied, no PFA appears on the surface of the oxide layer (M3012L, M0756L), or the PFA layer appears partially detached from the oxide layer (M0756L), or PFA layer remains attached to the surface of the metal substrate (M2515L).

From Figure 5-3, in case of samples that were produced at 1 bar pressure, it is seen that the surface of the oxide layers are bare, or show a crack in the interface between oxide and adhesive when they are broken in order to analyse their cross-section. This is a clear indication that the failure that occurs is interfacial. This is probably due to the fact that the adhesives have not infiltrated the nanopores due to lack of necessary pressure. It must also be noted this observation is consistent for all the samples of this production method (M0623L, M3012L, M0756L, and M2515L).

When samples were produced at a high pressure of 6 bars, it is seen that interfacial failure occurs in case of M0756H. But, cohesive failure in the adhesive layer is witnessed in all other samples (M0623H, M3012H, and M2515H). This observation leads to the understanding that polymer-surface interaction in the case of M0756H sample is unlike other samples. The difference could be a factor of pore topology, processing conditions, substrate chemistry, etc. Also, in the other samples (M0623H, M3012H, and M2515H), clear partial infiltration of polymers into nanopores is seen.

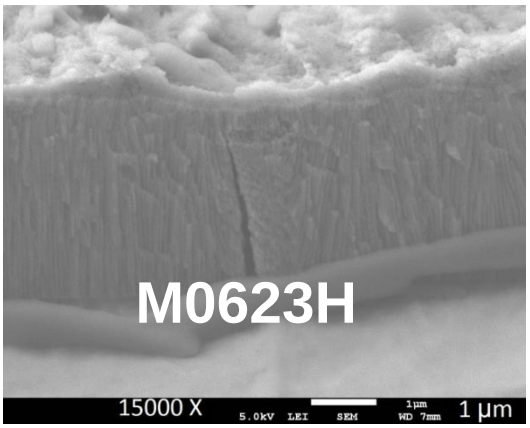

(a)

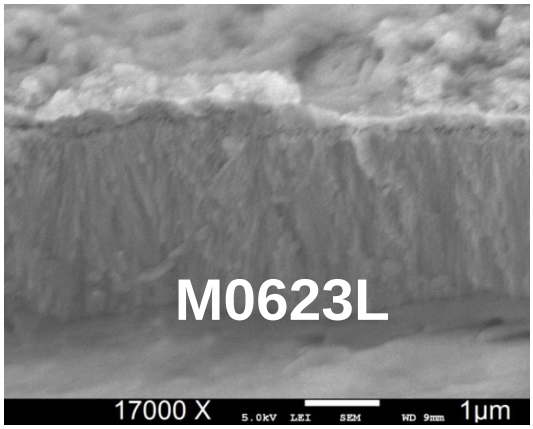

(b)

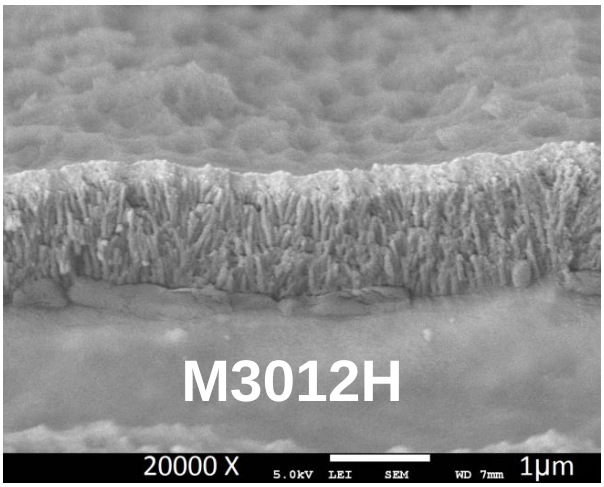

(c)

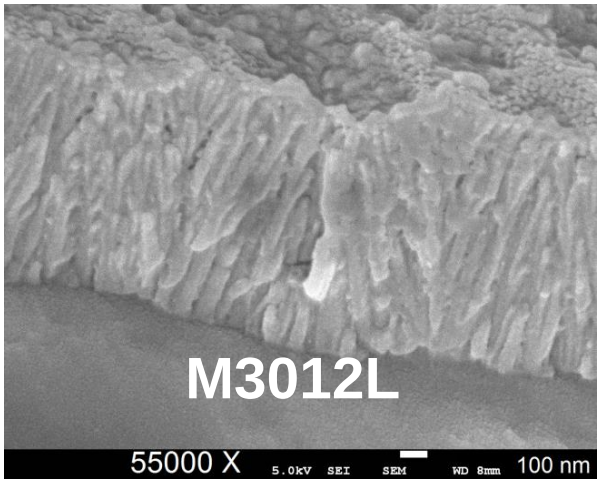

(d)

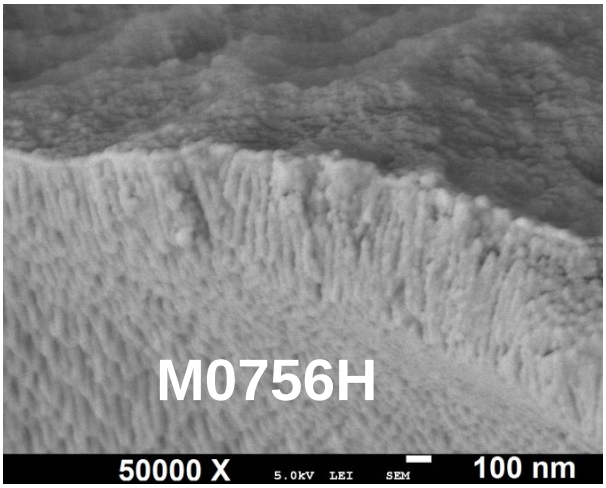

(e)

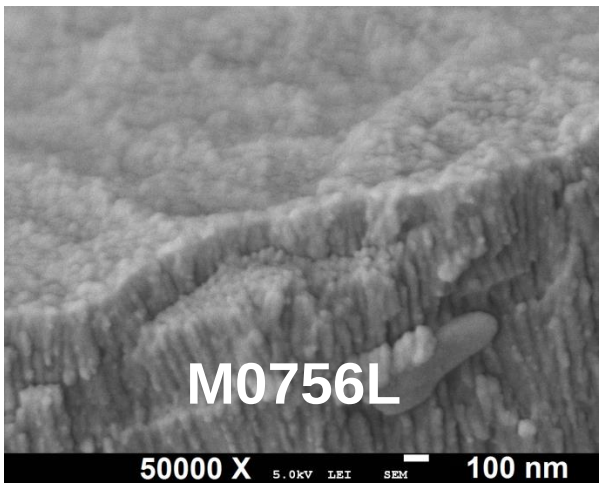

(f)

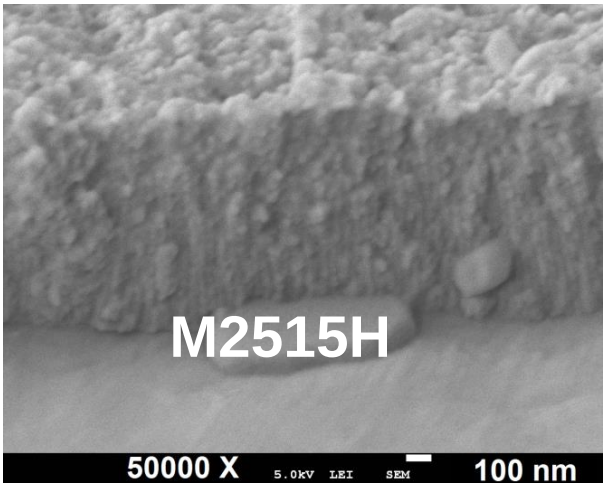

(g)

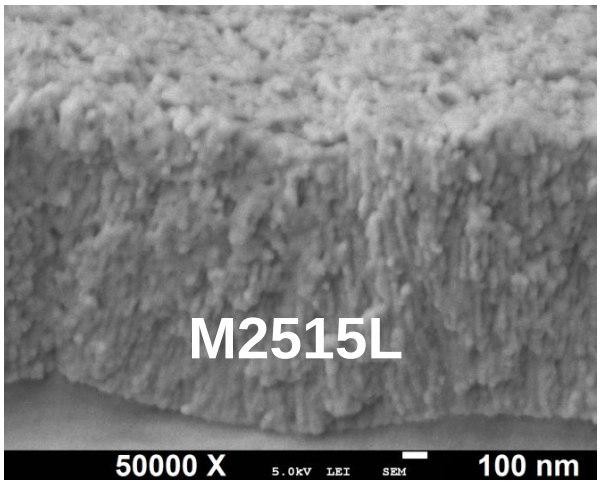

(h)

Figure 5-3 Cross-sectional view of the infiltration of PFA into nanopores of oxide layers different samples. *(Sample code provided on the images)*

Further, from Figure 5-1, it is also seen that the substrate of M2515H has a different oxide topology than the other samples. So, even upon the infiltration of adhesive into the nanopores, its behaviour might vary. Overall, it appears that in the case of samples produced at high pressure, only M0623H and M3012H have comparable oxide structure and show clear infiltration of polymers. Thus, only these two samples can be reliably compared to find the difference in dielectric behaviour of the polymer confined in different geometries.

From all these samples it is also seen that the polymer never fully infiltrates the oxide nanopores. Thus, the definition of CSA and TF does not hold any meaning in this scenario as the depth of the pore is never fully infiltrated. The only parameters that appear to be useful for comparison between infiltration of the polymer into the nanopores are the diameter of the nanopores. Thus, in this chapter, the discussions are also concentrated based on the nanopore diameter of different substrates.

5.3.2. Dielectric behaviour of a polymeric sample (M2515H)

Several important parameters such as capacitance, storage modulus, loss modulus (2D plot) and loss modulus (3D plot) of a sample are shown in Figure 5-4, Figure 5-5, Figure 5-6 and Figure 5-7 respectively in order to explain the behaviour of the polymeric system in the given conditions. Much of the descriptions on the behaviour seen in these figures are similar to explanations in Section 4.5.1, where detailed descriptions are provided.

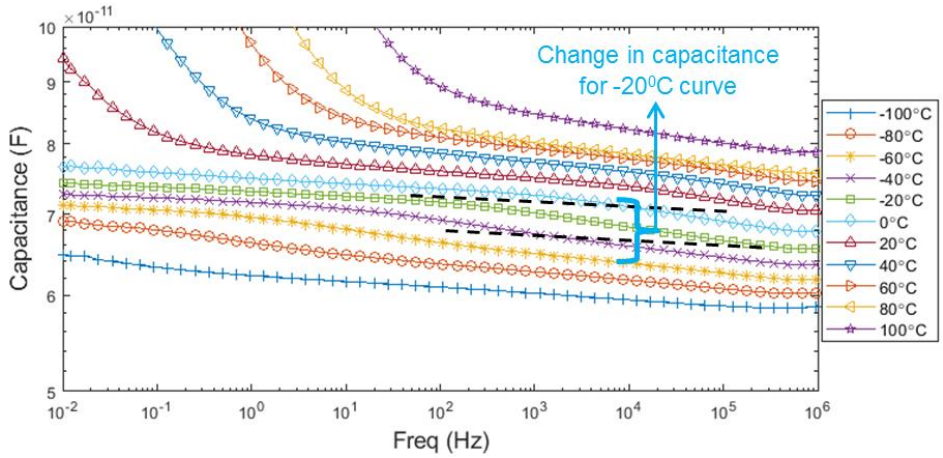

Figure 5-4 Capacitance of M2515H, as observed through dielectric analysis

As expected, it can be seen that at particular combinations of frequencies and temperatures, change in capacitance can be observed in Figure 5-4. This change is due to the similar reasons as explained in Section 4.5.1. This change in capacitance coincides with the change in storage modulus (ε‘), as observed in Figure 5-5. These drops in storage modulus are reflected as peaks in loss modulus (ε‘‘) curves. From Figure 5-6 and Figure 5-7, it can be seen that there are two sets of loss peaks or relaxation peaks.

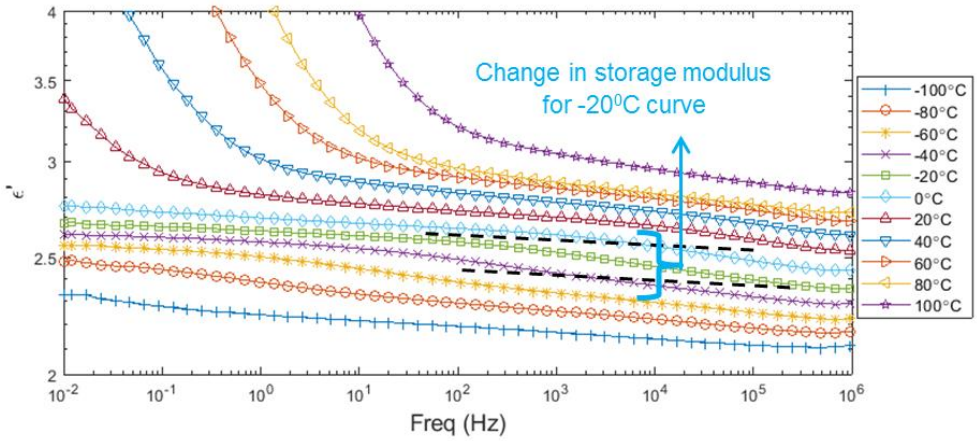

Figure 5-5 Storage modulus (ε‘) of M2515H, as observed through dielectric analysis

One set of loss peaks (Loss peaks I) form distinct fully-formed loss peaks inside the frequency domain under monitoring. These peaks occur at temperatures that are far less than the glass transition temperature of PFA (Tg~108^{0}C or 381 K). Thus, it can be expected that these peaks probably relate to other relaxation processes such as β or γ relaxation. In case of the second loss peak (Loss peaks II), it can be seen that the peaks are not fully formed within the frequency range of analysis. Additional tests were performed for similar samples at higher temperature ranges in order to witness any distinct and fully-formed loss peaks in the Loss peaks II set. From Figure 5-8, it can be seen that even at higher temperatures of analysis, loss curved do not form distinct peaks.

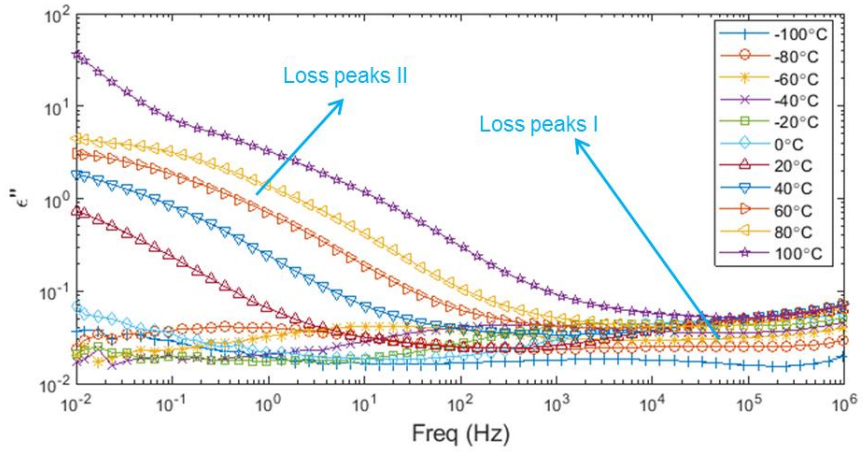

Figure 5-6 Loss modulus (ε‘‘) of M2515H, as observed through dielectric analysis

It is also seen from Figure 5-7 and Figure 5-8 that there are no peaks seen that could be a contribution of Tg (α relaxation). It is possible that these peaks might be suppressed due to the very high electrode polarisation. So, in this chapter, the analyses are performed on loss peaks I in an attempt to understand the molecular dynamics of the samples.

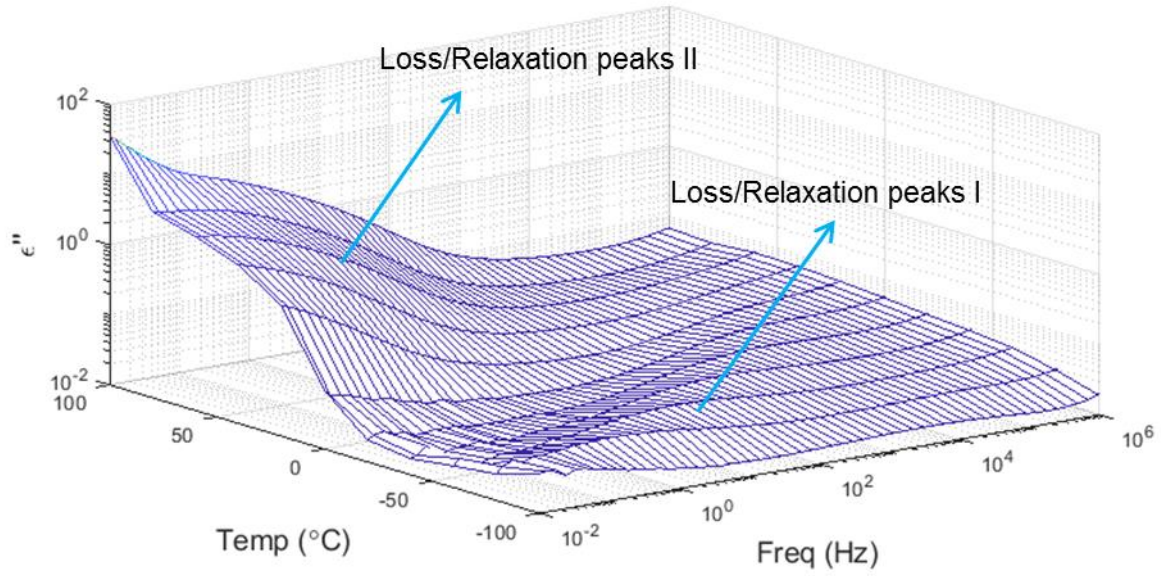

Figure 5-7 Loss modulus (ε'') of M2515H at low temperatures (-100°C to +100°C), as observed through dielectric analysis - 3D

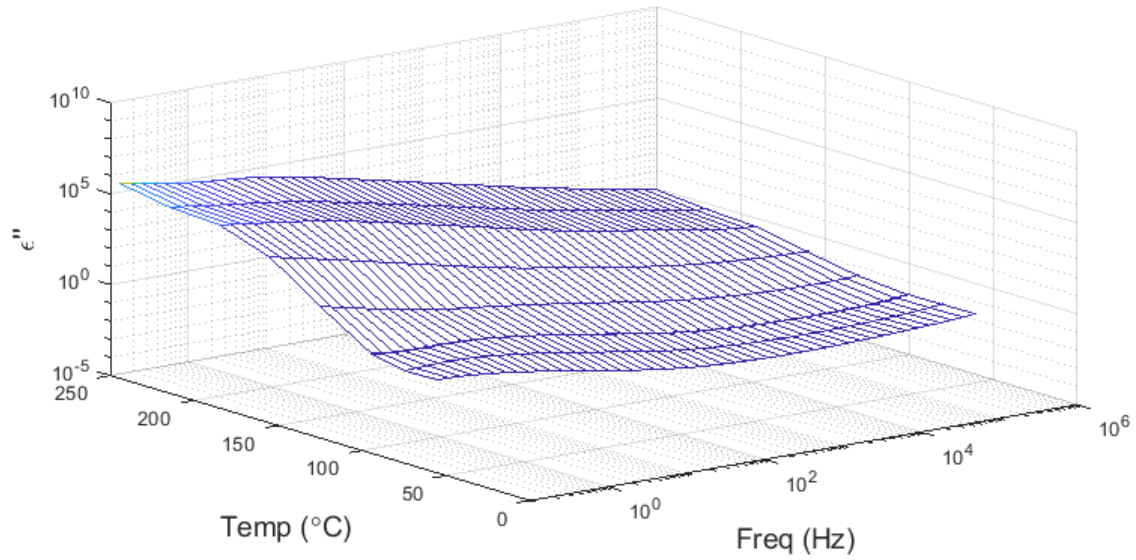

Figure 5-8 Loss modulus (ε'') of M2515H at high temperatures (+80°C to +250°C), as observed through dielectric analysis - 3D

From this section, it can be seen that distinct relaxation peaks (of loss peak I) are formed between -80^{0}C and -20^{0}C for the polymeric samples. For the purpose of comparison, the curves corresponding to -40^{0}C are used in Section 5.3.4 for data processing. It can also be noted, through Figure 5-6, that that electrode polarisation does not play a major role at this temperature, and so its contribution is neglected. For all cases, the goodness of HN and VFT fits are given in Appendix A.

5.3.3. Broadening of loss (ε”) peaks

Like in Section 4.5.2, it is expected that the normalised loss peak must change its breadth for changes in the confining pore topologies. From Figure 5-9, it can be seen that different samples (high pressure, and temperature enabled curing) appear to have different breadths for loss peaks. But in case of low pressure enabled curing, such broadening is missing. Also, the broadening is quite unclear explicitly. So, in order to quantify this phenomenon, the area under various loss peaks was quantified using integration. Some of them are shown in Figure 5-10. Further, Figure 5-11 shows the distribution of these areas for different materials as a function of CSA and pore diameter (inset).

In the case of samples produced at low pressure, it is seen that the area under the graph shows a constant trend, but with considerable error. In case of samples produced with high pressure, a decreasing trend is observed as a function of pore diameter. In all the cases, considerable differences between the areas are found between the samples with same surface topology but produced under different conditions (eg. M0623H vs. M0623L). However, all the values are very close to each other, so the observation of change in area is not conclusive.

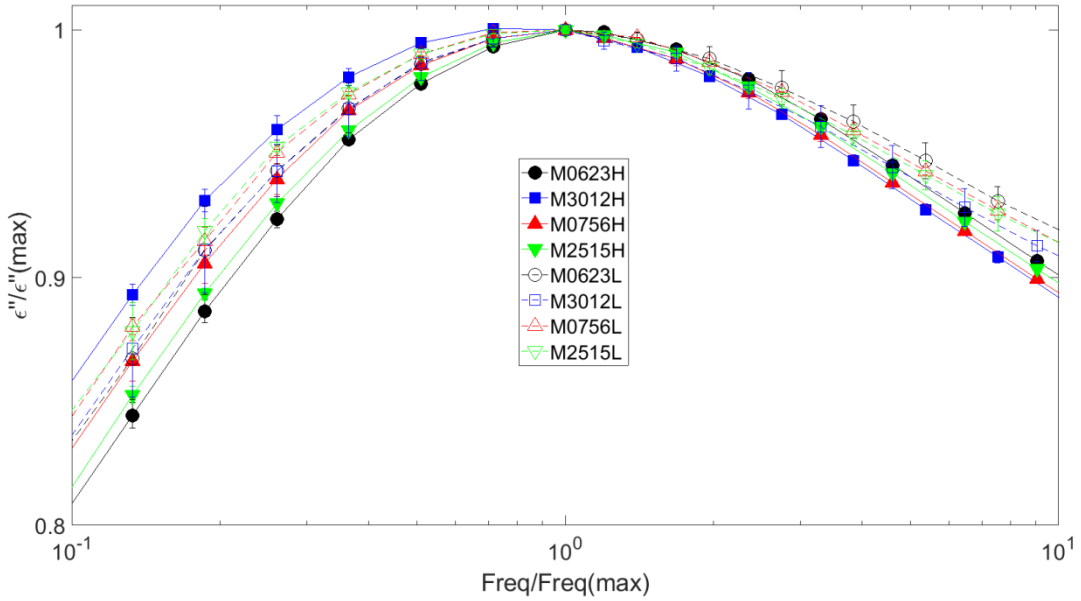

Figure 5-9 Compiled loss peaks (normalised) for different polymeric samples (at -40°C)

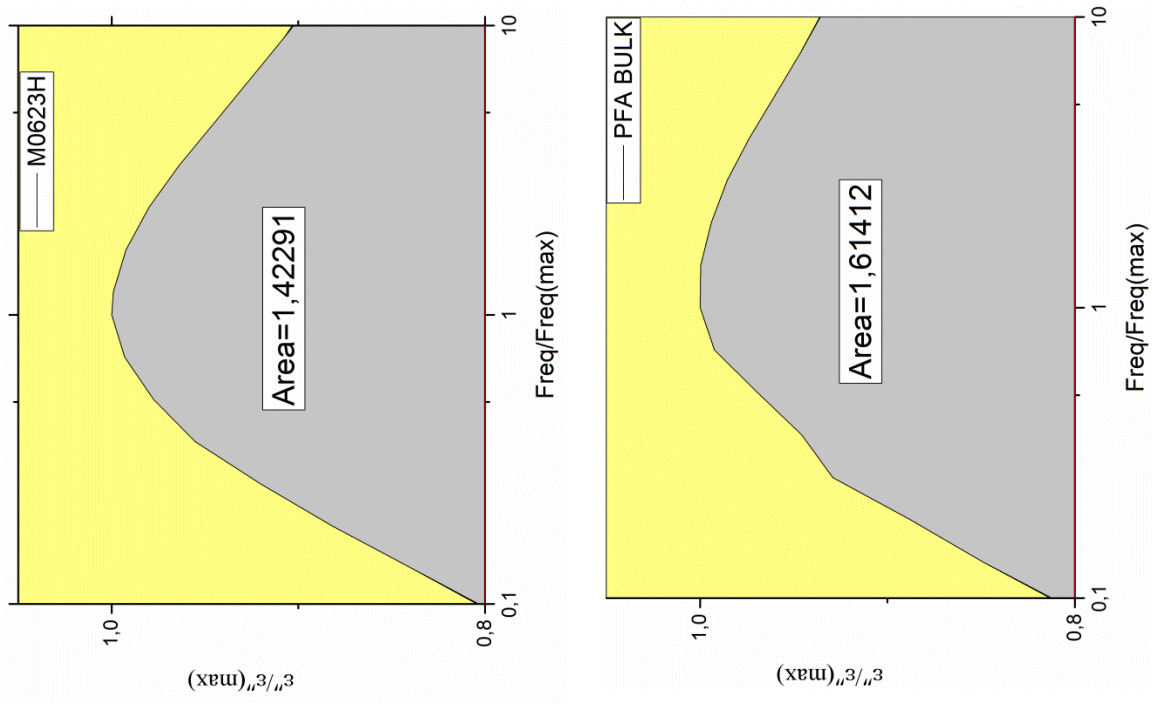

(a) (b)

Figure 5-10 Area under the normalised loss curves for different samples of PFA on a) M0623H, and b) Bulk

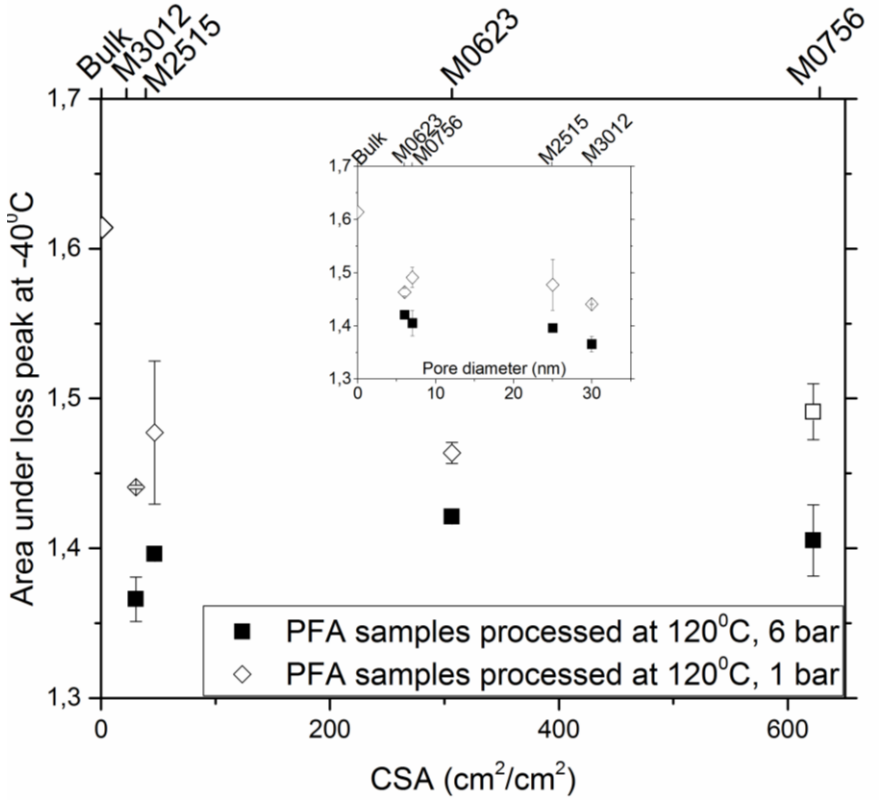

Figure 5-11 Distribution of area under the curve for different samples
(Inset: Same, but as a function of pore diameter)

5.3.4. Curve fitting parameters

To quantify the dielectric data to get information on molecular dynamics of the samples, the loss peaks were fitted with the following: (a) Single-HN peak, (b) Double-HN peaks as explained in Section 3.1.3, where the fitting procedures and equations are provided. Furthermore, Arrhenius fits* are also used for this purpose instead of VFT fits.

For Single-HN curve fit, the different fitting parameters of different samples, such as Δε, τ_{HN}, α and β are provided in Table 5-2. It can be seen that Δε and τ_{HN} of different samples are comparable to each other. Similarly, the shape parameters (α and αβ) show almost comparable values for different samples. In all scenarios, noticeable differences in fitting parameters such as Δε, τ_{HN}, α and β for samples with same substrates but different processing conditions (eg. M0623H vs. M0623L) are witnessed.

Table 5-2 HN curve fitting parameters for different polymeric samples (Single-HN curve)

Sample	Δε	τ_{HN} (s)	α	β	αβ
Bulk	10,6	5,8E-03	0,39	0,37	0,12
M0623H	9,7	3,6E-03	0,39	0,33	0,14
M3012H	9,9	3,8E-03	0,42	0,46	0,14
M0756H	9,8	2,8E-03	0,37	0,39	0,17
M2515H	10,0	3,5E-03	0,36	0,34	0,14
M0623L	9,8	4,2E-03	0,39	0,30	0,13
M3012L	9,7	4,5E-03	0,43	0,33	0,13
M0756L	11,4	6,6E-03	0,39	0,40	0,13
M2515L	10,3	5,1E-03	0,37	0,37	0,15

When the loss peaks were fitted with Double-HN peaks, a set of fitting parameters, as seen in Table 5-3 is obtained. It can be observed that the HN2 curve appears to be smaller than the HN1 peak ($\Delta\varepsilon_{HN2} < \Delta\varepsilon_{HN1}$). Also, it can be observed that $\Delta\varepsilon_{HN2}$ and $\Delta\varepsilon_{HN1}$ values tend to be of comparable values across different samples. The relaxation time of HN2 peak (τ_{HN2}) is observed to be faster than that of the HN1 peak (τ_{HN1}). Also, for each type of metal substrate, there are considerable differences in Δε and τ_{HN} found between samples processed under different conditions (eg. M0623H vs. M0623L).

* Equation for Arrhenius fit: $\tau(T) = \tau_0 \frac{E_a}{k_B T}$, where τ_0 – Relaxation time at maximum energy, Ea- Activation energy, k_B- Boltzmann constant

Table 5-3 HN curve fitting parameters for polymeric samples (Double-HN curves)

Sample code	$\Delta\varepsilon_{HN1}$	τ_{HN1} (s)	α_{HN1}	β_{HN1}	$\Delta\varepsilon_{HN2}$	τ_{HN2} (s)	α_{HN2} , β_{HN2}
Bulk	10,6	5,8E-3	0,39	0,30	-	-	1
M0623H	10,2			0,27	0,14	5,1E-04	
M3012H	11,0			0,26	0,14	5,3E-04	
M0756H	10,5			0,29	0,06	4,5E-04	
M2515H	10,9			0,27	0,10	5,9E-04	
M0623L	12,6			0,20	0,16	4,4E-04	
M3012L	12,5			0,21	0,16	4,2E-04	
M0756L	12,6			0,21	0,13	4,3E-04	
M2515L	12,5			0,21	0,15	3,9E-04	

Unlike monomeric samples, the polymeric samples have Arrhenius type dependence for their relaxations. The Arrhenius fits for HN1 and HN2 curves are showed in Figure 5-12. Further, the fit parameters are also provided in Table 5-4. Here, it can be seen that the fitting parameters τ_0 and E_a tend to show a constant trend for all the samples.

Table 5-4 Arrhenius fit parameters for different polymeric samples

Sample	τ_o-HN1 (s)	E_a HN1 (eV)	τ_o-HN2 (s)	E_a HN2 (eV)
Bulk	1,5E-19	7,1E-01	-	-
M0623H	4,7E-18	6,4E-01	8,1E-15	5,0E-01
M3012H	1,3E-19	7,0E-01	7,0E-15	5,1E-01
M0756H	1,8E-19	7,0E-01	3,0E-14	4,8E-01
M2515H	1,4E-19	7,0E-01	4,5E-15	5,2E-01
M0623L	6,3E-20	7,1E-01	5,0E-16	5,5E-01
M3012L	4,6E-20	7,1E-01	6,7E-15	5,0E-01
M0756L	2,8E-20	7,2E-01	7,2E-15	5,0E-01

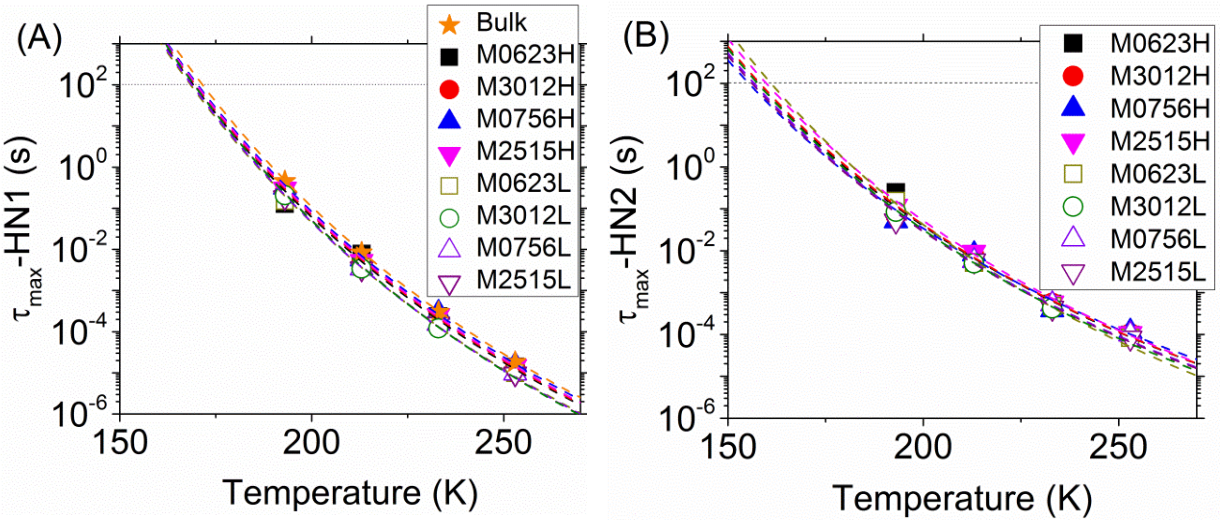

Figure 5-12 Arrhenius fits for the (A) HN1 and (B) HN2 curves of polymeric samples

5.3.5. Significance of different fits

The observed loss peaks do not show clear evidence of any trend in changes to their shape. So, changes to molecular dynamics are not explicitly observed unlike the case of monomers (Section 4.5.2). In order to extract information on molecular dynamics, HN and Arrhenius fits were performed.

From the MSD values of the different HN fits (Appendix A), it can be seen that the loss peaks are better represented by Single-HN peaks rather than Double-HN peaks, as the former shows lesser MSD. The addition of new HN peak appears to decrease the accuracy of the fits. However, in order to decouple the new behaviour from the bulk behaviour, it was done.

It can be seen from the Single-HN fit that the fit parameters $\Delta\varepsilon$ and τ_{HN} of different samples tend to be of comparable values. Constant value observed in the case of $\alpha\beta$ is a clear indicator that there are no changes observed in molecular dynamics of the PFA at higher frequencies. Furthermore, from α values (Figure 5-13), a clear trend is not established with respect to pore topology. If the samples M2515H and M2515L are ignored*, it is seen that a trend appears in α. However, as this change is very small, they are not considered. Increase in α for M3012H and M3012L when compared to bulk polymer shows that confining PFA in big pores decrease the diversity of polymer behaviour at low-frequency regime.

When the loss peaks are fitted with Double-HN peaks in order to separately observe the contribution of adsorbed polymers (if any), it is seen that fit parameters, τ_{HN} and $\Delta\varepsilon$, appear to be constant for different substrates. Decrease in for $\Delta\varepsilon$ high pressure enabled cured samples is probably due to decrease in quantity of PFA due to overflow at high pressure. A bulk sample which was made in-house also appears to replicate this phenomenon. Furthermore, it is seen that the HN2 peaks show faster dynamics than HN1 peaks in this case.

Arrhenius fits were also performed for the relaxation times for different samples at different temperatures. The fitting parameters obtained from this fitting were paramount in deducting the molecular dynamics behaviour of different samples. The information obtained from this fitting is further discussed in the upcoming sections.

* Due to their “bird-nest” oxide pores in M2515, as seen in Figure 5-1

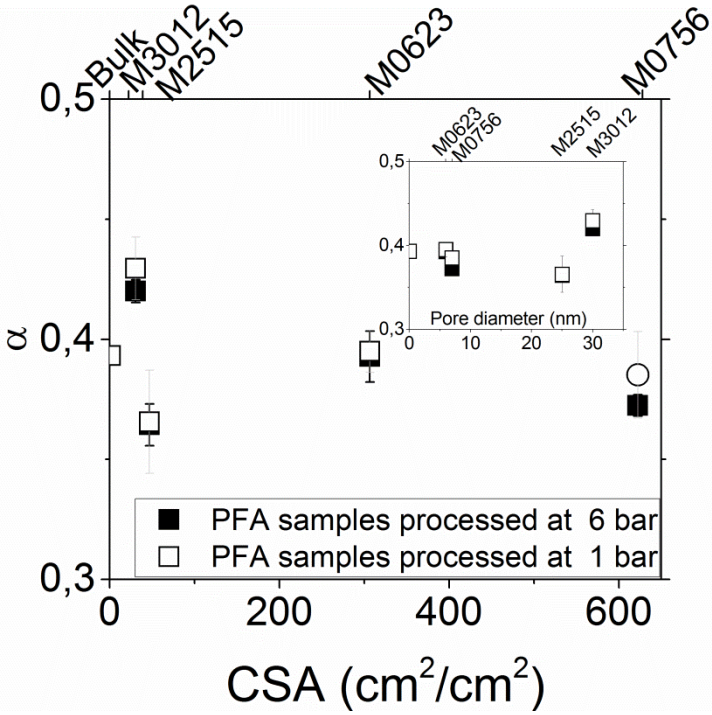

Figure 5-13 α parameter for Single-HN curve for normalised loss peaks of different polymeric samples *(Inset: Same, but as a function of pore diameter)*

5.3.6. Temperature dependence of relaxation time of HN2 peak

The HN and Arrhenius based relaxation times for different samples show comparable values with a change in pore topology. However, the overall trend of the HN2 peaks with respect to HN1 peaks tends to change.

HN fit based relaxation time (Figure 5-14(a)) shows that the HN2 peak has faster dynamics compared to HN1 peaks. When Arrhenius fit based relaxation times are considered (Figure 5-14(b)), it is seen that HN2 peaks show slower dynamics than HN1 peaks. It establishes the idea that HN2 peaks are more temperature-dependent than HN1 peaks. This is a clear indicator of the difference in the molecular arrangement between HN1 and HN2 peaks.

When different pore topologies are considered, it is seen that the relaxation times tend to remain constant. In all the cases, different substrates do not lead to different relaxation times. However, when different processing conditions are considered (eg. M0623H vs. M0623L), it is seen that high pressure leads to an increase in relaxation time. This shows that high pressure enables the formation of a different molecular arrangement of relatively slower dynamics for the HN2 peak. This further strengthens the idea that higher pressure enables slowing down of the molecular dynamics, probably due to better infiltration of polymers into nanopores.

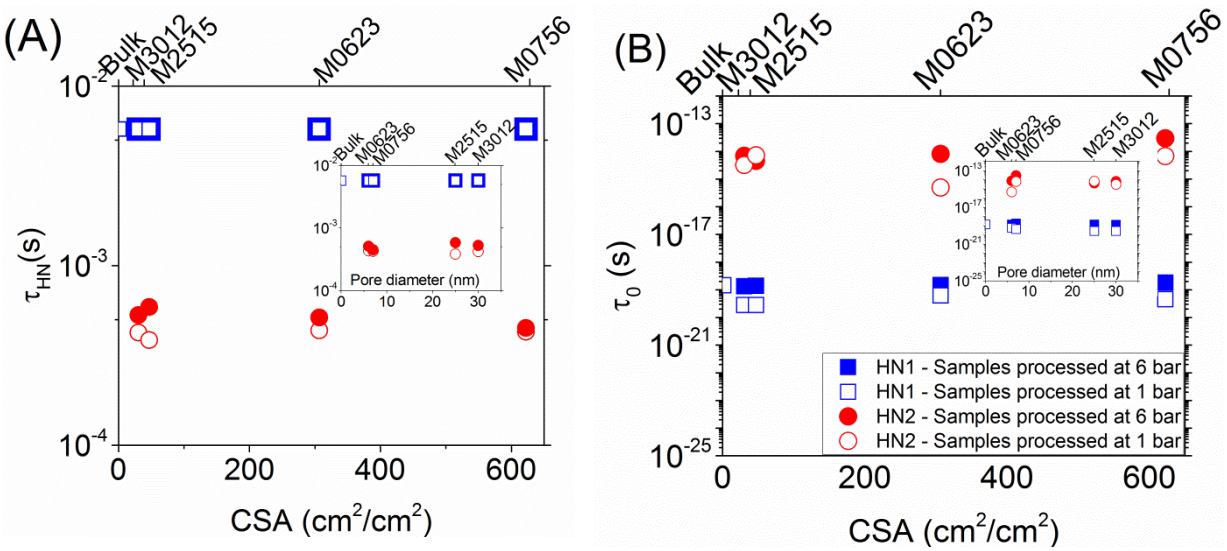

Figure 5-14 (A) Havriliak-Negami τ_{HN}, and (B) Arrhenius τ_0 – based relaxation time for different polymeric samples, with shared legend. *(Inset: Same, but as a function of pore diameter)*

5.3.7. Transition temperatures for different relaxation processes

In general, when Arrhenius curves reach a value of 100 s on time axis, the corresponding temperature is considered as the transition temperature of the process under consideration Based on this convention, the transition temperature (considered as Tx) corresponding to HN1 and HN2 peaks for different samples were obtained, as seen in Table 5-5 and Figure 5-15.

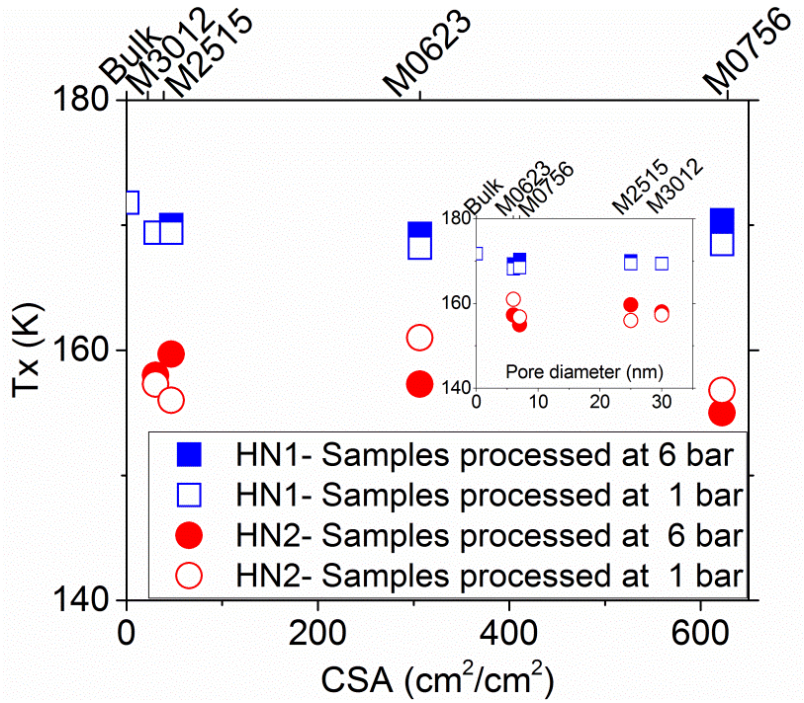

Figure 5-15 Transition temperature of different samples, obtained from Arrhenius fits
(Inset: Same, but as a function of pore diameter)

Table 5-5 Transition temperature (Tx) of different samples corresponding to τ_{max}=100s for HN1 and HN2 peaks

Sample	Tx HN1	Tx HN2
Bulk	172	--
M0623H	169	157
M3012H	169	158
M0756H	170	155
M2515H	170	160
M0623L	168	161
M3012L	169	157
M0756L	169	157
M2515L	169	156

In all the cases, it is seen that Bulk PFA shows the highest transition temperature that is consistent with the transition temperature of HN1, as expected. Further, it is observed that relaxations attributed to HN2 peaks show lower transition temperature than HN1 peaks. Infiltration of PFA into the nanopores leads to the formation of new dynamics that requires lesser temperature (or energy) for transition. It also shows that the polymer inside the pores are subjected to confinement effects, and have less restricted dynamics, as suggested by Donth et al [30]. Further, the dependence of molecular dynamics on the pore topology is not seen.

In order to validate this observation, DSC tests were done on PFA film from -150°C to +150°C (2 cycles) at ±10°C/min ramp up/down rate under Helium. Here, it is seen that DSC does not pick up any changes in heat flow about Tx values (Figure 4-19). The transition temperature predicted by Arrhenius fit is not seen probably as such a transition might be too small (or delicate) to be predicted by DSC. However, since the type of transition is unknown, binding conclusions cannot be made at this juncture.

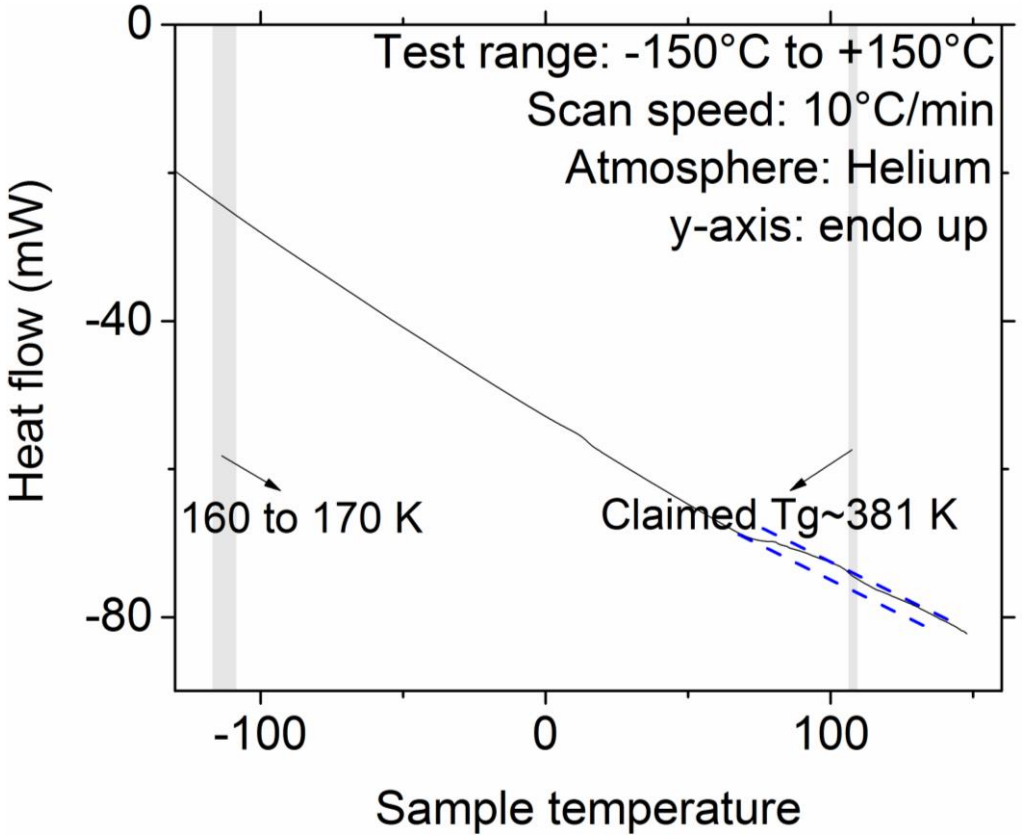

Figure 5-16 DSC data of PFA film (baseline uncorrected)

5.3.8. Activation energy required to initiate dielectric excitations

When the activation energy of different samples are seen, it appears that HN2 peaks show a lower activation energy than HN1 peaks, as seen in Figure 5-17. This indicates that the part of the sample represented by HN2 peaks needs lesser energy to activate motions to polymer chains. This observation appears to be in line with the discussions in Section 5.3.7. It is an indicator of the fact that the polymer infiltration into nanopores could lead to the formation of a region of the sample with high free volume (or short chains).

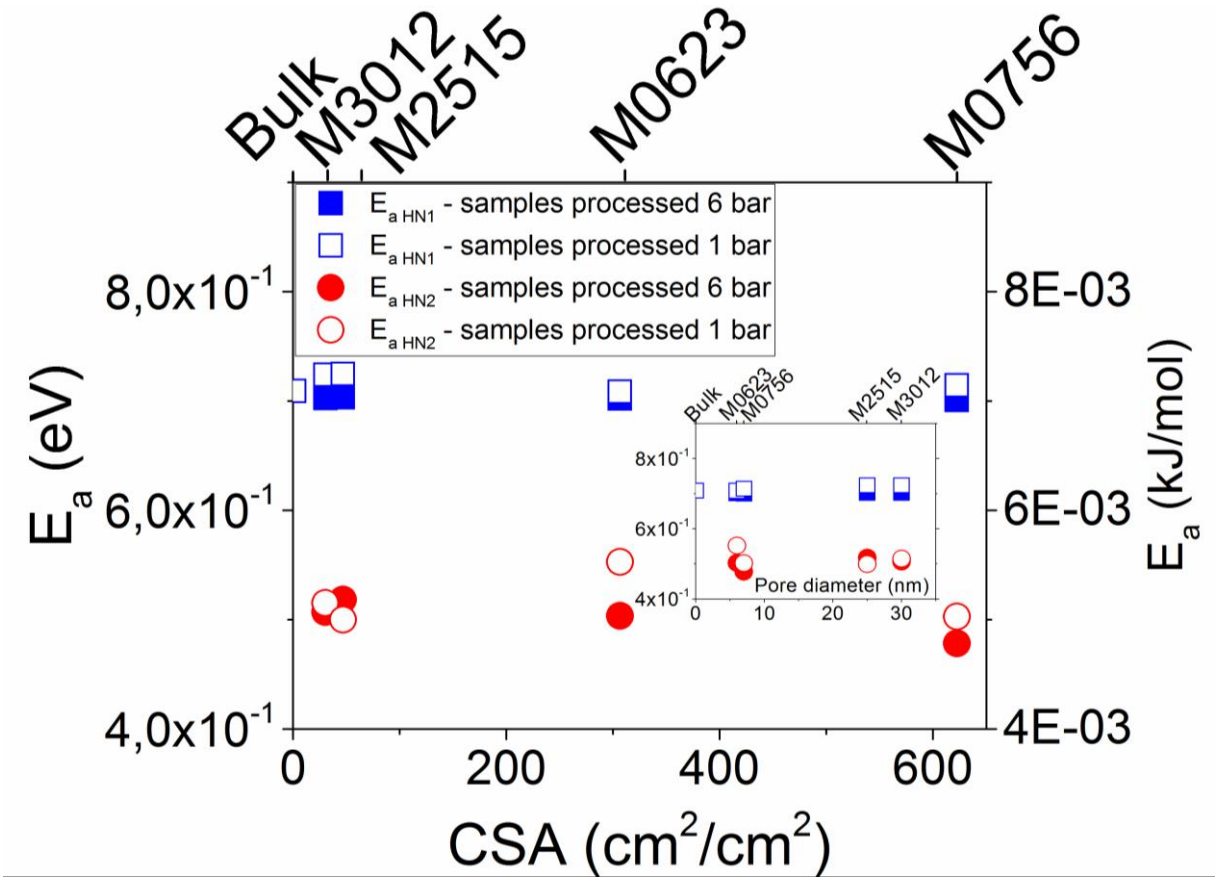

Figure 5-17 Activation energy of different samples, obtained from Arrhenius fits
(Inset: Same, but as a function of pore diameter)

5.3.9. Influence of production methods

It appears that the sample production methods do not cause any significant changes to the dielectric behaviour of the sample. The only insight provided by Single-HN fit is the high pressure enabled sample leads to the formation of thinner PFA layers that lead to a decrease in Δε. This observation and discussion are also seen in the case of HN1 peaks when the loss peaks are fitted with Double-HN curves.

High pressure enabled production also appears to slow down the dynamics, as observed by HN and Arrhenius fits. This change is probably due to a denser arrangement of polymers chains due to high pressure. Relaxation temperature for different production methods does not appear to follow any clear trend with respect to sample production methods.

5.3.10. Implication on Loss Peak-I

It was shown through Section 5.3.2 that the reason for selection of loss peak I for analysis was that it formed full peaks within the frequency range under analysis. However, the transition process associated with it remains unidentified. Thus, explanations based on this relaxation remains questionable. Since the samples are made of a commercial polymer AF163-2K0.060, there is not enough literature to identify the type of relaxation this peak corresponds to. It must also be noted that this loss peak does not reflect in the DSC data.

5.3.11. Validity of hypotheses

Based on the above discussions, it appears that the following hypothesis is valid: '*Confinement of mono/polymers will lead to restricted molecular dynamics in one part of the sample, that could be identified through Broadband Dielectric Spectroscopy (BDS)*'. However, there is not enough supportive data to validate that '*Change in contact area between the mono/polymers and the walls of the nanopores will lead to change in fraction of molecules under restricted dynamics*'. Further, due to limitations on variety of samples and data on adhesive strength of the samples, no conclusions can be made on the hypothesis that *'the data obtained from dielectric studies could be correlated to the strength of the adhesion between the polymeric adhesive and the metal substrates'*.

5.4. Chapter synopsis

Through the discussions provided in Section 5.3, it is seen that it is possible to identify new molecular dynamics in various samples. When AF163-2K0.060 polymers were applied and cured on metal substrates, the difference in dielectric behaviour between different samples is not seen explicitly at any one temperature.

Fitting the peaks with Single-HN peak gives lesser MSD. But, they do not provide sufficient information on the molecular dynamics of the samples. When Double-HN curves were used to fit the loss peaks, the fitting became poorer, as indicated by an increase in MSD. However, by this process of deconvolution, the secondary molecular dynamics was observed.

Newly formed molecular dynamics (represented by HN2) appears to be highly temperature dependent. At lower temperatures of around -40°C, they are faster than bulk effects (HN1), but at higher temperatures, they are slower (Section 5.3.6). It appears to indicate that the molecular arrangements of polymer chains attributed to HN2 appear to be different than that of HN1. The chains represented by HN2 also show lesser transition temperature and activation energy than bulk (Section 5.3.7 and 5.3.8). It is possible that this is due to the fact these polymeric chains are relatively less restricted than the bulk. It is a clear indicator that the molecular dynamics is enhanced due to confinement effects. Due to limited varieties of available samples, and production methods, a trend in the influence of substrate topologies or production methods is not established.

5.4.1. Summary

The summary of this chapter can be stated as follows:

1. When the polymeric adhesive is applied on an anodised aerospace aluminium alloy, a new region of molecular dynamics is formed
2. The newly formed region has faster dynamics (τ_{HN}) and requires lesser energy for dielectric excitation (Tx and E_a) due to the hindering of dynamics i.e. domination of confinement effects
3. The substrate topography does not influence the dielectric behaviour of samples
4. Sample production method does not influence the dielectric behaviour of samples substantially
5. With a limited variety of samples, binding conclusions cannot be made on the effectiveness of BDS to study molecular dynamics of confined polymers

Chapter 6
Conclusions

6.1. Reflection on project goal

Based the literature study, experiments performed, and data analysis, it is seen that BDS can reliably be used to assess the molecular dynamics of mono/polymers confined with the nanopores of anodised aerospace aluminium alloys.

In case of monomers, the broadening of loss peak, and subsequent analysis reveals the formation of a new region of restricted dynamics. Through BDS, it is possible to clearly identify the infiltration of monomers into nanopores. Furthermore, the contribution of substrate topology to this phenomenon is also identified. In case of polymers, clear broadening of loss peaks is not seen. However, the subsequent analysis reveals that a new region of lesser restriction is formed. In this case, it is also not possible to differentiate between different sample manufacturing methods.

Overall, within the scope of this project, it is seen it is difficult to use BDS to identify different sample manufacturing processes, and different sample (substrate) types for polymeric samples. So, within the limited scope of this project, it appears that further tests on different polymeric samples are needed to arrive at a decisive conclusion.

6.2. Establishment of a testing method

For using BDS as NDT characterisation tool, the following protocol is suggested to be followed:

Step 1: Prepare ideal samples using proven manufacturing methods (verified by other test methods*) and test them at a wide range of temperatures and frequencies to identify the combination of temperatures (T_a…T_b) and frequencies (f_a…f_b) where relaxation peaks are seen

Step 2: Dielectric tests must be done for the above-mentioned temperature and frequency range (T_a…T_b, and f_a…f_b) for all the ideal samples

Step 3: Loss peaks must be fitted with Single-HN fit, Double-HN fit (or Multiple-HN curves fit depending on the samples), and VFT fit to extract fitting data, and a database must be prepared using the statistical data from all samples

Step 4: For all comparable samples, dielectric tests must be done for the above mentioned temperate and frequency range (T_a…T_b, and f_a…f_b)

Step 5: Molecular dynamics can be directly extracted from these fit parameters by correlating them to the ideal case from the established database

* Including destructive methods such as peel tests and shear tests

6.3. Future scope of this study

While this project sheds light into several aspects of the analysis of molecular dynamics of confined mono/polymers in oxide pores, there are some concepts that could be explored further to get a wholesome understanding of the topic under consideration.

Firstly, the increase in observed activation energy for adsorbed monomers is counterintuitive to other measured data (relaxation time, Vogel temperature, transition temperature). Unfortunately, the study of molecular dynamics confined monomers is not a well-established research field, the explanation provided for this phenomenon is highly speculative. So, in order to establish a reasonable and validated explanation for this observation, it is suggested to do a molecular dynamics simulation of confined monomers. For this purpose, the simulation of monomers as a Lennard-Jones fluid confined within infinite slit-like pores can be explored [62], [63].

One of the challenges faced in this project was the lack of customisable nanoporous substrates. The substrates used in this project were of industrial standard, with pre-designed pore topology. So, an in-house anodisation opportunity could provide a way to produce samples with highly controlled pore diameter, pore depth, and substrate chemistry. Such samples will enable elimination of any remaining uncontrolled variables in this analysis. Further, the in-house production of polymeric samples could also allow a way to monitor the infiltration of polymers into the oxide nanopores. This will also enable the production of samples that are suitable for in-house strength testing. Such control over substrate topology, substrate chemistry, and production process could enable the establishment of a much more systematic approach for analysing the molecular dynamics by studying the influence of each parameter separately.

Further, the influence of substrate chemistry on the molecular dynamics of the polymerisation of polymeric adhesives could also be explored. In-situ BDS using disposable electrodes could be used for this purpose.

Overall, it appears that BDS could be an effective NDT tool for characterising adhesive bonds. While this thesis has laid the groundwork for such a development, there is still a long way to go before BDS characterisation of an adhesive bond is applicable on an industrial scale.

References

[1] K. Zhao and L. R. Xu, “Size Effect of the Adhesive Bonding Strengths of Metal/Polymer Similar and Dissimilar Material Joints,” *J. Adhes.*, vol. 91, no. 12, pp. 978–991, Dec. 2015.

[2] K. B. Katnam, A. D. Crocombe, H. Khoramishad, and I. A. Ashcroft, “The Static Failure of Adhesively Bonded Metal Laminate Structures: A Cohesive Zone Approach,” *J. Adhes. Sci. Technol.*, vol. 25, no. 10, pp. 1131–1157, Jan. 2011.

[3] T. Sinmazçelik, E. Avcu, M. Ö. Bora, and O. Çoban, “A review: Fibre metal laminates, background, bonding types and applied test methods,” *Materials and Design*, vol. 32, no. 7. pp. 3671–3685, 2011.

[4] E. M. Petrie, “Adhesives for the assembly of aircraft structures and components,” *Met. Finish.*, vol. 106, no. 2, pp. 26–31, Feb. 2008.

[5] S. Y. Park, W. J. Choi, H. S. Choi, H. Kwon, and S. H. Kim, “Recent Trends in Surface Treatment Technologies for Airframe Adhesive Bonding Processing: A Review (1995–2008),” *J. Adhes.*, vol. 86, no. 2, pp. 192–221, Feb. 2010.

[6] C. W. Jennings, “Surface Roughness and Bond Strength of Adhesives,” *J. Adhes.*, vol. 4, no. 1, pp. 25–38, May 1972.

[7] A. Kwakernaak, J. Hofstede, J. Poulis, and R. Benedictus, “Improvements in bonding metals for aerospace and other applications,” in *Welding and Joining of Aerospace Materials*, 2011, pp. 235–287.

[8] S. T. Abrahami, J. M. M. de Kok, V. C. Gudla, R. Ambat, H. Terryn, and J. M. C. Mol, “Interface strength and degradation of adhesively bonded porous aluminum oxides,” *npj Mater. Degrad.*, vol. 1, no. 1, p. 8, Dec. 2017.

[9] M. Davis and D. Bond, “Principles and practices of adhesive bonded structural joints and repairs,” *Int. J. Adhes. Adhes.*, vol. 19, no. 2, pp. 91–105, Apr. 1999.

[10] R. A. Pethrick, “Design and ageing of adhesives for structural adhesive bonding - A review,” *Proc. Inst. Mech. Eng. Part L J. Mater. Des. Appl.*, vol. 229, no. 5, pp. 349–379, Oct. 2015.

[11] LPD lab Services, “Interface Adhesion, Adhesives and Coatings.” [Online]. Available: http://www.lpdlabservices.co.uk/problem_solving/typical_technical_expertise/interfaces_adhesion_adhesives_and_coatings.php. [Accessed: 23-Jul-2017].

[12] A. Higgins, “Adhesive bonding of aircraft structures,” *Int. J. Adhes. Adhes.*, vol. 20, no. 5, pp. 367–376, 2000.

[13] J. R. G. Evans and D. E. Packham, “Adhesion of polyethylene to metals: The role of surface topography,” *J. Adhes.*, vol. 10, no. March 2013, pp. 177–191, Jan. 1979.

[14] P. Molitor and T. Young, “Adhesives bonding of a titanium alloy to a glass fibre reinforced composite material,” *Int. J. Adhes. Adhes.*, vol. 22, no. 2, pp. 101–107, Jan. 2002.

[15] D. J. Bland, A. J. Kinloch, and J. F. Watts, “The role of the surface pretreatment in the durability of aluminium-alloy structural adhesive joints: Mechanisms of failure,” *J. Adhes.*, vol. 89, no. 5, pp. 369–397, May 2013.

[16] V. M. Papadakis, S. Teixeira De Freitas, R. M. Colijn, J. J. Goedhart, J. A. Poulis, and R. M. Groves, “Post peel test assessment of metal-metal bonded interface using hyperspectral imaging,” *Spie Proc.*, vol. 9899, no. 9899, 2016.

[17] J. Martín, C. Mijangos, A. Sanz, T. A. Ezquerra, and A. Nogales, “Segmental Dynamics of Semicrystalline Poly(vinylidene fluoride) Nanorods,” *Macromolecules*, vol. 42, no. 14, pp. 5395–5401, Jul. 2009.

[18] J. L. Lutkenhaus, K. McEnnis, A. Serghei, and T. P. Russell, “Confinement Effects on Crystallization and Curie Transitions of Poly(vinylidene fluoride-co-trifluoroethylene),” *Macromolecules*, vol. 43, no. 8, pp. 3844–3850, Apr. 2010.

[19] A. Houachtia, P. Alcouffe, G. Boiteux, G. Seytre, J.-F. Gérard, and A. Serghei, “Nanofluidics Approach to Separate between Static and Kinetic Nanoconfinement Effects on the Crystallization of Polymers,” *Nano Lett.*, vol. 15, no. 7, pp. 4311–4316, Jul. 2015.

[20] I. Blaszczyk-lezak, M. Hernández, and C. Mijangos, “One Dimensional PMMA Nano fi bers from AAO Templates. Evidence of Con fi nement E ff ects by Dielectric and Raman Analysis,” *Macromolecules*, vol. 46, no. 12, pp. 4995–5002, Jun. 2013.

[21] J. Maiz *et al.*, “Dynamic study of polystyrene-block-poly(4-vinylpyridine) copolymer in bulk and confined in cylindrical nanopores,” *Polym. (United Kingdom)*, vol. 55, no. 16, pp. 4057–4066, 2014.

[22] A. Serghei, W. Zhao, X. Wei, D. Chen, and T. P. Russell, “Nanofluidics with phase separated block-copolymers: Glassy dynamics during capillary flow,” *Eur. Phys. J. Spec. Top.*, vol. 189, no. 1, pp. 95–101, Oct. 2010.

[23] I. Blaszczyk-Lezak, V. Desmaret, and C. Mijangos, “Electrically conducting polymer nanostructures confined in anodized aluminum oxide templates (AAO),” *Express Polym. Lett.*, vol. 10, no. 3, pp. 259–272, 2016.

[24] S. Zhao, H. Roberge, A. Arthur Yelon, and T. Veres, “New Application of AAO Template: A Mold for Nanoring and Nanocone Arrays,” 2006.

[25] A. Serghei, D. Chen, D. H. Lee, and T. P. Russell, “Segmental dynamics of polymers during capillary flow into nanopores,” *Soft Matter*, vol. 6, no. 6, pp. 1111–1113, 2010.

[26] L. Li *et al.*, “Glass transitions of poly(methyl methacrylate) confined in nanopores: Conversion of three- and two-layer models,” *J. Phys. Chem. B*, vol. 119, no. 15, pp. 5047–5054, Apr. 2015.

[27] Y. B. Mel’nichenko, J. Schüller, R. Richert, B. Ewen, and C.-K. Loong, “Dynamics of hydrogen-bonded liquids confined to mesopores: A dielectric and neutron spectroscopy study,” *J. Chem. Phys.*, vol. 103, no. 6, p. 2016, 1995.

[28] M. Arndt, R. Stannarius, W. Gorbatschow, and F. Kremer, “Dielectric investigations of the dynamic glass transition in nanopores,” *Phys. Rev. E*, vol. 54, no. 5, pp. 5377–5390, 1996.

[29] M. Alcoutlabi and G. B. McKenna, “Effects of confinement on material behaviour at the nanometre size scale,” *J. Phys. Condens. Matter*, vol. 17, no. 15, pp. R461–R524, Apr. 2005.

[30] E.-J. Donth, *The Glass Transition Relaxation Dynamics in Liquids and Disordered Materials*, vol. 48. Springer Berlin Heidelberg, 2001.

[31] M. Arndt, R. Stannarius, H. Groothues, E. Hempel, and F. Kremer, “Length Scale of Cooperativity in the Dynamic Glass-Transition,” *Phys. Rev. Lett.*, vol. 79, no. 11, pp. 2077–2080, 1997.

[32] A. Schönhals, H. Goering, and C. Schick, “Segmental and chain dynamics of polymers: From the bulk to the confined state,” *J. Non. Cryst. Solids*, vol. 305, no. 1–3, pp. 140–149, 2002.

[33] A. Huwe and F. Kremer, “Molecular dynamics in confining geometries,” in *Liquid Dynamics: Experiment, Simulation and Theory*, vol. 820, no. PR7, EDP Sciences, 2002, pp. 59–65.

[34] S. Spange, A. Graser, A. Huwe, F. Kremer, C. Tintemann, and P. Behrens, “Cationic host-guest polymerization of N-vinylcarbazole and vinyl ethers in MCM-41, MCM-48, and nanoporous glasses,” *Chemistry*, vol. 7, no. 17, pp. 3722–3728, Sep. 2001.

[35] C. C. Lin, E. Parrish, and R. J. Composto, “Macromolecule and Particle Dynamics in Confined Media,” *Macromolecules*, vol. 49, no. 16, pp. 5755–5772, Aug. 2016.

[36] Y. Long, R. A. Shanks, and Z. H. Stachurski, “Kinetics of polymer crystallisation,” *Progress in Polymer Science*, vol. 20, no. 4. pp. 651–701, Jan-1995.

[37] B. Sanz, N. Ballard, J. M. Asua, and C. Mijangos, “Effect of Confinement on the Synthesis

of PMMA in AAO Templates and Modeling of Free Radical Polymerization," *Macromolecules*, p. acs.macromol.6b02282, 2017.

[38] R. M. Michell and A. J. Müller, "Confined crystallization of polymeric materials," *Prog. Polym. Sci.*, vol. 54–55, pp. 183–213, 2016.

[39] M. Tarnacka *et al.*, "Following kinetics and dynamics of DGEBA-aniline polymerization in nanoporous native alumina oxide membranes - FTIR and dielectric studies," *Polym. (United Kingdom)*, vol. 68, pp. 253–261, 2015.

[40] M. Tarnacka *et al.*, "Polymerization of Monomeric Ionic Liquid Confined within Uniaxial Alumina Pores as a New Way of Obtaining Materials with Enhanced Conductivity," *ACS Appl. Mater. Interfaces*, vol. 8, no. 43, pp. 29779–29790, Nov. 2016.

[41] J. M. Giussi, I. Blaszczyk-Lezak, M. S. Cortizo, and C. Mijangos, "In-situ polymerization of styrene in AAO nanocavities," *Polym. (United Kingdom)*, vol. 54, no. 26, pp. 6886–6893, 2013.

[42] H. Y. Zhao, Z. N. Yu, F. Begum, R. C. Hedden, and S. L. Simon, "The effect of nanoconfinement on methyl methacrylate polymerization: Tg, molecular weight, and tacticity," *Polym. (United Kingdom)*, vol. 55, no. 19, pp. 4959–4965, 2014.

[43] M. Hernández, J. Carretero-González, R. Verdejo, T. A. Ezquerra, and M. A. López-Manchado, "Molecular Dynamics of Natural Rubber/Layered Silicate Nanocomposites As Studied by Dielectric Relaxation Spectroscopy," *Macromolecules*, vol. 43, no. 2, pp. 643–651, Jan. 2010.

[44] M. Hernández, T. A. Ezquerra, R. Verdejo, and M. A. López-Manchado, "Role of vulcanizing additives on the segmental dynamics of natural rubber," *Macromolecules*, vol. 45, no. 2, pp. 1070–1075, 2012.

[45] A. Schönhals, H. Goering, C. Schick, B. Frick, and R. Zorn, "Glassy dynamics of polymers confined to nanoporous glasses revealed by relaxational and scattering experiments," *Eur. Phys. J. E*, vol. 12, no. 1, pp. 173–178, 2003.

[46] P. Pissis, D. Daoukakidiamanti, L. Aspekis, and C. Christodoulides, "The glass transition in confined liquids," *J. Phys. Condens. Matter*, vol. 6, no. 21, p. L 325-L, 1994.

[47] S. Malynych, I. Luzinov, and G. Chumanov, "Poly(vinyl pyridine) as a universal surface modifier for immobilization of nanoparticles," *J. Phys. Chem. B*, vol. 106, no. 6, pp. 1280–1285, 2002.

[48] B. K. Sharma, A. K. Gupta, N. Khare, S. K. Dhawan, and H. C. Gupta, "Synthesis and characterization of polyaniline-ZnO composite and its dielectric behavior," *Synth. Met.*, vol. 159, no. 5–6, pp. 391–395, 2009.

[49] P. Klonos *et al.*, "Interaction of poly(ethylene glycol) with fumed silica and alumina/silica/titania," *Colloids Surfaces A Physicochem. Eng. Asp.*, vol. 360, no. 1–3, pp. 220–231, 2010.

[50] X. Huang, T. Iizuka, P. Jiang, Y. Ohki, and T. Tanaka, "Role of interface on the thermal conductivity of highly filled dielectric epoxy/AlN composites," *J. Phys. Chem. C*, vol. 116, no. 25, pp. 13629–13639, Jun. 2012.

[51] B. Lambert, "Mauritz - Dielectric Spectroscopy." [Online]. Available: https://web.archive.org/web/20010307184808/http://www.psrc.usm.edu:80/mauritz/dilect.html. [Accessed: 23-Jun-2017].

[52] K.-C. C. Kao, *DIELECTRIC PHENOMENA IN SOLIDS - With Emphasis on Physical Concepts of Electronic Processes*. Academic Press, 2004.

[53] M. Hernández, A. M. Grande, S. van der Zwaag, and S. J. García, "Monitoring Network and Interfacial Healing Processes by Broadband Dielectric Spectroscopy: A Case Study on Natural Rubber," *ACS Appl. Mater. Interfaces*, vol. 8, no. 16, pp. 10647–10656, Apr. 2016.

[54] F. Kremer and A. Schönhals, *Broadband Dielectric Spectroscopy*. Berlin, Heidelberg: Springer Berlin Heidelberg, 2003.

[55] A. Vassilikou-Dova and I. M. Kalogeras, “Dielectric Analysis (DEA),” in *Thermal Analysis of Polymers: Fundamentals and Applications*, Hoboken, NJ, USA: John Wiley & Sons, Inc., 2008, pp. 497–613.

[56] S. Havriliak and S. Negami, “A complex plane analysis of α-dispersions in some polymer systems,” *J. Polym. Sci. Part C Polym. Symp.*, vol. 14, no. 1, pp. 99–117, Mar. 1966.

[57] P. Ben Ishai, M. S. Talary, A. Caduff, E. Levy, and Y. Feldman, “Electrode polarization in dielectric measurements: A review,” *Measurement Science and Technology*, vol. 24, no. 10. IOP Publishing, p. 102001, 01-Oct-2013.

[58] J. D. Mencel and R. B. Prime, “Thermal analysis of polymers: Fundamentals and applications.” John Wiley, p. 688, 2009.

[59] A. Rathi *et al.*, “Identifying the effect of aromatic oil on the individual component dynamics of S-SBR/BR blends by broadband dielectric spectroscopy,” *J. Polym. Sci. Part B Polym. Phys.*, Mar. 2018.

[60] R. A. Pethrick, “Non-destructive evaluation (NDE) of composites: dielectric methods for testing adhesive bonds in composites,” in *Non-Destructive Evaluation (NDE) of Polymer Matrix Composites*, 2013, pp. 185–219.

[61] A. Schönhals, H. Goering, C. Schick, B. Frick, and R. Zorn, “Glass transition of polymers confined to nanoporous glasses,” *Colloid Polym. Sci.*, vol. 282, no. 8, pp. 882–891, 2004.

[62] T. J. H. Vlugt, J. P. J. M. van der Eerden, M. Dijkstra, B. Smit, and D. Frenkel, *Introduction to Molecular Simulation and Statistical Thermodynamics*. 2009.

[63] J. M. Y. Carrillo and B. G. Sumpter, “Structure and dynamics of confined flexible and unentangled polymer melts in highly adsorbing cylindrical pores,” *J. Chem. Phys.*, vol. 141, no. 7, p. 74904, Aug. 2014.

Appendix A
Goodness of fit

In this section, the mean square deviation (MSD) of different HN and VFT fits are provided. They can be considered as a measure of goodness of different fits.

B.1. For monomer (DGEBA) based samples

Table A-1 Mean squared deviation (MSD) for different monomeric samples for loss peaks fitted with Single-HN curves*

Sample	MSD
Bulk	2,21E-02
N1015	2,78E-02
N1030	5,64E-03
N1512	4,10E-03
N4011	2,66E-02
M0623	2,63E-02
M3012	2,29E-02
M0756	5,23E-02
M2515	4,17E-03

Table A-2 Mean squared deviation (MSD) for different monomeric samples for loss peaks fitted with Double-HN curves†

Sample	MSD
Bulk	-
N1015	7,95E-03
N1030	9,95E-03
N1512	8,25E-03
N4011	1,19E-02
M0623	2,84E-02
M3012	1,19E-03
M0756	1,25E-02

* For normalised loss peaks ($\varepsilon''/\varepsilon''_{max}$) at 0°C
† For normalised loss peaks ($\varepsilon''/\varepsilon''_{max}$) at 0°C

Table A-3 Mean squared deviation (MSD) of VFT fit curves for HN1 and HN2 for different monomeric samples fitted with Double-HN curves*

Sample	MSD (HN1)	MSD (HN2)
Bulk	7,07E-02	-
N1015	1,72E-02	7,77E-02
N1030	3,92E-02	2,05E-01
N1512	4,44E-03	2,18E-01
N4011	1,88E-02	2,77E-01
M0623	1,72E-02	2,00E-01
M3012	1,40E-02	7,54E-02
M0756	5,76E-02	4,86E-02

* VFT fit performed for τ_{max} (s) from -15°C to +5°C

B.2. For polymeric film adhesive (PFA) based samples

Table A-4 Mean squared deviation (MSD) for different polymeric samples for loss peaks fitted with Single-HN curves*

Sample	MSD
Bulk	1,07E-02
M0623H	9,96E-03
M3012H	8,43E-03
M0756H	1,63E-02
M2515H	2,25E-02
M0623L	1,18E-02
M3012L	7,84E-03
M0756L	1,56E-02
M2515L	1,53E-02

Table A-5 Mean squared deviation (MSD) for different polymeric samples for loss peaks fitted with Double-HN curves†

Sample	MSD
Bulk	-
M0623H	4,79E-03
M3012H	4,35E-03
M0756H	2,26E-02
M2515H	1,55E-02
M0623L	4,78E-03
M3012L	3,30E-03
M0756L	1,26E-02
M2515L	8,63E-03

* For normalised loss peaks ($\varepsilon''/\varepsilon''_{max}$) at -40°C
† For normalised loss peaks ($\varepsilon''/\varepsilon''_{max}$) at -40°C

Table A-6 Mean squared deviation (MSD) of Arrhenius fit curves for HN1 and HN2 for different polymeric samples fitted with Double-HN curves*

Sample	MSD (HN1)	MSD (HN2)
Bulk	2,81E-02	-
M0623H	1,52E-01	5,03E-02
M3012H	1,15E-02	4,02E-02
M0756H	4,23E-02	1,12E-01
M2515H	4,21E-02	5,52E-02
M0623L	1,52E-02	1,94E-02
M3012L	4,35E-02	1,27e-02
M0756L	8,17E-03	3,22E-02
M2515L	1,42E-02	4,86E-02

* VFT fit performed for τ_{max} (s) from -80°C to -20°C

Appendix B
Mechanical strength test data for polymeric samples

For the purpose of assessment of the strength of the adhesive bond between the polymeric adhesive (AF163-2K0.060) and the metal oxide layer, bell peel tests were performed by Fokker for different samples. The results of the test are given in Table B-1.

Table B-1 Bell peel test data for different polymeric samples

Sample	Dry Bell peel (N/inch)	Wet Bell peel (N/inch)
M0623H	167	67,1
M3012H	303,6	156,7
M0756H	187,4	49,6
M2515H	330	352,7

This page is intentionally left blank.